3. Results and discussion

Fig. 2 shows the performances of a typical SOFC with uniform potential operation (SOFC-UP). Each line represents the results at a constant value of fuel utilization (U_f). It should be noted that because concentration polarization becomes an importance loss at high current densities and small fuel concentrations ($U_f \geq 80\%$) [15], the simulations were performed only in the ranges of high voltages (low current densities) and fuel utilizations (U_f) of lower than 80%. In order to validate the calculations, the simulation results from a previous literature [19] at a condition close to our work ($U_f = 85\%$) are included in Fig. 2. Our calculations show good agreement within a range of high operating voltages (0.65–0.75 V). However, at lower voltages, the data from the literature shows higher power density. This is probably due to the observed temperature increase (within 100 K) which is particularly pronounced at high current density (low voltage) whereas our calculations were based on the isothermal condition. From Fig. 2, regarding the electrical efficiency, it is favorable to operate the SOFC at high voltage in order to obtain high efficiency. However, when taking into account the power density, operation at a high value of voltage is not practical due to the achievement of low power density. Therefore, in practice suitable operating voltage and fuel utilization should be carefully selected. Some workers suggested to operate the cell at 70% of maximum power density [20] and fuel utilization of 80–95% [21–24]. In the present work, the fuel utilization (U_f) of 80% was considered and SOFC with non-uniform potential operation (SOFC-NUP) was investigated with the aim to improve the power density without lowering the electrical efficiency.

Fig. 3 shows the relationship between power density and electrical efficiency of a simple SOFC-NUP with a cell divided into two sections of equal range of fuel utilization ($S_{p,1} = S_{p,2} = 0.5$). V_1 and V_2 represent the operating voltages of sections 1 and 2, respectively. The thick solid line indicates the results of the SOFC-UP. It is indicated that there are some ranges of operation in which the SOFC-NUP offers higher power density than the SOFC-UP without lowering the electrical efficiency (area above of the thick solid line). The improvement becomes significant when the cell is operated at high electrical efficiency.

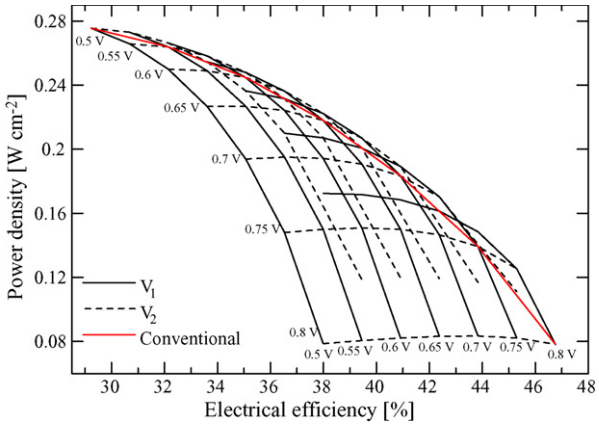

Fig. 3. Relationship between power density and electrical efficiency of SOFC-UP and SOFC-NUP ($U_f = 80\%$ and $T = 1173$ K; for SOFC-NUP: $n = 2$, $S_{p,1} = 0.5$).

In order to indicate suitable operating voltages which offer the highest average power density, the value of electrical efficiency was specified and the value of V_1 was varied. Then V_2, which gives the desired value of the electrical efficiency, and its corresponding power density can be calculated. For example, as shown in Fig. 4, for an electrical efficiency of 43%, the values of V_2 are 0.623, 0.673 and 0.723 V for $V_1 = 0.7$, 0.75 and 0.80 V, respectively, and the corresponding values of the power density are 0.178, 0.156 and 0.159 W cm^{-2}, respectively. By varying V_1, the maximum power density of 0.162 W cm^{-2} is obtained at $V_1 = 0.773$ V and $V_2 = 0.700$ V.

According to the above study, the section splits were maintained at $S_{p,1} = S_{p,2} = 0.5$. Those values were then adjusted in order to achieve better performance. Fig. 5 shows the effect of section split ($S_{p,1}$) on the power density improvement at different values of electrical efficiency. It should be noted that the reported values are based on the operation using optimum voltages for each value of the section split. It was found that the power density improvement as high as 9.2% can be achieved at the electrical efficiency of 45% but the improvement becomes less significant when the SOFC is operated at lower electrical efficiency. In addition, the optimum $S_{p,1}$ for all cases was found

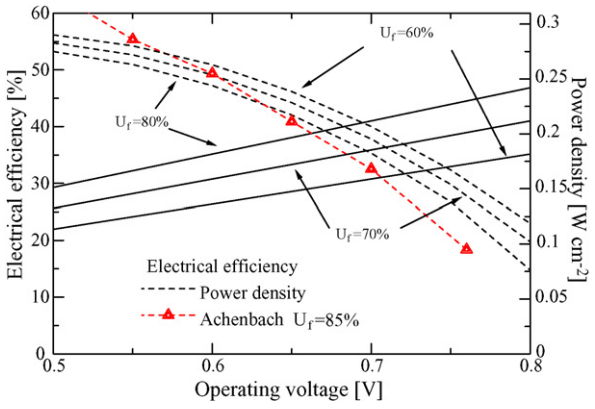

Fig. 2. Performance characteristic curves of typical SOFC-UP (H_2O/CH_4 ratio = 2.2 and $T = 1173$ K).

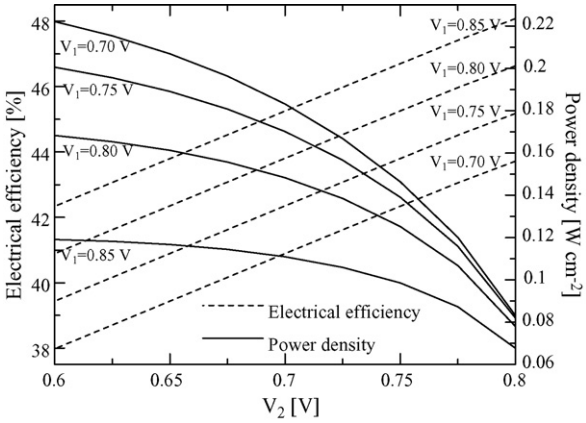

Fig. 4. Effect of operating voltages on performance of SOFC-NUP ($n = 2$, $U_f = 80\%$, $T = 1173$ K, $S_{p,1} = 0.5$ and $S_{p,2} = 0.5$).

Table 3
Comparison of power density between SOFCs with different number of section and section splits

Electrical efficiency (%)	Power density (W cm^{-2})			
	$n=1$	$n=2$ ($S_{p,1}=S_{p,2}=0.5$)	$n=2$ ($S_{p,1}=0.55$, $S_{p,2}=0.45$)	$n=3$ ($S_{p,1}=S_{p,2}=S_{p,3}=(1/3)$)
35	0.246 (0.598 V)	0.248 (0.619, 0.571 V)	0.249 (0.631, 0.560 V)	0.250 (0.644, 0.608, 0.544 V)
37	0.229 (0.632 V)	0.232 (0.669, 0.598 V)	0.232 (0.666, 0.594 V)	0.233 (0.682, 0.632, 0.583 V)
40	0.196 (0.683 V)	0.201 (0.721, 0.649 V)	0.201 (0.717, 0.645 V)	0.202 (0.740, 0.666, 0.647 V)
43	0.154 (0.734 V)	0.162 (0.7726, 0.7001 V)	0.162 (0.768, 0.697 V)	0.164 (0.782, 0.736, 0.688 V)
45	0.120 (0.768 V)	0.131 (0.8069, 0.7342 V)	0.131 (0.803, 0.731 V)	0.134 (0.817, 0.772, 0.720 V)

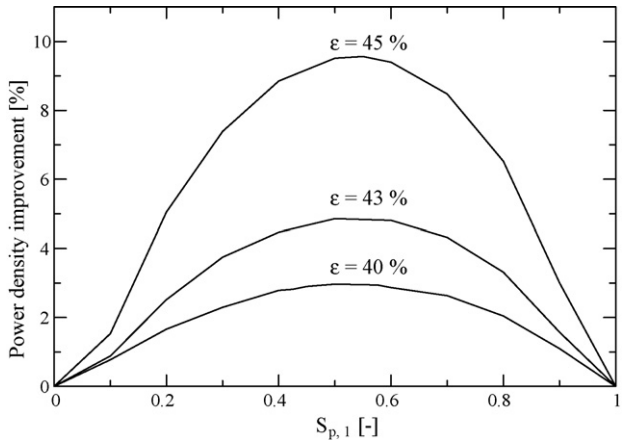

Fig. 5. Effect of section split on power density improvement of SOFC-NUP ($n=2$, $U_f=80\%$ and $T=1173$ K).

to be around 0.55. Table 3 summarizes the values of the power density and the corresponding optimum voltages at different electrical efficiency of the SOFC-UP and the SOFC-NUPs with $S_{p,1}=S_{p,2}$ and with the optimum $S_{p,1}$ and $S_{p,2}$. It was found that the results of the SOFC-NUP with the optimum $S_{p,1}$ and $S_{p,2}$ are not significantly different from those of the SOFC-NUP with $S_{p,1}=S_{p,2}$ although the voltages are different.

To further enhance the performance of the SOFC-NUP, the number of separated section (n) was increased. Fig. 6 shows the effect of the number of section on the power density improvement for three values of electrical efficiency. The section splits of all sections are specified to be at the same value of $S_{p,k}=1/n$ in order to simplify the calculations. The optimum voltages of the SOFC-NUPs which offer the highest power density for each case were determined by following the procedure described earlier for the case with $n=2$. It was assumed that the maximum power density achieved from the case with adjustable section splits does not significantly differ from that achieved from the case with equally divided sections. This assumption is valid at least for the case of the SOFC-NUP with $n=2$ as shown earlier. The calculated results indicate that the obtained maximum power density increases with increasing the number of sections (n). However, the improvement becomes less significant after $n>3$. The SOFC-NUP with $n=3$ is likely to be a suitable system for improving the power density without the reduction of electrical efficiency. Table 3 also shows the values of the maximum power density and the corresponding voltages at different values of electrical efficiency. At the electrical efficiency of 45%, the power density of the SOFC-NUP with $n=3$ is 11.7% higher than that of the typical SOFC-UP.

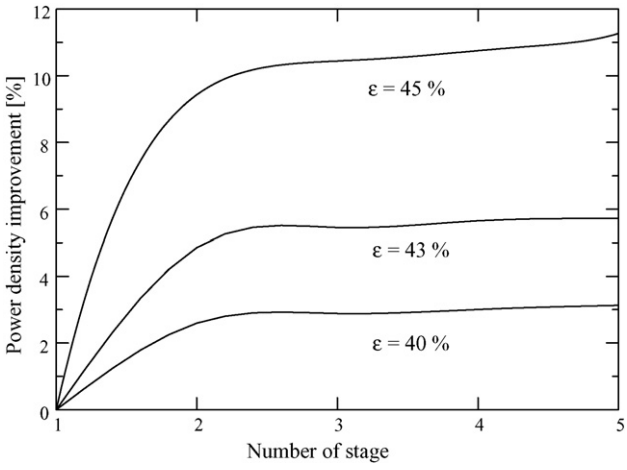

Fig. 6. Effect of number of stage on power density improvement of SOFC-NUP ($U_f=80\%$, $T=1173$ K and $S_{p,k}=1/n$).

From the above results, it has been demonstrated that the use of the non-uniform potential operation with SOFC is technically feasible. The cell area can be reduced without lowering the electrical efficiency. However, the SOFC-NUP would require more sophisticated cell arrangement, power conditioning system and so on. The system control would inevitably become more complicated. Further investigations are required before implementing this system for commercial use.

4. Conclusions

An SOFC-NUP can provide higher power density than a typical SOFC-UP without a reduction of electrical efficiency. The optimum SOFC-NUP was determined by allowing the operating voltage and section split of each section to be appropriately adjusted to achieve the highest power density for each level of electrical efficiency. The maximum power density can be further improved by increasing the number of separated section (n) of the cell; however, it became less pronounced after $n>3$. Although it is obvious that the non-uniform operation can allow the SOFC to be operated at higher performance, further investigation is necessary to determine whether the cost reduction by the reduced stack size would be sufficiently attractive compared to the increases of power conditioning cost and complication of the SOFC operation.

Acknowledgements

The supports from The Thailand Research Fund and Commission on Higher Education are gratefully acknowledged. The second author also would like to acknowledge kind supports from Professor Piyasan Praserthdam.

References

[1] P. Kuchonthara, S. Bhattacharya, A. Tsutsumi, J. Power Sources 124 (2003) 65–75.
[2] A. Heinzel, J. Roes, H. Brandt, J. Power Sources 145 (2005) 312–318.
[3] P.W. Li, S.P. Chen, M.K. Chyu, J. Power Sources 140 (2005) 311–318.
[4] Y.G. Yoon, W.Y. Lee, G.G. Park, T.H. Yang, C.S. Kim, Electrochim. Acta 50 (2004) 709–712.
[5] S.P. Yoon, J. Han, S.W. Nam, T.H. Lim, S.A. Hong, J. Power Sources 136 (2004) 30–36.
[6] S.D. Kim, S.H. Hyun, J. Moon, J.H. Kim, R.H. Song, J. Power Sources 139 (2005) 67–72.
[7] S.P. Simner, J.F. Bonnett, N.L. Canfield, K.D. Meinhardt, J.P. Shelton, V.L. Sprenkle, J.W. Stevenson, J. Power Sources 113 (2003) 1–10.
[8] A. Kazim, J. Power Sources 143 (2005) 9–16.
[9] F. Standeart, Analytical fuel cell modelling and exergy analysis of fuel cells, Ph.D. Thesis, Delft University of Technology, 1998.
[10] A. Selimovic, J. Palsson, J. Power Sources 106 (2002) 76–82.
[11] S.F. Au, N. Woudstra, K. Hemmes, J. Power Sources 122 (2003) 28–36.
[12] S.M. Senn, D. Poulikakos, Electrochem. Commun. 7 (2005) 773–780.
[13] M.A. Khaleel, Z. Lin, P. Singh, W. Surdoval, D. Collin, J. Power Sources 130 (2004) 136–148.
[14] S.H. Chan, C.F. Low, O.L. Ding, J. Power Source 103 (2002) 188–200.
[15] E. Hernandez-Pacheco, D. Singh, P.N. Hutton, N. Patel, M.D. Mann, J. Power Sources 138 (2004) 174–186.
[16] S.H. Clarke, A.L. Dicks, K. Pointon, T.A. Smith, A. Swann, Catal. Today 38 (1997) 411–423.
[17] A.L. Dicks, J. Power Sources 71 (1998) 111–122.
[18] W. Sangtongkitcharoen, S. Assabumrungrat, V. Pavarajarn, N. Laosiripojana, P. Praserthdam, J. Power Source 142 (2005) 75–80.
[19] E. Achenbach, J. Power Sources 49 (1994) 333–348.
[20] A.K. Demin, P. Tsiakaras, E. Gorbova, S. Hramova, J. Power Sources 131 (2004) 231–236.
[21] J.R. Rostrup-Nielsen, Phys. Chem. Chem. Phys. 3 (2001) 283–288.
[22] S. Campanari, J. Power Sources 92 (2001) 26–34.
[23] E. Riensche, U. Stimming, G. Unverzagt, J. Power Sources 73 (1998) 251–256.
[24] A. Criscuoli, A. Basile, E. Drioli, O. Loiacono, J. Membr. Sci. 181 (2001) 21–27.

Appendix 7

ELSEVIER

Chemical Engineering Journal 138 (2008) 436–441

Chemical Engineering Journal

www.elsevier.com/locate/cej

Performance analysis of methanol-fueled solid oxide fuel cell system incorporated with palladium membrane reactor

W. Sangtongkitcharoen [a], S.Vivanpatarakij [a], N. Laosiripojana [b], A. Arpornwichanop [c], S. Assabumrungrat [a,*]

[a] *Center of Excellence in Catalysis and Catalytic Reaction Engineering, Department of Chemical Engineering, Faculty of Engineering, Chulalongkorn University, Bangkok 10330, Thailand*

[b] *The Joint Graduate School of Energy and Environment, King Mongkut's University of Technology Thonburi, Bangkok 10140, Thailand*

[c] *Control and Systems Engineering, Department of Chemical Engineering, Faculty of Engineering, Chulalongkorn University, Bangkok 10330, Thailand*

Received 3 January 2007; received in revised form 8 June 2007; accepted 25 June 2007

Abstract

The paper presents preliminary results from the performance analysis of a methanol-fueled solid oxide fuel cell (SOFC) system incorporated with a palladium membrane reactor. A conventional SOFC system comprises major components of preheaters, a reformer, an SOFC unit and a burner. The performance of the SOFC unit was dependent on operating current density, fuel utilization and temperature. When the conventional reformer is replaced by a palladium membrane reactor, pure hydrogen is extracted from the reformed gas and fed to the anode of the SOFC unit. It was demonstrated that the incorporation of the palladium membrane reactor to the SOFC system could improve the performance of the SOFC unit. When the membrane reactor is operated at a hydrogen recovery of 90%, the maximum power density is about 12.6% higher than that from the system with the conventional reformer. The performance comparison between the two SOFC systems which provide the same net electrical efficiency indicates that the SOFC system with the membrane reactor requires a smaller SOFC stack than the conventional SOFC system; however, the former requires an extra cost on palladium membranes and extra electrical power for operating the compressor for the membrane reactor. The preliminary economic analysis reveals that the implementation of the membrane reactor to the SOFC system is not cost-effective due to high cost of palladium membranes. Finally it was indicated that the use of the palladium membrane reactor in the SOFC system is still technically attractive even when an SOFC cell with lower resistance can be further developed.

Keywords: Solid oxide fuel cell; Palladium membrane reactor; Performance analysis

1. Introduction

Fuel cell is considered as an efficient electrical power generator compared to conventional heat engines, steam and gas turbine, and combined cycles. Among the various types of fuel cell, solid oxide fuel cell (SOFC) has attracted considerable interest as it offers wide application ranges, flexibility in the choice of fuel, high system efficiency and possibility of operation with an internal reformer. Hydrogen is a main fuel for most type of fuel cells. Nevertheless, other fuels such as methane, methanol, ethanol, gasoline and oil derivatives can also be used when a reformer is included in a fuel cell system for converting the fuel to hydrogen. A thermodynamic analysis was carried out to evaluate the performances of SOFCs fuelled by different fuels; that is, methane, methanol, ethanol and gasoline. The results obtained in terms of electromotive force and efficiency indicate that ethanol and methanol are very promising alternatives to hydrogen [1]. However, methanol is a preferable choice with respect to its availability, high energy density and ready storage and distribution [2,3].

A number of research efforts have been carried out on advanced SOFC operations such as development of intermediate temperature-SOFCs [4] and integration of SOFCs with intercool gas turbine [5]. Some researchers attempted to improve the performance of SOFC systems by focusing on the different integration modes of a reformer and an SOFC unit (i.e., external reforming, indirect internal reforming and direct internal reforming) [4]. Because it has been demonstrated that hydrogen

* Corresponding author. Fax: +662 218 6877.
E-mail address: Suttichai.A@chula.ac.th (S. Assabumrungrat).

1385-8947/$ – see front matter © 2007 Elsevier B.V. All rights reserved.
doi:10.1016/j.cej.2007.06.021

Nomenclature

a	Constant in Eq. (8) (Ω m)
A	Area (m^2)
b	Constant in Eq. (8) (K)
$E_{A,pol}$	Activation energy involved in activation loss ($kJ\,mol^{-1}$)
E_D	Activation energy for diffusion through membrane ($kJ\,mol^{-1}$)
E_0	Open circuit voltage (V)
f	Volumetric flow rate of permeated hydrogen ($m^3\,s^{-1}$)
F	Faraday constant ($C\,mol^{-1}$)
i	Current density ($A\,cm^{-2}$)
n_i	Number of moles of component i (mol)
N_{H_2}	Permeation flux of hydrogen through membrane ($mol\,m^{-2}$)
P	Total pressure (kPa)
P_{com}	Power requirement of the compression unit (kW)
p_i	Partial pressure of component i (Pa)
Q_0	Pre-exponential constant for membrane permeability ($mol\,m^{-1}\,s^{-1}\,Pa^{-0.5}$)
Q_i	Heat involved in each unit (kW)
R	Universal gas constant (8.31447×10^{-3}) ($kJ\,mol^{-1}\,K^{-1}$)
T	Absolute temperature (K)
U_f	Fuel utilization (%)
V	Operating voltage (V)

Greeks letters

η	Overpotential (V)
δ	Thickness (m)
ϕ	Hydrogen recovery (%)
ψ_{com}	Efficiency of compressor (−)
ρ	Specific ohmic resistant (Ω m)
ξ	Level of SOFC cell resistance (%)

Subscripts

a	Anode
Act	Activation
c	Cathode
Conc	Concentration
Ohm	Ohmic
p	Permeate side
r	Reaction side

concentration in feed influences SOFC performance [6], the use of a palladium membrane reactor, which has been successfully implemented in a number of hydrogen-generating reactions [7], should provide potential advantages when it is incorporated with the SOFC system. It is expected that due to a high concentration of hydrogen obtained from the membrane reactor, the SOFC unit should be operated at a higher stack power density, and therefore a smaller SOFC stack as well as a cell area is required. However, the operation of the palladium membrane reactor requires additional costs on membrane and compressor. Unfortunately, there is still no effort in the literatures to analyze the potential benefits and economics of the incorporation of the palladium membrane reactor to the SOFC system.

In this study, the performances of the methanol-fuelled SOFC system incorporated with the palladium membrane reactor are compared with those of the conventional SOFC system. The benefits from the use of the membrane reactor and the preliminary economic analysis are investigated. The obtained information from this study is important for determining whether the research effort should be carried out further on this proposed system.

2. Theory

A conventional SOFC system normally consists of preheaters, a reformer, an SOFC unit, and a burner (Fig. 1(a)). As shown in the figure, a mixture of methanol and water is firstly preheated in Preheater I before being converted to hydrogen-rich gas in the reformer. Simultaneously, air is also preheated (in Preheater II) by the exhaust heat from Preheater I before feeding to the SOFC unit where electrical power is generated. Heat required in the system is obtained from the combustion of exhaust gases and the irreversible losses in the SOFC unit.

For the SOFC system with a palladium membrane reactor, the conventional reformer is replaced by the membrane reactor

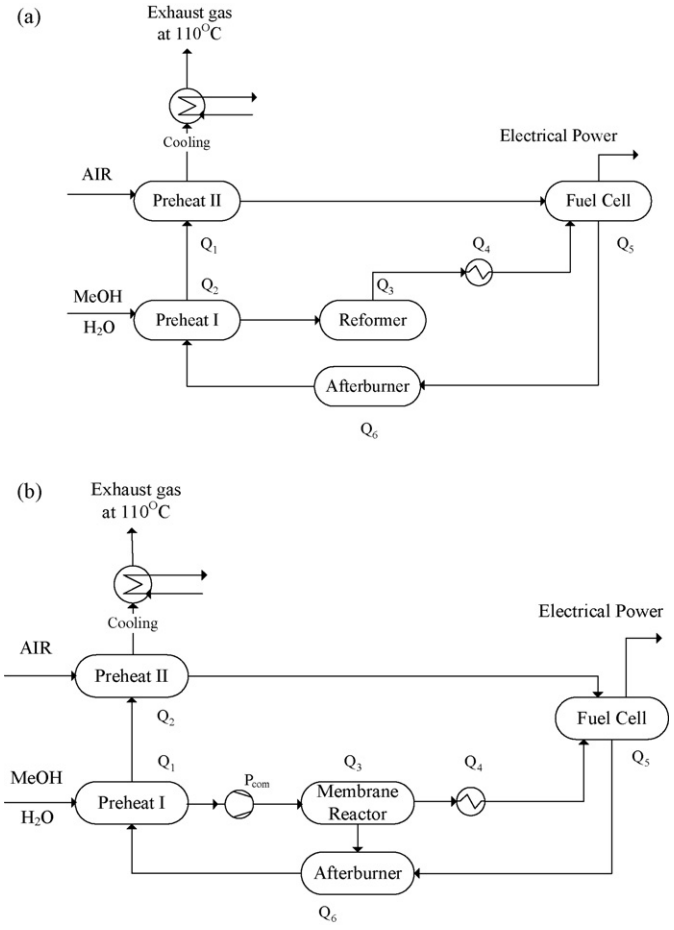

Fig. 1. Flow diagrams of SOFC systems; (a) a conventional SOFC system and (b) an SOFC system with a membrane reactor.

(Fig. 1(b)). In addition, a compressor is required for this system in order to increase the driving force for hydrogen separation. According to this operating system, pure hydrogen is extracted from the reformed gas and fed to the anode compartment of the SOFC unit, whereas the residual reformed gas is combined with the exhaust gases from the SOFC unit and combusted in the burner in order to supply heat to the system.

2.1.1. Reformer/membrane reactor

At the reformer/membrane reactor, the reactions involved in the production of hydrogen from the steam reforming of methanol can be represented by the following equations [8,9]

$$CH_3OH = 2H_2 + CO \quad (1)$$

$$CO + H_2O = H_2 + CO_2 \quad (2)$$

$$CO + 3H_2 = CH_4 + H_2O \quad (3)$$

In this work, the reactor is assumed to be operated at equilibrium condition. This assumption may be reasonable because the rates of methanol steam-reforming and the water gas shift reaction are fast, particularly at high temperature [10]. It was reported that the conversion of methanol from the methanol steam-reforming always close to 100% when the operating temperature above 623 K is performed [11]. According to the substantial works on developing selective hydrogen permeable membranes, a dense palladium-based membrane reactor has attracted many research interests. Recent research efforts have focused on the fabrication of thin membrane layers and determination of alloy compositions with better stability and resistance to poisonings. In the present work, the palladium membrane reactor with a membrane thickness of 10 μm was chosen due to its minimum in palladium material cost, defects and manufacturing difficulties of a thin membrane [12].

The hydrogen flux through a palladium membrane (N_{H_2}) is typically limited by the diffusion of hydrogen atoms through the membrane film, in which the flux can be represented by Eq. (4)

$$N_{H_2} = \frac{Q_0}{\delta} \exp\left(\frac{-E_D}{RT}\right)(p_{H_2,r}^{0.5} - p_{H_2p}^{0.5}) \quad (4)$$

The flux is inversely proportional to the membrane thickness (δ) and proportional to the difference in the square roots of the hydrogen partial pressure on the reaction side and the permeate side of the membrane. The resistance of the porous support is assumed negligible. The parameters of Eq. (4) are presented in Table 1. It should be noted that the required area of the palladium membrane can be calculated from the average hydrogen flux through the membrane as shown in the following equation:

$$\text{Area}_{\text{Mem}} = \frac{\text{molar flowrate of } H_2 \text{ recovered}}{\bar{N}_{H_2}} \quad (5)$$

As described earlier, the SOFC system with the palladium membrane reactor needs to install the compressor to operate in the palladium membrane reactor. The required power for the compressor (P_{com}) can be calculated from the following equation.

$$P_{com} = \frac{\Delta(Pf)}{\psi_{com}} \quad (6)$$

where f and P are volumetric flow rate and total pressure, respectively. It is assumed that the efficiency of compressor (ψ_{com}) is 80%.

Table 1
Parameters for hydrogen permeation through a palladium membrane [13]

Q_0 (mol m^{-1} s^{-1} Pa$^{-0.5}$)	4.40×10^{-7}
E_D (kJ mol^{-1})	15.7
Thickness (μm)	10

Table 2
Summary of parameters of ohmic resistance and thickness of each cell component [14]

Materials for anode/electrolyte/cathode	Ni–YSZ/YSZ/LSM–YSZ
Anode thickness (μm)	150
Constants for anode ohmic resistance	$a = 0.0000298$, $b = -1392$
Cathode thickness (μm)	200
Constants for cathode ohmic resistance	$a = 0.0000811$, $b = 600$
Electrolyte thickness (μm)	40
Constants for electrolyte ohmic resistance	$a = 0.0000294$, $b = 10350$
Interconnect thickness (μm)	100
Constants for interconnect ohmic resistance	$a = 0.001256$, $b = 4690$

2.2. SOFC unit

An SOFC unit consists of two porous ceramic electrodes (i.e. an anode and a cathode), a solid ceramic electrolyte, and an interconnector. The theoretical open-circuit voltage of the cell, which is the maximum voltage under specific operating conditions, can be calculated from the following equation:

$$V = E_0 - (\eta_{ohm} + \eta_{Act,a} + \eta_{Act,c} + \eta_{Conc,a} + \eta_{Conc,c}) \quad (7)$$

where E_0 is open circuit voltage determined by Nernst's equation and η_i is a polarization loss in the SOFC unit.

It is well established that several losses could occur during SOFC operation. The voltage drop is normally caused by three major irreversibilities; that is, ohmic polarization (Eq. (8)), activation polarization (Eq. (9)) and concentration polarization. The summaries of ohmic polarization and activation polarization parameters are given in Tables 2 and 3, respectively. In the present work, the concentration polarization is assumed to be negligible. This assumption is valid when the cell is not operated at too high current density or too low concentration [16].

$$\eta_{Ohm} = \frac{i\rho\delta}{A} \quad (8)$$

Table 3
Summary of activation polarization parameters [15]

	k (A m^{-2})	$E_{A,pol}$ (kJ mol^{-1})	m
Cathode	14.9×10^9	160	0.25
Anode	0.213×10^9	110	0.25

where $\rho = a\exp(b/T)$; a and b are the constant values dependent on a type of material.

$$\tilde{\eta}_{\mathrm{Act}} = i\left[\left[\frac{4F}{RT}k_{\mathrm{O_2}}(p_{\mathrm{O_2},c})^{m_{\mathrm{O_2}}}\exp\left(-\frac{E_{\mathrm{A,pol,O_2}}}{RT}\right)\right]^{-1} + \left[\frac{2F}{RT}k_{\mathrm{H_2}}(p_{\mathrm{H_2,a}})^{m_{\mathrm{H_2}}}\exp\left(-\frac{E_{\mathrm{A,pol,H_2}}}{RT}\right)\right]^{-1}\right] \quad (9)$$

The electrical power can be calculated by Eq. (10). Generally, the SOFC is suggested to operate at the relative power (ratio of power to the maximum achievable power at the specific condition) of 0.7 [17]. The fuel cell operation at lower power is attractive from the point of view that the higher efficiency is obtained. However, too low power is not practical due to high cost of SOFC cell.

$$\text{Electrical power} = \text{Current} \times \text{Operating Voltage} \quad (10)$$

The amount of heat involved in each unit (Q_i) shown in Fig. 1 can be calculated from the enthalpy change of each unit based on the assumption that no heat loss occurs in the unit.

3. Results and discussion

Various operating parameters influence the performance of SOFC stack. In operation, hydrogen in the fuel is consumed along the fuel channel by the electrochemical reaction. Fig. 2 shows the voltage (dashed lines) and average power density (solid lines) at different operating current density (i) and fuel utilization (U_f) for the conventional system fed by a feed with a H_2O:MeOH ratio of 1:1 at a temperature of 1173 K. The voltage decreases with the increase of operating current density due to the increased voltage loss from the irreversible SOFC cell resistances. Power density increases initially to a maximum value and then decreases. These characteristics are often observed in most SOFC systems. However, it should be noted that the values at high current density are likely to be overestimated because the concentration polarization is neglected. When the stack is operated at high fuel utilization, both the voltage and power density decrease. This is mainly due to the fuel depletion particularly near the exit of the anode chamber. Fig. 3 shows the

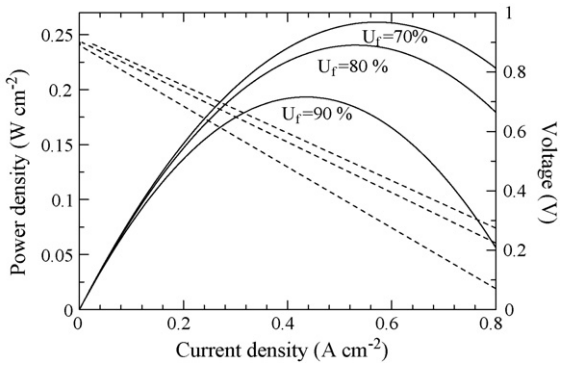

Fig. 2. Characteristic curves of SOFC stack at different fuel utilization (inlet H_2O:MeOH = 1:1 and T = 1173 K).

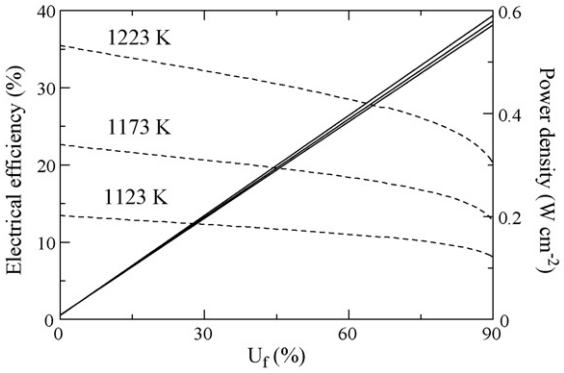

Fig. 3. Maximum power density and electrical efficiency at different operating fuel utilization and temperature (inlet H_2O:MeOH = 1:1).

effect of fuel utilization on the maximum power density (dashed lines) and its corresponding electrical efficiency (solid line) at three temperature levels. It is clearly shown that although the operation at high fuel utilization is desirable in term of achieving high electrical efficiency, the main drawback is its lower power density, implying that larger cell area is required to operate the system. Therefore, the fuel utilization should be carefully selected to achieve a high electrical efficiency at a reasonable stack power density. The fuel utilization of 80–95% has been reported in many studies [17–19]. It was also found that the temperature significantly influences the values of maximum power density. At high temperature the cell resistance becomes smaller and therefore the maximum power density increases. However, it does not affect the corresponding electrical efficiency at the maximum power density. It should be noted that high operating temperature is a favorable operating condition regarding the SOFC performance; however, it is limited by the presence of some technical constraint, such as availability of high temperature seal. The operating temperature of 1173 K is used in the further studies in this work.

When an SOFC system is incorporated with a palladium membrane reactor, pure hydrogen is extracted from the reformed gas and fed to the SOFC stack. The operating temperature of the palladium membrane was reported in a range of 673–873 K [20,21]. In this study, the operating temperature of 873 K was considered as it provided the highest hydrogen flux. Fig. 4 shows the characteristic curves of the SOFC unit fed by pure hydrogen at different hydrogen recovery (ϕ). The SOFC unit is operated at T = 1173 K and a fuel utilization of 80%. The dashed line and solid lines show the power density for the case of the conventional SOFC system and the case of the SOFC system with the membrane reactor, respectively. It is obvious that hydrogen recovery significantly influences the performance of the SOFC unit. The value must be sufficiently high to offer superior performance to the case with the conventional reformer. The maximum power density increases from 0.238 W cm^{-2} for the conventional SOFC system to 0.247 W cm^{-2} (3.8%) and 0.268 W cm^{-2} (12.6%), for the SOFC system with the palladium membrane operated at hydrogen recovery of 85% and 90%, respectively. When the SOFC unit is operated at constant fuel utilization, the hydrogen concentration along the fuel channel is governed by

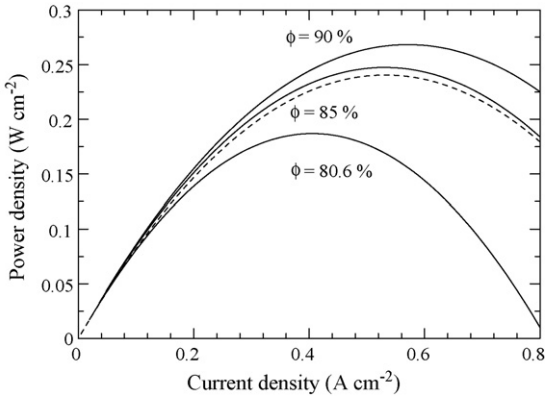

Fig. 4. Comparison of characteristic curves between the conventional SOFC system and the SOFC system with palladium membrane reactor operated at different values of percentage hydrogen recovery (ϕ; inlet H_2O:MeOH = 1:1, U_f = 80%, T = 1173 K).

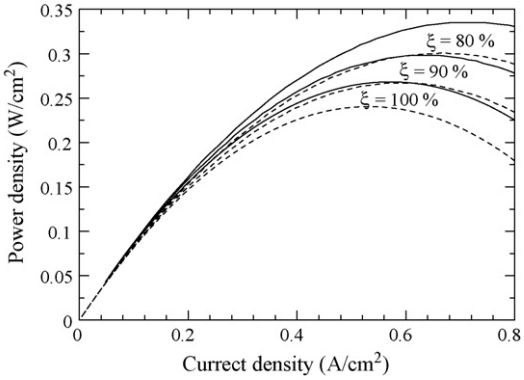

Fig. 5. Comparison of characteristic curves between the conventional SOFC system and the SOFC system with palladium membrane reactor at different cell resistance (inlet H_2O:MeOH = 1:1, U_f = 80%, ϕ = 90%, T = 1173 K).

the value of hydrogen recovery. At low hydrogen recovery, the fuel depletion near the exit of the SOFC unit is pronounced, which deteriorates the SOFC performance as observed by the reduction of power density. From this study, it is obvious that the percentage hydrogen recovery is an important factor which determines whether the inclusion of the membrane reactor in the SOFC system is beneficial to the SOFC system.

Although it was clearly demonstrated that the use of the membrane reactor shows a potential technical benefit for the SOFC system, it requires additional cost on expensive palladium membranes and a compressor to operate the membrane reactor. A preliminary analysis is necessary to determine whether the SOFC system with the membrane reactor is economically feasible. Table 4 shows the calculation results of two cases; i.e., case I the conventional SOFC system and case II the SOFC system with a palladium membrane reactor. For both cases the SOFC is operated at 1173 K and a fuel utilization of 80%. Details of the other operating conditions are also provided in the table. The net electrical efficiency for both cases is 287.2 kW which is equivalent to an electrical efficiency of 45%. For the case II, the extra electrical power (21.6 kW) is generated in the SOFC stack to provide the electrical power for operating the compressor. It was found that the SOFC cell area for case II (131.7 m^2) is lower than that of case I (143.6 m^2), resulting in the reduction of SOFC cell area of 11.9 m^2 when using the membrane reactor in the system. However, the operation in case II requires a palladium membrane area of 120.1 m^2 at 873 K. From the literatures, the prices of SOFC cell and palladium membrane are 1,500 US$/$m^2$ [22] and 746 US$/$m^2$ [23], respectively. Assuming the equivalent life time for both the SOFC cell and the palladium membrane and neglecting the cost of the compressor, it is obvious that the saving of 62.2 US$/kW from the reduction of the SOFC cell area is still much lower than the extra palladium membrane cost of 312.0 US$/kW, indicating that the incorporation of the palladium membrane reactor in the SOFC system is not economical at the present state of art. To make it economical, significant effort is required to reduce the price of the membrane. However, it should be noted that nowadays an SOFC cell is also progressively developed to improve the cell performance as well as to reduce its price. The calculations of heat requirement in the system indicate that both systems can be operated without additional requirement of an external heat source.

Table 4
Performance comparison between the conventional SOFC system and the SOFC system with the palladium membrane reactor

Items	Unit	Case I	Case II
Inlet H_2O:MeOH ratio	–	1	1
Reformer/palladium membrane reactor			
Pressure	kPa	101.3	2026
Temperature	K	973	873
Afterburner stack data	K	1173	1173
Pressure	kPa	101.3	101.3
Temperature	K	1173	1173
Fuel utilization (U_f)	%	80	80
Cell voltage	V	0.62	0.67
Current density	A cm^{-2}	0.323	0.35
Power density	W cm^{-2}	0.203	0.234
Cell area	m^2	143.6	131.7
Palladium membrane reactor			
% recovery	%	–	90.0
Membrane area	m^2	–	120.1
Power production			
Electrical power	kW	287.2	308.8
Power consumption			
Compressor	kW	–	21.6
Net electrical efficiency	%	45	45

In order to determine whether the use of palladium membrane reactor is technically advantageous for the SOFC system when a better cell is developed, the characteristic curves of the SOFC at different levels of cell resistance (ξ = 80%, 90% and 100%) are calculated (see Fig. 5). The dashed lines indicate the results for the conventional SOFC system while the solid lines represent those for the SOFC system with the palladium membrane reactor. The fuel utilization is kept at 80% for both cases and the hydrogen recovery is fixed at 90% for the case with the palladium membrane reactor. From the results, it is clear that when the cell is further developed to have lower resistance, the use of a palladium membrane reactor still shows a potential technical benefit to the SOFC system. It should be noted that the

use of other membranes (such as zeolite membrane) which offer similar or slightly lower separation efficiency may be another attractive option to be considered.

4. Conclusions

Performance of the SOFC system fuelled by methanol was analyzed to investigate the potential benefit from incorporating a palladium membrane reactor to the system. The electrical efficiency and power density of the SOFC unit were governed by the operating current density, fuel utilization and temperature. It was demonstrated that the SOFC unit can be operated at higher power density when the system is equipped with the membrane reactor. Compared with the conventional SOFC system, the system with the membrane reactor requires lower SOFC cell area, resulting in lower cost of the stack. However, the cost of the required palladium membrane was found to be much more expensive than the saving cost. Therefore the SOFC system incorporated with the palladium membrane is not economically attractive unless the membrane can be made at much lower cost. Finally it was revealed that the improvement of the stack power density by the use of the palladium membrane reactor is still technically significant even when an advanced cell with lower cell resistance can be developed.

Acknowledgements

The supports from The Thailand Research Fund, Commission on Higher Education, and the Chulalongkorn University Graduate Scholarship commemorating the 72nd Anniversary of H.M. King RAMA IX are gratefully acknowledged. The authors also would like to acknowledge the support from Professor Piyasan Praserthdam.

References

[1] S.L. Douvartzides, F.A. Coutelieris, K. Demin, P.E. Tsiakaras, AIChE 49 (2003) 248–257.
[2] B. Emonts, J.B. Hansen, S.L. Jorgensen, B. Hohlein, R. Peters, J. Power Sources 71 (1998) 288.
[3] K. Ledjeff-Hey, V. Formanski, T. Kalk, J. Roes, J. Power Sources 71 (1998) 199–207.
[4] P. Aguiar, C.S. Adjiman, N.P. Brandon, J. Power Sources 138 (2004) 120–136.
[5] Y. Yi, A.D. Rao, J. Brouwer, G.S. Samuelsen, J. Power Sources 132 (2004) 77–85.
[6] S.H. Chan, O.L. Ding, Int. J. Hydrogen Energy 30 (2005) 167–179.
[7] E. Kikuchi, Catal. Today 56 (2000) 97–101.
[8] J.C. Amphlett, M.J. Evans, R.A. Jones, R.F. Mann, R.D. Weir, Can. J. Chem. Eng. 59 (1981) 720–727.
[9] J.C. Amphlett, R.F. Mann, R.D. Weir, Can. J. Chem. Eng. 66 (1988) 950–956.
[10] C. Pakornphant, C. Sumaeth, S. Johannes, Chem. Eng. J. 97 (2004) 161–171.
[11] H. Amanduson, L.G. Ekedahl, H. Dannetun, Surf. Sci. 442 (1999) 199–205.
[12] R. Dittmeyer, V. Hollein, K. Daub, J. Mol. Catal. A: Chem. 173 (2001) 135–184.
[13] G.L. Hollock, J. Phys. Chem. 74 (1970) 503–511.
[14] S.H. Chan, C.F. Low, O.L. Ding, J. Power Sources 103 (2002) 188–200.
[15] E. Achenbach, J. Power Sources 49 (1994) 333–348.
[16] M. Pfafferodt, P. Heidebrecht, M. Stelter, K. Sundmacher, J. Power Sources 140 (2005) 53–62.
[17] A.K. Demin, P. Tsiakaras, E. Gorbova, S. Hramova, J. Power Sources 131 (2004) 231–236.
[18] J.R. Rostrup-Nielsen, Phys. Chem. Chem. Phys. 3 (2001) 283–288.
[19] S. Campanari, J. Power Sources 92 (2001) 26–34.
[20] G. Marigliano, G. Barbieri, E. Drioli, Chem. Eng. Process. 42 (2003) 231–236.
[21] F.A.N. Fernandes, A.B. Soares Jr., Fuel 85 (2006) 569–573.
[22] E. Riensche, U. Stimming, G. Unverzagt, J. Power Sources 73 (1998) 251–256.
[23] A. Criscuoli, A. Basile, E. Drioli, O. Loiacono, J. Membr. Sci. 181 (2001) 21–27.

Appendix 8

ELSEVIER

Chemical Engineering Journal xxx (2007) xxx–xxx

Chemical Engineering Journal

www.elsevier.com/locate/cej

Selection of appropriate fuel processor for biogas-fuelled SOFC system

P. Piroonlerkgul [a], S. Assabumrungrat [a,*], N. Laosiripojana [b], A.A. Adesina [c]

[a] *Center of Excellence in Catalysis and Catalytic Reaction Engineering, Department of Chemical Engineering, Faculty of Engineering, Chulalongkorn University, Bangkok 10330, Thailand*

[b] *The Joint Graduate School of Energy and Environment, King Mongkut's University of Technology Thonburi, Bangkok 10140, Thailand*

[c] *Reactor Engineering & Technology Group, School of Chemical Sciences & Engineering, University of New South Wales, Sydney, NSW 2052, Australia*

Received 9 August 2007; received in revised form 4 October 2007; accepted 5 October 2007

Abstract

The performance of biogas-fed solid oxide fuel cell (SOFC) systems utilizing different reforming agents (steam, air and combined air/steam) has been investigated via thermodynamic analysis to determine the most suitable feed. The boundary of carbon formation was first calculated to specify the minimum amount of each reforming agent necessary to avoid carbon formation. The SOFC performance (electrical efficiency and power density) was determined at different biogas compositions and reforming agent:biogas ratios. The SOFC performance is better when the methane content in the biogas is higher. Steam is considered to be the most suitable reforming agent in this study as the steam-fed SOFC offers much higher power density than the air-fed SOFC although its electrical efficiency is slightly lower. When steam is added in the air-fed SOFC as in the case of the co-fed SOFC, the power density can be improved but the electrical efficiency becomes lower compared with the case of the air-fed SOFC. Finally, in order to improve the electrical efficiency of the steam-fed SOFC, the biogas split option was proposed. It was found that a higher electrical efficiency can be achieved. In addition, although the power density is lowered by this operation, the value is still higher than the case of the air-fed SOFC.

Keywords: Biogas; Dry reforming; Partial oxidation; Solid oxide fuel cell; Steam reforming; Thermodynamic analysis

1. Introduction

The demand for fossil fuel in electrical power generation has significantly increased in the past decade due to the rapid changes in global economic activities. This upsurge in fossil fuel consumption poses serious fuel supply insecurity and increases the amount of greenhouse gases accumulating in the environment. To alleviate these problems, several environmental-friendly fuels have been proposed alternatives to conventional fossil fuels. Biogas is an attractive fuel as it is derived renewably from biomass and it contains only trace amount of non-methane hydrocarbons. A common problem for biogas utilization is that most biogas is derived from small-scale sources, e.g. farm and municipal wastes. Hence, the use of biogas is applicable to a small-size power generation (5–100 kW) [1]. Moreover, the biogas composition fluctuates markedly, depending on its source [2]. Generally, biogas contains methane (40–65%), carbon dioxide (30–40%) and trace of nitrogen.

A solid oxide fuel cell (SOFC) is an appropriate technology for generating electricity from biogas due to its high efficiency (30–40%) for small-size power generations (<20 kW) [1]. Recently, a 100 kW class SOFC system fed by biogas has been proposed, and the electrical efficiency of almost 48.7% [3] was reported compared to 41.5% of a conventional system [4]. Additionally, its performance is still remarkable even at low methane contents in biogas. In laboratory test, the performance of SOFC drops only 5% when the biogas composition (CH_4:CO_2) is reduced from 70:30 to 30:70 [5].

An SOFC system can be divided into three main parts: (1) a fuel processor to reform the raw fuel into hydrogen gas, (2) SOFC stacks which subsequently generate electricity and useful heat from the reformed gas and (3) an afterburner where the residual fuel is combusted in order to supply heat to the preheaters and the fuel processor. Within the fuel processor, four main chemical reactions, namely steam reforming, dry

* Corresponding author. Tel.: +66 2 218 6868; fax: +66 2 218 6877.
E-mail address: Suttichai.A@chula.ac.th (S. Assabumrungrat).

1385-8947/$ – see front matter © 2007 Elsevier B.V. All rights reserved.
doi:10.1016/j.cej.2007.10.007

Please cite this article in press as: P. Piroonlerkgul, et al., Selection of appropriate fuel processor for biogas-fuelled SOFC system, Chem. Eng. J. (2007), doi:10.1016/j.cej.2007.10.007

Nomenclature

$D_{A–B}$	ordinary diffusivity of gas A versus gas B [$cm^2\ s^{-1}$]
$D_{A–B(eff)}$	ordinary diffusivity of gas A versus gas B [$cm^2\ s^{-1}$]
$D_{A,k}$	Knudsen diffusivity of gas A [$cm^2\ s^{-1}$]
$D_{A,k(eff)}$	effective Knudsen diffusivity of gas A [$cm^2\ s^{-1}$]
$D_{i(eff)}$	effective diffusion coefficient of species i (i = anode, cathode) [$cm^2\ s^{-1}$]
D_p	catalyst pore diameter [μm]
E	open circuit voltage [V]
$E_{act,a}$	activation energy at anode [$J\ mol^{-1}$]
$E_{act,c}$	activation energy at cathode [$J\ mol^{-1}$]
F	Faraday constant (9.6495×10^4) [$C\ mol^{-1}$]
ΔG_i	Gibb's free energy of reaction i [$J\ mol^{-1}$]
i	current density [$A\ cm^{-2}$]
$i_{0,i}$	exchange current density (i = anode, cathode) [$A\ cm^{-2}$]
$K_{eq,dry}$	equilibrium constant of dry reforming reaction [Pa^2]
$K_{eq,pox}$	equilibrium constant of partial oxidation reaction [$Pa^{3/2}$]
$K_{eq,RWGS}$	equilibrium constant of reverse water gas shift reaction (RWGS)
$K_{eq,steam}$	equilibrium constant of steam reforming reaction [Pa^2]
l_a	thickness of anode [μm]
l_c	thickness of cathode [μm]
L	thickness of electrolyte [μm]
M_A	molecular weight of gas A [g]
n	electrode porosity
p_i^I	inlet pressure of species i [Pa]
P	operating pressure [Pa]
P_i	partial pressure of species i [Pa]
r	average radius of the catalyst pore [μm]
R	gas constant (8.3145) [$J\ mol^{-1}\ K^{-1}$]
T	operating temperature [K]
V	cell voltage [V]

Greek letter

α_c	carbon activity
ε_{AB}	Lennard-Jones energy interaction parameter scaled with respect to the Boltzman constant
γ_a	pre-exponential factor for anode exchange current density [$A\ m^{-2}$]
γ_c	pre-exponential factor for cathode exchange current density [$A\ m^{-2}$]
$\eta_{act,a}$	activation overpotential at anode [V]
$\eta_{act,c}$	activation overpotential at cathode [V]
$\eta_{Conc,a}$	concentration overpotential at anode [V]
$\eta_{Conc,c}$	concentration overpotential at cathode [V]
η_{ohmic}	ohmic overpotential [V]
σ_{AB}	collision diameter [Å]
Ω_D	collision integral
ξ	electrode tortuosity

reforming, partial oxidation and autothermal reforming are possible [6]. Dry reforming is perhaps the most interesting option for the conversion of biogas since the major constituents of the biogas are carbon dioxide and methane. However, it gives less hydrogen yields compared with steam reforming reaction. For steam and dry reforming, an external heat source is required to supply the endothermic fuel processor and to preheat the reforming agent (steam and CO_2) and this reduces the overall efficiency of the fuel processor. This problem can be overcome by applying an exothermic partial oxidation reaction which utilizes air as the reforming agent. However, it is accompanied by a lower hydrogen yield. Moreover, the hydrogen partial pressure of the gas product obtained from the partial oxidation is low due to the dilution effect of nitrogen present in air. In order to circumvent this drawback, the partial oxidation can operate simultaneously with steam reforming to improve hydrogen yield in a route referred to as autothermal reforming. If methane is the fuel, autothermal reforming leads to a higher efficiency (93.9%) – defined as the lower heating value (LHV) of hydrogen generated divided by the LHV of the methane fuel – than that of the steam reforming (91.3%) even though the latter gives a higher hydrogen yield. This is because higher heating power is required to generate steam in the case of the steam reforming. In addition, steam reforming is more prone to carbon formation compared to the partial oxidation and autothermal reforming [7].

When biogas is considered as a feedstock for the reformer, dry reforming may become a co-reaction due to the large amount of CO_2 present in biogas. However, the quantity of carbon dioxide available is not sufficient to convert all methane in biogas into hydrogen. Air and steam are the common reforming agents to combine with CO_2 in the fuel processor. The combination of the dry reforming with partial oxidation helps reduce the reformer size and softens the operating conditions. Furthermore, the desired H_2/CO ratio can be achieved by tuning the composition of the reforming agent [8–10]. Combined steam and dry reforming gives a higher H_2:CO ratio compared to sole dry reforming, however, large amount of heat must be supplied to the fuel processor [11,12].

Although the advantages and disadvantages of the use of each reforming agent in the fuel processor have been widely reported [11,12], the determination of a suitable reforming agent when the fuel processor is integrated with an SOFC system is still a matter for further investigation. The performance analysis of integrated biogas-fed SOFC systems should provide better insights into proper selection guidelines and hence, the rationale for this study. Thermodynamic analysis was performed to compare the relevant performance indices (overall electrical efficiency and the power density) of the SOFC systems with different reforming agents.

2. Modeling

2.1. Fuel processors

The main reaction in the fuel processor fed by biogas is the dry reforming reaction (Eq. (1)) due to the high content of carbon dioxide in biogas. When this is supplemented with steam, Eq.

Please cite this article in press as: P. Piroonlerkgul, et al., Selection of appropriate fuel processor for biogas-fuelled SOFC system, Chem. Eng. J. (2007), doi:10.1016/j.cej.2007.10.007

(2) also takes place in the fuel processor. In a third option, air is fed along with biogas to the system so that the exothermic partial oxidation (Eq. (3)) occurs and provides the energy for the endothermic dry reforming.

$$CH_4 + CO_2 \rightarrow 2H_2 + 2CO \quad \text{(Dry reforming)} \tag{1}$$

$$CH_4 + H_2O \rightarrow 3H_2 + CO \quad \text{(Steam reforming)} \tag{2}$$

$$CH_4 + \tfrac{1}{2}O_2 \rightarrow 2H_2 + CO \quad \text{(Partial oxidation)} \tag{3}$$

It should be noted that the mildly endothermic reverse water gas shift reaction (RWGS) (Eq. (4)) always takes place in the fuel processor due to the present of CO_2 in biogas feed. This reaction inhibits the generation of hydrogen.

$$CO_2 + H_2 \rightarrow H_2O + CO \quad \text{(RWGS)} \tag{4}$$

The thermodynamics of dry and steam reforming are similar (since both are highly endothermic) while the methane partial oxidation is exothermic. However, carbon formation during dry reforming is more severe compared with that of steam reforming due to its lower H/C ratio [13]. In order to simplify the calculations, in this study the reformer is assumed to operate at isothermal condition and the exit gas reaches its equilibrium composition. The relationships of the thermodynamic equilibrium for the dry reforming, steam reforming, partial oxidation and RWGS are shown in Eqs. (5)–(8), respectively.

$$K_{eq,dry} = \frac{P_{H_2}^2 P_{CO}^2}{P_{CH_4} P_{CO_2}} \tag{5}$$

$$K_{eq,steam} = \frac{P_{H_2}^3 P_{CO}}{P_{CH_4} P_{H_2O}} \tag{6}$$

$$K_{eq,pox} = \frac{P_{H_2}^2 P_{CO}}{P_{CH_4} P_{O_2}^{1/2}} \tag{7}$$

$$K_{eq,RWGS} \rightleftarrows = \rightleftarrows \frac{P_{H_2O} P_{CO}}{P_{H_2} P_{CO_2}} \tag{8}$$

where $K_{eq,i}$, the equilibrium constant of reaction i, can be calculated from this expression:

$$K_{eq,i} = e^{-\Delta G_i/RT} \tag{9}$$

The possibility of carbon formation may be examined from the estimation of the carbon activity (α_c). The carbon formation is thermodynamically possible when $\alpha_c \geq 1$. The details of carbon activity calculations are described in our recent work [14]. In this study, the following carbon formation reactions are assumed to occur in the reformer.

$$2CO = CO_2 + C \tag{10}$$

$$CH_4 = 2H_2 + C \tag{11}$$

$$CO + H_2 = H_2O + C \tag{12}$$

where the carbon activities (α_c) for these carbon formation reactions can be calculated by Eqs. (13)–(15):

$$\alpha_{c,CO} = \frac{K_1 P_{CO}^2}{P_{CO_2}} \tag{13}$$

$$\alpha_{c,CH_4} = \frac{K_2 P_{CH_4}}{P_{H_2}^2} \tag{14}$$

$$\alpha_{c,CO\text{–}H_2} = \frac{K_3 P_{CO} P_{H_2}}{P_{H_2O}} \tag{15}$$

2.2. SOFC stack model

Electrochemical reaction takes place via the reaction between fuel and oxidizing agent. At the cathode section, oxygen in air is reduced to oxygen ions (Eq. (16)) which permeate via the solid electrolyte to react with the hydrogen fuel at the anode section (Eq. (17)). Only hydrogen is assumed to react electrochemically with oxygen ions. It was observed that the H_2 electro-oxidation is much faster than the CO electro-oxidation [15] and in addition the rate of WGS reaction is fast at high temperatures [16–18]. It is also assumed that little amount of methane remaining from the fuel processor is consumed via the steam reforming and that the anode compositions always reach their equilibrium along the cell length due to the fast kinetics at high temperature. For the SOFC stack, Ni-YSZ, YSZ and LSM-YSZ are used as the materials in the anode, electrolyte and cathode, respectively.

$$\tfrac{1}{2}O_2 + 2e^- \rightarrow O^{2-} \tag{16}$$

$$H_2 + 2O^{2-} \rightarrow H_2O + 2e^- \tag{17}$$

The open circuit voltage (E) of the cell can be calculated from the Nernst equation which is expressed as:

$$E = E^0 + \frac{RT}{2F} \ln\left(\frac{P_{H_2} P_{O_2}^{1/2}}{P_{H_2O}}\right) \tag{18}$$

The actual cell potential (V) is always less than the open circuit voltage (E) owing to the existence of overpotentials as shown in Eq. (19). The overpotentials can be categorized into three main sources: ohmic overpotential (η_{ohmic}), activation overpotential (η_{act}) and concentration overpotential (η_{Conc}).

$$V = E - \eta_{act} - \eta_{ohmic} - \eta_{Conc} \tag{19}$$

2.2.1. Ohmic overpotential (η_{ohmic})

This overpotential is the resistance to flow of electron through the electrodes and the interconnections as well as resistance to the flow of ions through electrolyte. This voltage drop is the vital one in all types of cells and is linearly proportional to current density (i). Due to the higher electronic conductivity of the electrodes compared to the electrolyte, only ohmic overpotential in the electrolyte is concerned. Hence, the ohmic overpotential of SOFC can be expressed by [19]:

$$\eta_{ohmic} = 2.99 \times 10^{-11} iL \exp\left(\frac{10300}{T}\right) \tag{20}$$

Please cite this article in press as: P. Piroonlerkgul, et al., Selection of appropriate fuel processor for biogas-fuelled SOFC system, Chem. Eng. J. (2007), doi:10.1016/j.cej.2007.10.007

2.2.2. Activation overpotential (η_{act})

Activation overpotential is controlled by the kinetics at the electrode surface. It is directly related to the activation barrier to be overcome by the reacting species in order to conduct the electrochemical reaction. The electrode reaction rate at high temperatures is fast, leading to low activation polarization as normally observed in SOFC.

These activation overpotentials in electrodes can be expressed by the Butler-Volmer equation,

$$i = i_0 \left[\exp\left(\frac{\alpha z F \eta_{act}}{RT}\right) - \exp\left(-\frac{(1-\alpha) z F \eta_{act}}{RT}\right)\right] \quad (21)$$

In case of SOFC, α and z are set to 0.5 and 2 [20]. Therefore, the activation potential at the anode and cathode can be explicitly written as:

$$\eta_{act,j} = \frac{RT}{F} \sinh^{-1}\left(\frac{i}{2i_0}\right), \quad j = a, c \quad (22)$$

The exchange current density (i_0) for the cathode side depends on partial pressure of both hydrogen and water as well as the operating temperature [21,22]. For the anode side, i_0 depends on oxygen partial pressure and operating temperature as expressed in Eqs. (23)–(24) [23].

$$i_{0,a} = \gamma_a \left(\frac{P_{H_2}}{P_{ref}}\right)\left(\frac{P_{H_2O}}{P_{ref}}\right) \exp\left(-\frac{E_{act,a}}{RT}\right) \quad (23)$$

$$i_{0,c} = \gamma_c \left(\frac{P_{O_2}}{P_{ref}}\right)^{0.25} \exp\left(-\frac{E_{act,c}}{RT}\right) \quad (24)$$

2.2.3. Concentration overpotential (η_{Conc})

The concentration overpotential is the electrical loss owing to the difference between the reactant concentration on the reaction site and that in the bulk of the gas stream. This is due to the effect of the diffusion of the reactant gas into the pore of the electrochemical catalyst. It can be calculated by Eqs. (25) and (26):

$$\eta_{Conc,a} = \frac{RT}{2F} \ln\left[\frac{(1 + (RT/2F)(l_a/D_{a(eff)} p^I_{H_2O})i)}{(1 - (RT/2F)(l_a/D_{a(eff)} p^I_{H_2})i)}\right] \quad (25)$$

$$\eta_{Conc,c} = \frac{RT}{4F} \ln\left[\frac{p^I_{O_2}}{(p_c - \delta_{O_2}) - ((p_c - \delta_{O_2}) - p^I_{O_2}) \exp\left[(RT/4F)(\delta_{O_2} l_c / D_{c(eff)} p_c) i\right]}\right] \quad (26)$$

where δ_{O_2}, $D_{a(eff)}$ and $D_{c(eff)}$ can be expressed by:

$$\delta_{O_2} = \frac{D_{O_2,k(eff)}}{D_{O_2,k(eff)} + D_{O_2-N_2(eff)}} \quad (27)$$

$$\frac{1}{D_{c(eff)}} = \frac{\xi}{n}\left(\frac{1}{D_{O_2,k}} + \frac{1}{D_{O_2-N_2}}\right) \quad (28)$$

$$D_{a(eff)} = \left(\frac{p_{H_2O}}{p_a}\right) D_{H_2(eff)} + \left(\frac{p_{H_2}}{p_a}\right) D_{H_2O(eff)} \quad (29)$$

$$\frac{1}{D_{H_2(eff)}} = \frac{\xi}{n}\left(\frac{1}{D_{H_2,k}} + \frac{1}{D_{H_2-H_2O}}\right) \quad (30)$$

$$\frac{1}{D_{H_2O(eff)}} = \frac{\xi}{n}\left(\frac{1}{D_{H_2O,k}} + \frac{1}{D_{H_2-H_2O}}\right) \quad (31)$$

The correlation between the effective parameter and the normal parameter can be expressed by Eq. (32)

$$D_{(eff)} = \frac{n}{\xi} D \quad (32)$$

Knudsen diffusivity can be computed by the correlation below:

$$D_{A,k} = 9700 r \sqrt{\frac{T}{M_A}} \quad (33)$$

Ordinary diffusivity can be calculated by Chapman-Enskog equation (Eq. (34)) [24]:

$$D_{A-B} = 1.8583 \times 10^{-3}\left(\frac{T^{3/2}((1/M_A)+(1/M_B))^{1/2}}{P\sigma^2_{AB}\Omega_D}\right) \quad (34)$$

where σ_{AB} is the collision diameter (Å) which is equal to $(\sigma_A + \sigma_B)/2$. Ω_D is computed from [25]:

$$\Omega_D = \frac{A}{T_k^B} + \frac{C}{\exp(DT_k)} + \frac{E}{\exp(FT_k)} + \frac{G}{\exp(HT_k)} \quad (35)$$

where T_k is equal to T/ε_{AB} and A, C, E and G are constants for each gas.

2.3. Afterburner and heat exchanger

At the exit of the SOFC stack, the anode exit gas and the cathode exit gas are mixed for post combustion. Complete combustion is assumed to take place in the afterburner; hence methane, carbon monoxide and hydrogen contents in the exhaust gas become zero. The heat exchanger is assumed to operate without heat loss.

2.4. Calculation procedure for determining SOFC stack performance

For the SOFC operation, a constant operating voltage along the cell length is assumed as the current collector usually has high electrical conductivity. The operating voltage is kept at 0.7 V in this study. The current density inside the stack varies with the distance from the stack entrance due to the changes in gas compositions in the cathode and anode sections and therefore the open circuit voltage. Hence, the average current density and power density of the SOFC stack can be calculated. In this work, the calculation takes place for each small fuel utilization region employing the mathematical model presented in Section 2.2. The thermodynamic equilibrium is assumed for the anode gas in each region because the anode material is also active for the reactions and the operating temperature of the SOFC stack is high. In each region, the open circuit voltage, overpotentials,

Please cite this article in press as: P. Piroonlerkgul, et al., Selection of appropriate fuel processor for biogas-fuelled SOFC system, Chem. Eng. J. (2007), doi:10.1016/j.cej.2007.10.007

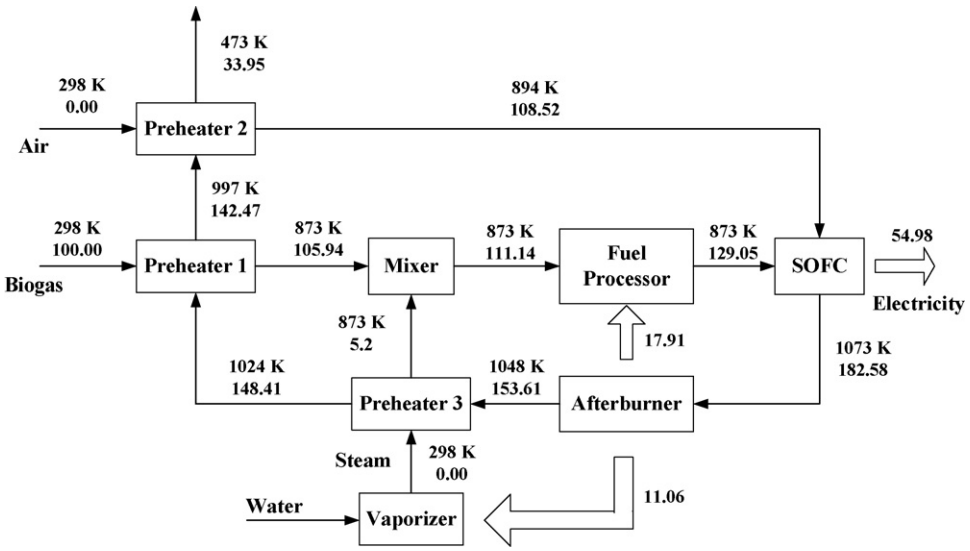

Fig. 1. The plant configuration and energy balance for the steam-fed SOFC system.

equilibrium composition of anode fuel, stack area and current density are computed. The stack areas calculated in each region are added up to yield the total stack area. Finally, the current calculated from the fuel utilized in the stack is divided by the total stack area to obtain the average current density and hence, the average power density is determined. The electrical efficiency may be computed from Eq. (36).

$$\text{SOFC plant efficiency} = \frac{\text{total electricity generated}}{\text{LHV of biogas feed}} \quad (36)$$

2.5. SOFC system configurations

Three biogas-fuelled SOFC systems are considered in this study, i.e. SOFC using steam as the reforming agent (steam-fed SOFC), SOFC using air as the reforming agent (air-fed SOFC) and SOFC using both air and steam as the reforming agents (co-fed SOFC). The plant configuration for the steam-fed SOFC is illustrated in Fig. 1. Several unit operations are included in this configuration consisting of a fuel processor, SOFC stack, an afterburner, a mixer, a vaporizer and preheaters. Steam is generated via the vaporizer, preheated and then mixed with biogas. The mixture gas is then fed into the fuel processor. In the fuel processor, the steam reforming, dry reforming and WGS take place to produce H_2-rich gas and the total heat consumed in these reactions is supplied from heat generated in the afterburner. The H_2-rich gas produced in the fuel processor is fed into the SOFC stack where the electrical energy is generated. The heat generated in the SOFC stack due to the irreversibility is utilized for air and H_2-rich gas preheating. The residue fuel gas released from the SOFC stack is burned up in the afterburner in order to supply heat to the vaporizer and the fuel processor. A high temperature flue gas which mainly contains carbon dioxide and steam released from the afterburner is used in preheating

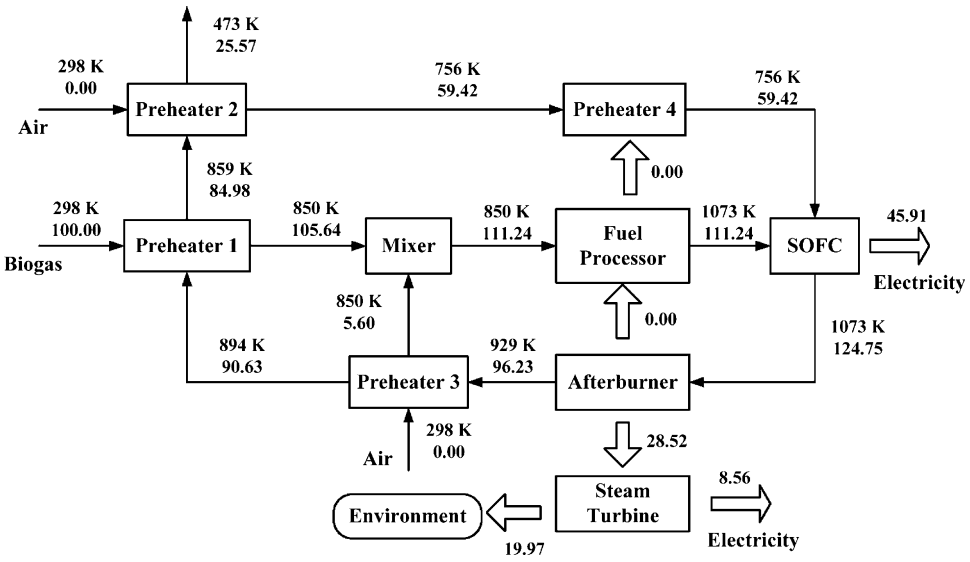

Fig. 2. The plant configuration and energy balance for the air-fed SOFC system.

Please cite this article in press as: P. Piroonlerkgul, et al., Selection of appropriate fuel processor for biogas-fuelled SOFC system, Chem. Eng. J. (2007), doi:10.1016/j.cej.2007.10.007

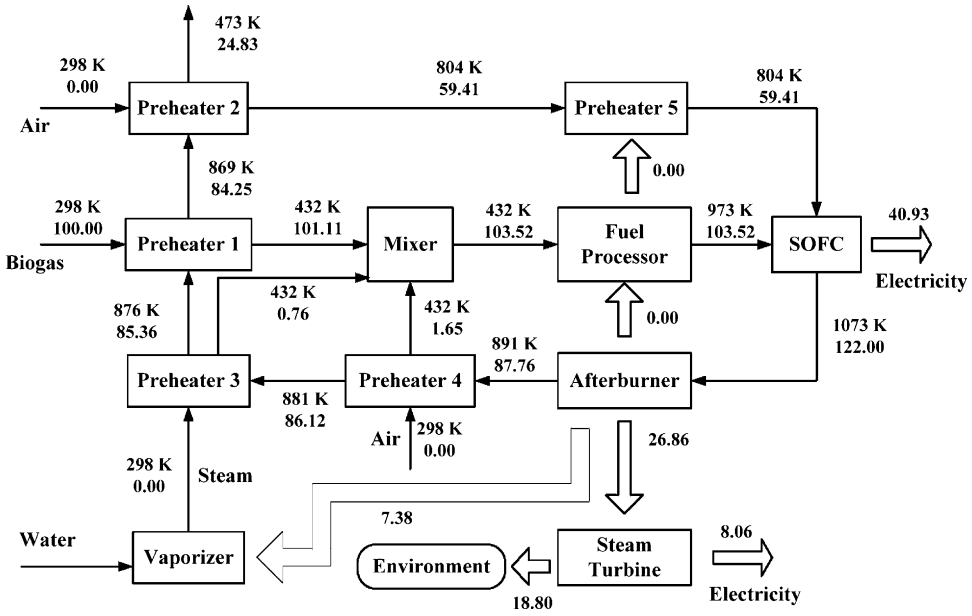

Fig. 3. The plant configuration and energy balance for the co-fed SOFC system.

biogas, steam and oxidizing agent (air) before being discharged to the environment at low temperature. For the calculation, the flue gas temperature released from the system is kept at 473 K. The total heating power used in preheating is computed and the afterburner outlet gas temperature and the quantity of the fuel combusted in the afterburner to achieve the required outlet gas temperature are then calculated. To achieve a desired temperature of the SOFC stack, an oxidizing agent (air) temperature is tuned up employing the energy balance in the SOFC stack. A trial-and-error is performed by tuning the fuel utilization until the total energy flowing into the afterburner is equal to the total energy flowing out of the afterburner. For the air-fed SOFC, its calculation procedure is similar to that of the steam-fed SOFC. However, the heating power used in preheating and the quantity of the fuel used in the afterburner of the former is extremely less than the latter. Therefore, almost all hydrogen in the anode gas can be utilized in the SOFC stack for the air-fed SOFC and the power density also reduces following to the increase in the fuel utilization. To achieve a reasonable power density, the hydrogen mole fraction of the SOFC anode output stream is controlled to be higher than 1.5 mol%. In this case, the heat residue from the afterburner is fed into the steam turbine to generate more electricity as illustrated in Fig. 2. The electrical efficiency of steam turbine is assumed to be 30%. The heat generated from the exothermic partial oxidation in the fuel processor is utilized in preheating the oxidizing agent.

According to the plant configuration of the co-fed SOFC, most of the configurations are identical to that of the air-fed SOFC as illustrated in Fig. 3; nevertheless, more heat is generated in the afterburner in order to generate steam. It should be noted that, in all cases, the quantities of air fed as the oxidant into the SOFC cathode are 5 times of theoretical air required to combust the biogas fuel. The excessive amount of air is required in order to avoid the overheating of the stack which would cause cell damages.

3. Results and discussion

The models of the SOFC systems are programmed in Visual Basic. The values of all parameters used in the calculations are summarized in Table 1. For model validation, the computed results are compared with the experimental results of Zhao and Virkar [26] and Tao et al. [27]. The feed compositions and the SOFC stack dimensions used in model validation are summarized in Table 2. As shown in Fig. 4, the simulation shows good agreement with the experimental data using pure hydrogen fuel [26] for all temperature levels particularly at the operating temperature of 1073 K which is used in the subsequent studies of this work. Moreover, with inlet gas containing various fuel types (CH_4–CO–H_2), the simulation could also predict the experimental data [27] well as illustrated in Fig. 5.

Table 1
Summary of model parameters [28]

Parameters	Value
γ_a	1.344×10^{10} A m^{-2}
γ_c	2.051×10^{9} A m^{-2}
$E_{act,a}$	1.0×10^{5} J mol^{-1}
$E_{act,c}$	1.2×10^{5} J mol^{-1}
n	0.48
ξ	5.4
D_p	1 μm
d_a	750 μm
d_c	50 μm
L	50 μm
V	0.7 V
T_{SOFC}	1073 K
Operating pressure (SOFC)	1 bar
Operating pressure (H_2 processor)	1 bar
$T_{Fuel\ processor\ (steam\ as\ reforming\ agent)}$	873 K
$T_{Fuel\ processor\ (air\ as\ reforming\ agent)}$	1073 K

Please cite this article in press as: P. Piroonlerkgul, et al., Selection of appropriate fuel processor for biogas-fuelled SOFC system, Chem. Eng. J. (2007), doi:10.1016/j.cej.2007.10.007

Table 2
Feed compositions and SOFC stack dimensions used in model validation

Parameters	Zhao and Virkar [26]	Tao et al. [27]
Fuel compositions (mole fraction)		
CH_4	–	0.21
H_2	0.97	0.4
CO	–	0.2
CO_2	–	0.18
N_2	–	0.01
H_2O	0.03	–
Stack dimensions		
Type of cell	Button cell	Planar SOFC with 100 cm^2 active surface area
n	0.48	0.48
ξ	5.4	5.4
D_p	1 μm	1 μm
d_a	1000 μm	500 μm
d_c	20 μm	50 μm
L	8 μm	10 μm
Stack average temperature	873–1073 K	1073 K

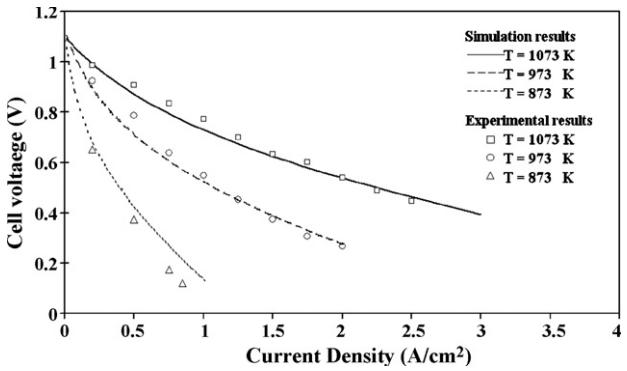

Fig. 4. Verification of the SOFC model.

The boundaries of carbon formation indicating the minimum amount of a reforming agent required to avoid the carbon formation for the biogas steam reforming and partial oxidation are illustrated in Fig. 6a and b, respectively. It is obvious that less reforming agent (steam or air) is required in order to inhibit the carbon formation when the reforming temperature increases. In fact, the moles of reforming agent per biogas required decreased almost hyperbolically with temperature attaining nearly constant value beyond about 1173 K. Biogas with a higher content of methane is more prone to carbon formation than that with a lower amount of methane. These trends are corresponding well with previous literatures [13,14,29]. Note that in the following studies the SOFC systems are always operated using a sufficient amount of the reforming agent to avoid the carbon formation.

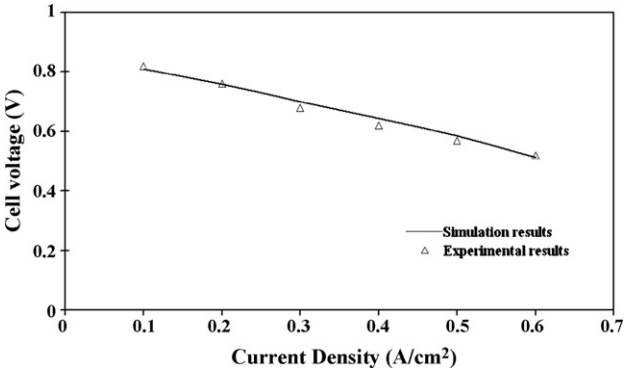

Fig. 5. Verification of SOFC model for the feed with CH_4, CO and H_2 mixtures.

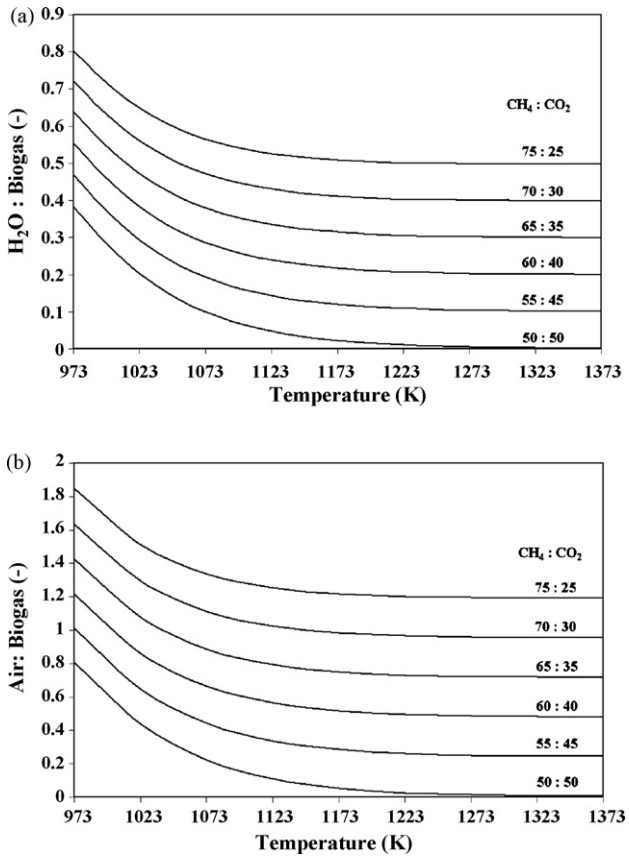

Fig. 6. Boundary of carbon formation for the biogas-fed fuel processors with different reforming agents: (a) steam and (b) air.

The electrical efficiency and power density of the steam-fed SOFC were first investigated. Energy value (lower number on each stream) and temperature (upper number) for different sections of the plant are shown in Fig. 1. The values of H_2O:biogas, CH_4:CO_2 in biogas and fuel processing temperature are 1.2, 60:40 and 873 K, respectively. It may be noted that the energy is given as a percentage of lower heating value of the biogas fuel. As seen in Fig. 1, large amounts of heat generated in afterburner, about 11.06 and 17.91% of biogas LHV, respectively, are supplied to the vaporizer and the fuel processor. An overall electrical efficiency of about 55% of biogas LHV was obtained for this SOFC system. Fig. 7 shows the plant electrical efficiency and power density of the steam-fed SOFC at various steam contents and CH_4:CO_2 ratios. As shown in Fig. 7, biogas with a higher CH_4:CO_2 ratio gives higher efficiency than that with a lower one. As the methane content in the biogas increases, the reformed gas contains hydrogen at a higher concentration and, therefore, a higher power density is achieved. The smaller content of CO_2 in the biogas reduces the energy loss by the exhaust gas of the system. Consequently, the electrical efficiency is improved. Inter-

Please cite this article in press as: P. Piroonlerkgul, et al., Selection of appropriate fuel processor for biogas-fuelled SOFC system, Chem. Eng. J. (2007), doi:10.1016/j.cej.2007.10.007

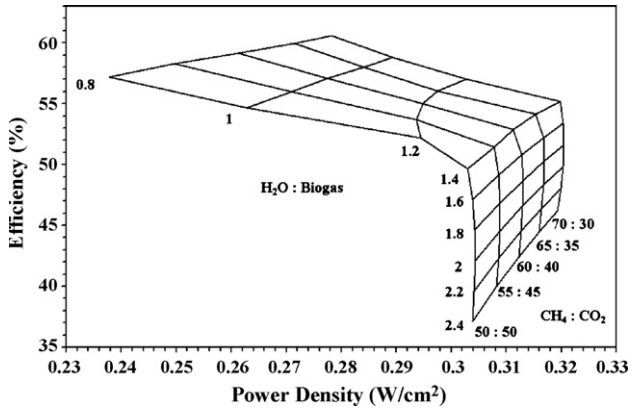

Fig. 7. Performance of the steam-fed SOFC at different H_2O:biogas and CH_4:CO_2 ratios (fuel processing temperature = 873 K).

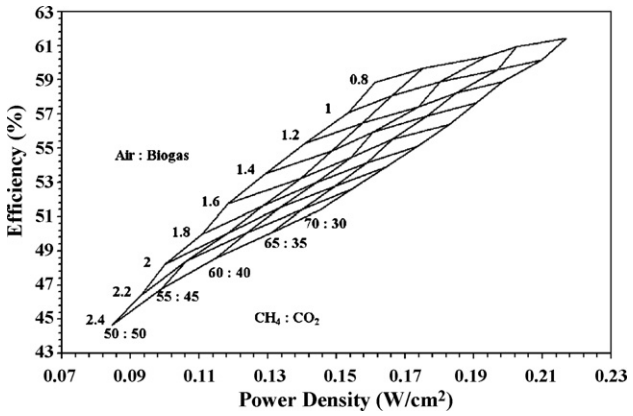

Fig. 8. Performance and current density of air-fed SOFC at different air:biogas and CH_4:CO_2 ratios in biogas (fuel processing temperature = 1073 K).

estingly, as the H_2O:biogas ratio increases, the plant electrical efficiency decreases. This is particularly pronounced when the H_2O:biogas ratio is higher than 1.6. Although excessive addition of steam in the system can increase the hydrogen yield from the reformer, significant amount of heat load is required to generate and preheat the excessive steam. Consequently, the SOFC cannot be operated at high fuel utilization, resulting in lower electrical efficiency. It is also observed that the power density increases initially, levels off and then slightly decreases. This behavior is most likely due to the fact that although steam is essential for promoting the production of hydrogen, it also acts as a diluent, leading to the decrease of hydrogen concentration and power density.

In the case of the air-fed SOFC, the plant configuration and its energy balance are illustrated in Fig. 2, the values of air:biogas, CH_4:CO_2 in biogas and fuel processing temperature are 1.6, 60:40 and 1073 K, respectively. Unlike the steam-fed SOFC, heating energy is not required for the steam generator and the fuel processor. However, hydrogen fuel cannot be used entirely in the SOFC stack, as some fuel must remain in the SOFC outlet stream in order to maintain a high power density for the SOFC. The residue gas combusted as well as the energy generated (28.52% of biogas LHV) is utilized in the steam turbine (assuming an electrical efficiency of 30%) to generate more electricity as shown in Fig. 2. Heat loss generated in the steam turbine (19.97% of biogas LHV) is released to the environment. The plant efficiency and power density for the air-fed SOFC with various air:biogas and CH_4:CO_2 ratios are illustrated in Fig. 8. Compared with the case of the steam-fed SOFC, the power density is much lower. This is due to the fact that the partial oxidation reaction (Eq. (2)) can produce only 2 moles of hydrogen per mole of methane compared with 3 moles of hydrogen per mole of methane in the case of the steam reforming reaction (Eq. (3)). In addition, the high proportion of nitrogen present in air also reduces the hydrogen concentration in the reformed gas. Consequently, the hydrogen partial pressure of the product gas derived from the partial oxidation is lower than that derived from the steam reforming, leading to a lower SOFC power density. However, the air-fed SOFC offers slightly higher electrical efficiency than the steam-fed system. This is due to the exothermicity of the partial oxidation route. Therefore, heat energy from the afterburner is not required to supply to the fuel processor unlike the steam-fed SOFC. Moreover, energy is not required for steam generation which usually consumes large amount of heat. These features help to annul the effect of reduced hydrogen yield in the partial oxidation route. Similar to the case of the steam-fed SOFC, both plant efficiency and power density improve as the quantity of methane in biogas increases as illustrated in Fig. 8. The effect of variation in the air:biogas ratio was also investigated. The results indicate that both power density and overall efficiency decrease with increasing the air content. The decrease in power density is mainly due to the significant increase in inert nitrogen in the inlet stream (anode). The decrease in the electrical efficiency may be ascribed to the excessive air fed to the reformer, occasioning higher energy loss from the increased amount of exhaust gas.

As a third option, the co-fed SOFC is also investigated and its energy balance is illustrated in Fig. 3. The values of H_2O:biogas, air:biogas, CH_4:CO_2 in biogas and fuel processing temperature are 0.8, 2, 60:40 and 973 K, respectively. Unlike the steam-fed SOFC, there is no energy supplied to the fuel processor due to the participation of exothermic partial oxidation reaction; however, some heating energy produced in the afterburner (7.38% of biogas LHV) must be supplied to the vaporizer to generate steam. Furthermore, the residue heat from the co-fed SOFC system (26.86% of biogas LHV) is supplied to the steam turbine to generate more electricity like in the case of the air-fed SOFC. The heat loss from the gas turbine (18.8% of biogas LHV) is released to the environment. The plant electrical efficiency and the power density at different air:biogas and H_2O:biogas ratios are illustrated in Fig. 9. In this study, the biogas composition (CH_4:CO_2) is kept at 60:40. From the foregoing analysis, the electrical efficiency of the co-fed SOFC decreases with the increase in the reforming agent content. The power density decreases as the air:biogas ratio increases due to the presence of large amount of nitrogen in air. However, an optimum H_2O:biogas ratio which provides a maximum power density is observed. This is due to the competing effects between the promotion of hydrogen production and the dilution effect by the addition of more water.

In order to select a suitable reforming agent, the performance of the SOFC systems with different reforming agents is com-

Please cite this article in press as: P. Piroonlerkgul, et al., Selection of appropriate fuel processor for biogas-fuelled SOFC system, Chem. Eng. J. (2007), doi:10.1016/j.cej.2007.10.007

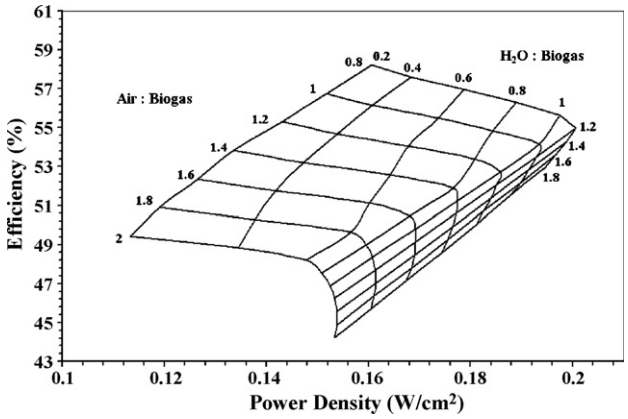

Fig. 9. Performance and current density of co-fed SOFC at different air:biogas and H_2O:biogas ratios (fuel processing temperature = 973 K).

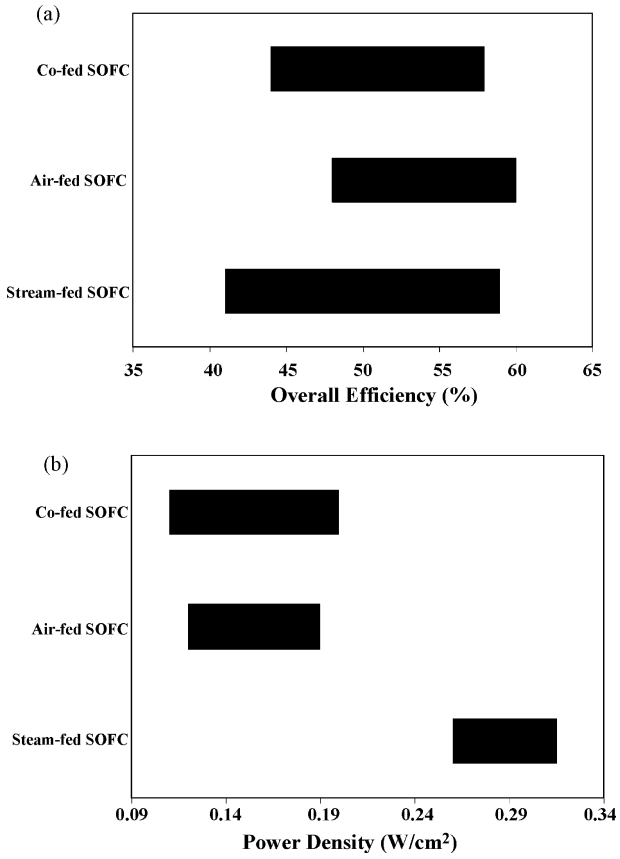

Fig. 10. SOFC performance: (a) overall electrical efficiency and (b) power density (CH_4:CO_2 = 60:40).

pared as shown in Fig. 10. It is obvious that steam is the most attractive reforming agent for the biogas-fed SOFC regarding the power density. Although the air-fed SOFC can provide slightly higher electrical efficiency than the steam-fed SOFC, the power density is much lower due to the high content of nitrogen in air. By adding steam to the air-fed SOFC, the power density can be improved but with the reduction of the electrical efficiency. Because the stack is among the most expensive part of the SOFC system, it is likely that the use of steam as the reforming agent is the most suitable for the biogas-fed SOFC although the electrical efficiency is slightly lower than the use of air.

In order to improve the efficiency of the steam-fed SOFC, the biogas split option is proposed as illustrated in Fig. 11. For this operation, part of biogas is split from the fuel processor and directly fed to the afterburner. This diminishes the heat load in the SOFC system due to the decrease in the quantities of steam added. Moreover, the extent of the endothermic steam reforming reaction is also diminished. As seen in Fig. 11, the heat load in steam generator and H_2 processor for the steam-fed SOFC with 9% of biogas split are 10.1 and 16.3% of biogas LHV, respectively, which are lower compared with those for the steam-fed SOFC without the biogas split (11.1 and 17.9% of biogas LHV for the heat load in steam generator and H_2 processor, respectively). The heating power and the heat exchanger area required in preheating are also reduced. Consequently, the electrical efficiency can be increased while the capital cost is also reduced. The results of the biogas split option shown in Fig. 12 indicate

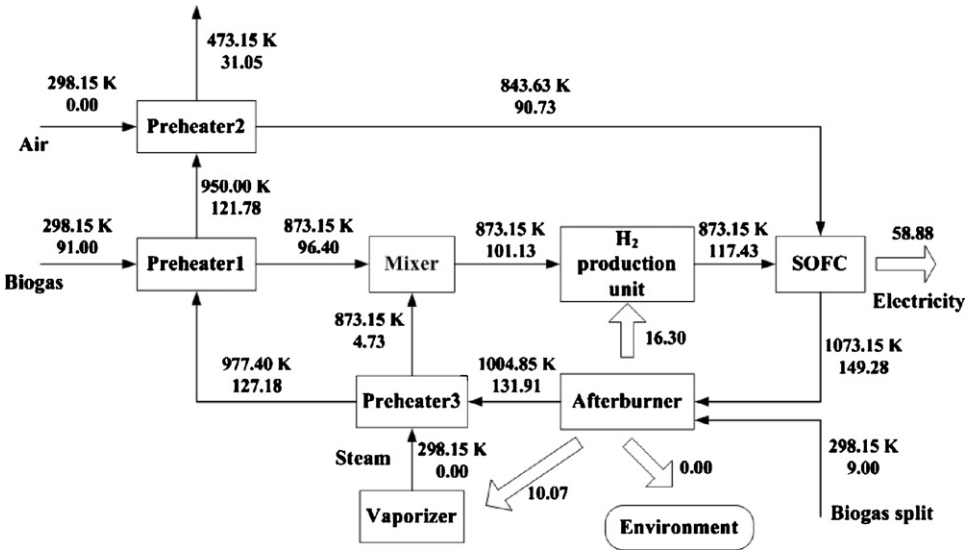

Fig. 11. The SOFC configuration with the biogas split operation.

Please cite this article in press as: P. Piroonlerkgul, et al., Selection of appropriate fuel processor for biogas-fuelled SOFC system, Chem. Eng. J. (2007), doi:10.1016/j.cej.2007.10.007

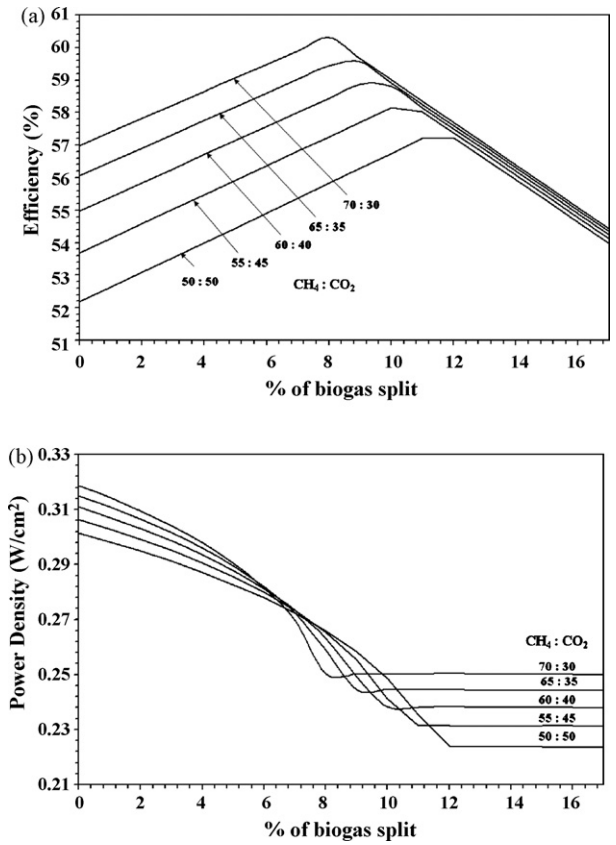

Fig. 12. The effect of %biogas split on (a) overall electrical efficiency and (b) power density at different biogas compositions (fuel processing temperature = 873 K, H_2O:biogas = 1.2).

that the increase in the percentage of biogas split can improve the plant efficiency. However, there is an optimal point at which the SOFC achieves a maximum electrical efficiency. For the operation over this point, the plant efficiency decreases with increasing the percentage of biogas split since the heat released from the afterburner is higher than that required in the vaporizer and the fuel processor. With the installation of biogas split operation, 59% of overall electrical efficiency can be achieved compared to 55% for the normal case with the CH_4:CO_2 ratio of 60:40. Although the biogas split can improve the plant electrical efficiency, the power density always decreases with the increasing biogas split, implying that more SOFC stack area is required for the higher percentage of biogas split. However, it should be noted that the use of steam-fed SOFC with biogas split still offers higher power density than the air-fed SOFC while the electrical efficiency becomes comparable.

4. Conclusions

Performance of the biogas-fed SOFC systems with different reforming agents (steam, air and combined steam/air) was determined in order to find a suitable reforming agent. The boundary of carbon formation was firstly calculated to specify a minimum amount of each reforming agent necessary to avoid carbon formation. Within the range of operating variables examined (chosen to avoid debilitating carbon formation), it seems that when the amount of reforming agent increases, the electrical efficiency always decreases. For the steam-fed SOFC, there is an optimal amount of steam which provides a maximum power density. However, for the air-fed SOFC, the power density always decreases with the increased amount of air due to the dilution effect of nitrogen in air. Steam is considered to be the most suitable reforming agent in this study as the steam-fed SOFC offers much higher power density than the air-fed SOFC although its electrical efficiency is slightly lower due to the high energy requirement in the steam generation. When steam is added in the air-fed SOFC as in the case of the co-fed SOFC, the power density can be improved but the electrical efficiency becomes lower compared with the case of the air-fed SOFC. In order to improve the electrical efficiency of the steam-fed SOFC, the biogas split option was considered. It was found that a higher electrical efficiency can be achieved. In addition, although the power density is lowered by this operation, the value is still higher than the case of the air-fed SOFC.

Acknowledgements

This research is financially supported by the Thailand Research Fund and Commission on Higher Education.

References

[1] J. Van Herle, Y. Membrez, O. Bucheli, Biogas as a fuel source for SOFC co-generators, J. Power Sources 127 (2004) 300–312.
[2] D.C. Dayton, Fuel cell integration—a study of the impacts of gas quality and impurities, NREL Final Report, 2001.
[3] J. Van herle, F. Maréchal, S. Leuenberger, Y. Membrez, O. Bucheli, D. Favrat, Process flow model of solid oxide fuel cell system supplied with sewage biogas, J. Power Sources 131 (2004) 127–141.
[4] R. Layi Fagbenle, A.B.C. Oguaka, O.T. Olakoyejo, A thermodynamic analysis of a biogas-fired integrated gasification steam injected gas turbine (BIG/STIG) plant, Appl. Therm. Eng. 27 (2005) 2220–2225.
[5] M. Jenne, T. Dörk, A. Schuler, in: U. Bossel (Ed.), Proceedings of the Fifth European Solid Oxide Fuel Cell Forum, Lucerne, Switzerland, July 2002, European Forum Secretariat, CH 5442 Oberrohrdorf, Switzerland, 2002, pp. 460–466.
[6] P. Ferreira-Aparicio, M.J. Benito, J.L. Sanz, New trends in reforming technologies: from hydrogen industrial plants to multifuel microreformers, Catal. Rev. 47 (2005) 491–588.
[7] S. Ahmed, M. Krumpelt, Hydrogen from hydrocarbon fuels for fuel cells, Int. J. Hydrogen Energy 26 (2001) 291–301.
[8] J.R. Rostrup-Nielsen, Syngas in perspective, Catal. Today 71 (2002) 243–247.
[9] P.D.F. Vernon, M.L.H. Green, A.K. Cheetham, A.T. Ashcroft, Partial oxidation of methane to synthesis gas, and carbon dioxide as an oxidising agent for methane conversion, Catal. Today 13 (1992) 417–426.
[10] A.M. O'Connor, J.R.H. Ross, The effect of O_2 addition on the carbon dioxide reforming of methane over Pt/ZrO_2 catalysts, Catal. Today 46 (1998) 203–210.
[11] G.F. Froment, Production of synthesis gas by steam- and CO_2-reforming of natural gas, J. Mol. Catal. A: Chem. 163 (2000) 147–156.
[12] J.R. Rostrup-Nielsen, J. Sehedsted, J.K. Norskov, Hydrogen and synthesis gas by steam- and CO_2 reforming, Adv. Catal. 47 (2002) 65–139.
[13] J.H. Edwards, A.M. Maitra, The chemistry of methane reforming with carbon dioxide and its current and potential applications, Fuel Proc. Technol. 42 (1995) 269–289.
[14] S. Assabumrungrat, N. Laosiripojana, P. Piroonlerkgul, Determination of the boundary of carbon formation for dry reforming of methane in a solid oxide fuel cell, J. Power Sources 159 (2006) 1274–1282.

Please cite this article in press as: P. Piroonlerkgul, et al., Selection of appropriate fuel processor for biogas-fuelled SOFC system, Chem. Eng. J. (2007), doi:10.1016/j.cej.2007.10.007

[15] M.A. Khaleel, Z. Lin, P. Singh, W. Surdoval, A finite element analysis modeling tool for solid oxide fuel cell development: coupled electrochemistry, thermal and flow analysis in MARC, D. Collin, J. Power Sources 130 (2004) 136–148.
[16] M.C.J. Bradford, M.A. Vannice, Catalytic reforming of methane with carbon dioxide over nickel catalysts. II: Reaction kinetics, Appl. Catal. A: Gen. 142 (1996) 97–122.
[17] H.M. Swaan, V.C.H. Kroll, G.A. Martin, C. Mirodatos, Deactivation of supported nickel catalysts during the reforming of methane by carbon dioxide, Catal. Today 21 (1994) 571–578.
[18] R. Blom, I.M. Dahl, A. Slagtem, B. Sortland, A. Spjelkavik, E. Tangstad, Carbon dioxide reforming of methane over lanthanum-modified catalysts in a fluidized-bed reactor, Catal. Today 21 (1994) 535–543.
[19] J.R. Ferguson, J.M. Fiard, R. Herbin, Three-dimensional numerical simulation for various geometries of solid oxide fuel cells, J. Power Sources 58 (1996) 109–122.
[20] S.H. Chan, K.A. Khor, Z.T. Xia, A complete polarization model of a solid oxide fuel cell and its sensitivity to the change of cell component thickness, J. Power Sources 93 (2001) 130–140.
[21] S.P. Jiang, S.P.S. Badwal, H_2 Oxidation reactions at the Ni and Pt electrodes on Y-TZP electrolytes, J. Electrochem. Soc. 144 (1997) 3777–3784.
[22] S.P. Jiang, S.P.S. Badwal, An electrode kinetics study of H_2 oxidation on Ni/Y_2O_3–ZrO_2 cermet electrode of the solid oxide fuel cell, Solid State Ionics 123 (1999) 209–224.
[23] J. Fleig, Solid oxide fuel cell cathodes: polarization mechanisms and modeling of the electrochemical performance, Annu. Rev. Mater. Res. 33 (2003) 361–382.
[24] W.J. Massman, A review of the molecular diffusivities of H_2O, CO_2, CH_4, CO, O_3, SO_2, NH_3, N_2O, NO, and NO_2 in air, O_2 and N_2 near STP, Atmos. Environ. 32 (1998) 1111–1127.
[25] H. Yakabe, M. Hishinuma, M. Uratani, Y. Matsuzaki, I. Yasuda, Evaluation and modeling of performance of anode-supported solid oxide fuel cell, J. Power Sources 86 (2000) 423–431.
[26] F. Zhao, A.V. Virkar, Dependence of polarization in anode-supported solid oxide fuel cells on various cell parameters, J. Power Sources 141 (2005) 79–95.
[27] G. Tao, T. Armstrong, A. Virkar, Intermediate temperature solid oxide fuel cell (IT-SOFC) research and development activities at MSRI, in: Nineteenth Annual ACERC&ICES Conference, Utah, 2005.
[28] M. Ni, M.K.H. Leung, D.Y.C. Leung, Parametric study of solid oxide fuel cell performance, Energy Convers. Manage. 48 (2007) 1525–1535.
[29] S.H. Lee, W. Cho, W.S. Ju, B.H. Cho, Y.C. Lee, Y.S. Baek, Tri-reforming of CH_4 using CO_2 for production of synthesis gas to dimethyl ether, Catal. Today 87 (2003) 133–137.

Please cite this article in press as: P. Piroonlerkgul, et al., Selection of appropriate fuel processor for biogas-fuelled SOFC system, Chem. Eng. J. (2007), doi:10.1016/j.cej.2007.10.007

Appendix 9

Elsevier Editorial System(tm) for Chemical Engineering Journal
Manuscript Draft

Manuscript Number:

Title: Performance improvement of solid oxide fuel cell system using palladium membrane reactor with different operation modes

Article Type: Original Article

Section/Category: Chemical Reaction Engineering

Keywords: SOFC; membrane reactor; palladium membrane; performance

Corresponding Author: Dr. Suttichai Assabumrungrat, PhD

Corresponding Author's Institution: Chulalongkorn University

First Author: Supawat Vivanpatarakij , BEng

Order of Authors: Supawat Vivanpatarakij , BEng; Suttichai Assabumrungrat, PhD; Navadol Laosiripojana , PhD; Amornchai Arpornwichanop , DEng

Abstract: The performance improvement of a solid oxide fuel cell (SOFC) system by replacing a conventional reformer with a palladium membrane reactor was investigated. When pure hydrogen was extracted from the reaction mixture via the palladium membrane, the power density of the SOFC was improved, depending on the value of hydrogen recovery (□). Three operation modes of membrane reactors; i.e., high pressure compressor (MR-HPC), vacuum pump (MR-V) and combined high pressure compressor and vacuum pump (MR-HPC-V) were considered. Their overall SOFC system characteristics were compared with those of the SOFC system with the conventional reformer. The economic analysis revealed that the total capital cost/net electrical power was dependent on hydrogen recovery, net electrical efficiency and operation mode. At high electrical efficiency, the replacement of the conventional reformer with the membrane reactor became attractive. Finally, it was demonstrated that the MR-HPC-V was the best operation mode for integration with the SOFC system.

Suggested Reviewers:

Opposed Reviewers:

Department of Chemical Engineering
Faculty of Engineering
Chulalongkorn University

December 1, 2007

Dear the editor of Chemical Engineering Journal,

I would like to submit a research article entitled "Performance improvement of solid oxide fuel cell system using palladium membrane reactor with different operation modes" for your consideration for inclusion in Chemical Engineering Journal. The article is original and unpublished and is not being considered for publication elsewhere.

If you have any query, please do not hesitate to contact me. I am looking forward to hearing from you.

Sincerely yours,

(Associate Professor Suttichai Assabumrungrat)
Department of Chemical Engineering, Faculty of Engineering,
Chulalongkorn University, Bangkok 10330, Thailand
Tel: 662-2186878-82; fax:662-2186877
E-mail: Suttichai.A@chula.ac.th

List of Suggested Reviewers

1. Professor E. Croiset
   Department of Chemical Engineering, University of Waterloo, Canada
   Email: ecroiset@cape.uwaterloo.ca

2. Professor S.H. Chan
   Fuel Cell Strategic Research Programme, School of Mechanical and Aerospace Engineering, 50, Nanyang Avenue, Nanyang Technological University, Singapore 639798, Singapore
   Email: mshchan@ntu.edu.sg

Submitted to Chemical Engineering Journal

Type of contribution: Full length article

Performance improvement of solid oxide fuel cell system using palladium membrane reactor with different operation modes

S. Vivanpatarakij [a], S. Assabumrungrat [a, *], N. Laosiripojana [b] and A. Arpornwichanop [c]

[a] *Center of Excellence in Catalysis and Catalytic Reaction Engineering, Department of Chemical Engineering, Faculty of Engineering, Chulalongkorn University, Bangkok 10330, THAILAND*

[b] *The Joint Graduate School of Energy and Environment, King Mongkut's University of Technology Thonburi, Bangkok 10140, THAILAND*

[c] *Control and Systems Engineering, Department of Chemical Engineering, Faculty of Engineering, Chulalongkorn University, Bangkok 10330, THAILAND*

[*] Corresponding author. fax: 662-218-6877,

E-mail address: Suttichai.A@chula.ac.th (S. Assabumrungrat)

Abstract

The performance improvement of a solid oxide fuel cell (SOFC) system by replacing a conventional reformer with a palladium membrane reactor was investigated. When pure hydrogen was extracted from the reaction mixture via the palladium membrane, the power density of the SOFC was improved, depending on the value of hydrogen recovery (ξ). Three operation modes of membrane reactors; i.e., high pressure compressor (MR-HPC), vacuum pump (MR-V) and combined high pressure compressor and vacuum pump (MR-HPC-V) were considered. Their overall SOFC system characteristics were compared with those of the SOFC system with the conventional reformer. The economic analysis revealed that the total capital cost/net electrical power was dependent on hydrogen recovery, net electrical efficiency and operation mode. At high electrical efficiency, the replacement of the conventional reformer with the membrane reactor became attractive. Finally, it was demonstrated that the MR-HPC-V was the best operation mode for integration with the SOFC system.

Keywords: SOFC; membrane reactor; palladium membrane; performance improvement

1. Introduction

A solid oxide fuel cell (SOFC) is a promising electrical power generator compared to conventional systems as it offers a wide range of applications, low emissions, fuel flexibility and high system efficiency. Although hydrogen is a main fuel for most type of fuel cells, the uses of various alternative fuels such as methane, methanol, ethanol, gasoline and other oil derivatives are possible in the presence of a reformer. To date, methane is a promising fuel as it is an abundant component in natural gas and the methane steam reforming technology is relatively well established. Therefore, it is the fuel of interest in this study.

A number of researches have been carried out aiming to improve performance of SOFCs. Novel cell components with better characteristics have been explored [1-3]. Some researchers have focused on the integration of SOFCs with other units such as a gas turbine for the efficient utilization of energy within the combined system [4-7]. A non-uniform cell potential operation (or multi-stage operation) has been proposed [8, 9, 10, 11]. Another attractive approach is to replace a conventional reformer with a palladium membrane reactor which has been successfully applied to many hydrogen-generating reactions [12]. As the fuel cell performance is dependent on hydrogen partial pressure in the anode feed [13], it was expected that by using the palladium membrane, pure hydrogen is extracted from the reaction mixture and, therefore, the performance of SOFC is improved.

Our preliminary study investigated a methanol-fueled SOFC system integrated with a palladium membrane reactor. The driving force for hydrogen separation was introduced by using a high pressure compressor which required high electrical power for the operation. It was demonstrated that the SOFC cells could be operated at a higher power density, resulting in a cost reduction of the SOFC cells. However, the

required large and expensive palladium membrane made the proposed system uneconomical [14].

Theoretically, a membrane reactor can be operated under different modes of driving force introduction, resulting in the differences in the required membrane area and power consumption. Therefore it is likely that the SOFC system integrated with a palladium membrane reactor may become economical than the system with a conventional reformer when appropriate choices of the operation mode of membrane reactor and operating condition are selected.

In this paper, the characteristics of the methane-fueled SOFC systems integrated with a palladium membrane reactor with different operation modes (i.e., high pressure compressor (MR-HPC), vacuum pump (MR-V) and combined high pressure compressor and vacuum pump (MR-HPC-V)) were investigated. Their economic analysis was compared with that of the SOFC system integrated with a conventional reformer in order to find a suitable operation mode of the membrane reactor for integrating with the SOFC system.

2. Theory

2.1 Methane steam reforming (MSR)

Methane steam reforming is a conventional method of hydrogen production. The major reactions taking place in the reactor are methane steam reforming (Eq.(1)), water gas shift reaction (Eq.(2)) and carbon dioxide methanation (Eq.(3)).

$$CH_4 + H_2O = CO + 3H_2 \quad (1)$$

$$CO + H_2O = CO_2 + H_2 \quad (2)$$

$$CH_4 + 2H_2O = CO_2 + 4H_2 \quad (3)$$

In order to avoid carbon formation problem, the feed containing a H_2O:CH_4 molar ratio of 2.5 (or high) is usually employed [15].

Mathematical models of methane steam reforming were reported by Xu and Froment (1989) [16]. The kinetic rates on Ni/$MgAl_2O_4$ catalyst were derived based on the Langmuir-Hinshelwood reaction mechanism. The rate expressions for reactions (1)-(3) are given by the following expressions:

$$r_1 = \frac{\frac{k_1}{p_{H_2}^{2.5}}\left(p_{CH_4}p_{H_2O} - \frac{p_{H_2}^3 p_{CO}}{K_1}\right)}{(DEN)^2} \quad (4)$$

$$r_2 = \frac{\frac{k_2}{p_{H_2}}\left(p_{CO}p_{H_2O} - \frac{p_{H_2}p_{CO_2}}{K_2}\right)}{(DEN)^2} \quad (5)$$

$$r_3 = \frac{\frac{k_3}{p_{H_2}^{3.5}}\left(p_{CH_4}p_{H_2O}^2 - \frac{p_{H_2}^4 p_{CO_2}}{K_3}\right)}{(DEN)^2} \quad (6)$$

where $DEN = 1 + K_{CO}p_{CO} + K_{H_2}p_{H_2} + K_{CH_4}p_{CH_4} + K_{H_2O}p_{H_2O}/p_{H_2}$ (7)

$$k_i = A_i \exp\left(\frac{-E_i}{RT}\right) ;\ i = 1, 2, 3 \quad (8)$$

$$K_j = B_j \exp\left(\frac{-\Delta H_j}{RT}\right) ;\ j = \mathrm{CO}, \mathrm{H_2}, \mathrm{CH_4}, \mathrm{H_2O} \quad (9)$$

The kinetic parameters for the methane steam reforming are summarized in Table 1.

2.2 Palladium membrane

A palladium membrane is well-known as a highly selective membrane for hydrogen separation. The ability of hydrogen transfer through the membrane is typically quantified in term of permeability. The hydrogen flux (N_{H_2}) is inversely proportional to the membrane thickness **(** δ **)** and directly proportional to the product of the hydrogen permeability (Q_0 **)** and the driving force (the difference in the square root of hydrogen partial pressure across the membrane).

$$N_{H_2} = \frac{Q_0}{\delta} exp(\frac{-E_D}{RT})(p_{H_2,r}^{0.5} - p_{H_2p}^{0.5}) \quad (10)$$

In order to achieve a high hydrogen flux, a thin film of palladium membrane is generally coated on a porous support with good mechanical property. In addition, the driving force is enhanced by installing a compressor and/or a vacuum pump. The required power (P_{pump}) for the compressor and vacuum pump can be calculated by using the Aspen Plus program. In this study, the efficiencies of both the compressor and the vacuum pump are assumed to be 85%.

2.3 Membrane reactor

A membrane reactor (MR) is a reaction system where separation unit and chemical reactors are combined together. The use of a palladium membrane reactor (Pd-MR) is a promising approach for methane steaming reforming (MSR). As the reactions are limited by equilibrium; the separation of hydrogen product via the selective palladium membrane can increase the conversion of methane and achieve a high-purity hydrogen product at the same time. To calculate the palladium membrane area, the membrane was divided into small increments represented by $dz_{Pd,i}$. The

corresponding hydrogen recovery ($H_{2,permeate_i}$) at each element can be computed by Eq. (11) and the total hydrogen recovery ($H_{2,permeate}$) obtained from the membrane reactor was the summation of hydrogen recovery at each element (Eq.(12)). The length of the membrane reactor ($z_{Pd,\ total}$) was extended until the hydrogen recovery reaches the target value ($H_{2,\ require}$) (Eq.(13)). The final membrane area which corresponds to the target hydrogen recovery represents the required membrane area (A_{Pd}) for the operation (Eq.(14)).

$$H_{2,permeate_i} = 2 \cdot \pi \cdot r_{ext} \cdot dz_{Pd,i} \cdot N_{H_2,i} \tag{11}$$

$$H_{2,permeate} = \sum_{i=1}^{n} H_{2,permeate_i} \tag{12}$$

$$z_{Pd,total} = \sum_{H_{2,permeate}=0}^{H_{2,permeate}=H_{2,require}} dz_{Pd,i} \tag{13}$$

$$A_{Pd} = 2 \cdot \pi \cdot r_{ext} \cdot z_{Pd,total} \tag{14}$$

2.4 SOFC

An SOFC unit consists of two porous ceramic electrodes (i.e. an anode and a cathode) and a solid ceramic electrolyte. In theory, both hydrogen and CO can react electrochemically with oxygen ions at the anode of the SOFC cells. However, it was reported that about 98% of current is produced by H_2 oxidation in common situations [17]. It is therefore assumed in this study that the CO electro-oxidation is neglected. The theoretical open-circuit voltage of the cell (E), which is the maximum voltage under specific operating conditions, can be calculated from the following equations [18]:

$$E = E_0 + \frac{RT}{2F}\ln\left(\frac{P_{H_2}P_{O_2}^{0.5}}{P_{H_2O}}\right) \quad (15)$$

$$E_0 = 1.253 - 2.4516\times10^{-4}T \quad (16)$$

The actual voltage (Eq.(17)) is usually lower than the open-circuit voltage due to the presence of polarization losses: ohmic polarization (Eq.(18)-(19)), activation polarization (Eq.(20)-(23)) and concentration polarization (Eq.(24)) [19].

$$V = E - (\eta_{ohm} + \eta_{Act} + \eta_{Conc}) \quad (17)$$

The ohmic polarization is the resistance of electron through electrode and electrolyte. The activation polarization is mostly illustration of a loss for driving the electrochemical reaction to completion. The concentration polarization occurs due to the mass transfer limitation through the porous electrodes.

Ohmic polarization:

$$\eta_{Ohm} = \sum \rho_j \delta_j \quad (18)$$

$$\rho_j = a_j \exp(b_j T) \quad (19)$$

Activation polarization:

$$i = i_0\left[\exp\left(\frac{\alpha n_e F \eta_{Act}}{RT}\right) - \exp\left(-\frac{(1-\alpha)n_e F \eta_{Act}}{RT}\right)\right] \quad (20)$$

$$\eta_{Act} = \frac{2RT}{n_e F}\sinh^{-1}\left(\frac{i}{i_0}\right); \text{ where } \alpha = 0.5 \quad (21)$$

$$i_{0,A} = 5.5\times10^{8}\left(\frac{p_{H_2}}{p}\right)\left(\frac{p_{H_2O}}{p}\right)\exp\left(\frac{-100\times10^{3}}{RT}\right) \quad (22)$$

$$i_{0,C} = 7.0\times10^{8}\left(\frac{p_{O_2}}{p}\right)^{m}\exp\left(\frac{-120\times10^{3}}{RT}\right) \quad (23)$$

Concentration polarization:

$$\eta_{Conc} = -\frac{2RT}{n_e F}\ln\left(\frac{y_{H_2}y^{I}_{H_2O}}{y^{I}_{H_2}y_{H_2O}}\right) \quad (24)$$

To simplify the calculation of the SOFC performance, it is assumed that both fuel and oxidant are well-diffused through the electrodes. Therefore, the concentration polarization losses ($\eta_{Conc,\,A}$ and $\eta_{Conc,\,C}$) are neglected. This assumption is valid when the current density is not very high [20]. Table 2 summarizes the values of the parameters of the ohmic polarization.

2.5 Configurations of different SOFC systems

The diagrams of different SOFC systems are illustrated in Figure 1. In a conventional system (Figure 1a.), methane and steam are fed to a reformer where they are converted to CO, CO_2 and H_2. The product gas containing hydrogen at a low concentration is directly introduced to the SOFC stack where electrical power is generated. The SOFC exhaust gases are combusted in a burner whose heat can be utilized for energy-demanding units in the system. When the conventional reformer is replaced by a membrane reactor, pure hydrogen is extracted from the reaction mixture and fed to the SOFC stacks. The term "hydrogen recovery (ξ)" is defined as the mole of hydrogen extracted by the membrane divided by the mole of hydrogen theoretically

produced based on the mole of methane feed (4 mol of H_2: 1 mol of CH_4). The term "fuel utilization (U_f)" represents the mole of hydrogen electrochemically consumed within the stack divided by the mole of hydrogen theoretically produced based on the mole of methane feed.

Three operation modes of a membrane reactor are considered in this study. For the membrane reactor with a high pressure compressor (MR-HPC) (Figure 1b.), the pressure of the permeation is kept at 1 atm while the driving force for hydrogen permeation is enhanced by using the high pressure compressor. In the second case (Figure 1c.), the permeation side is kept at below atmospheric pressure by using a vacuum pump. It is noted that the low pressure compressor is still required at the inlet of the conventional reformer and the membrane reactor in order to feed the reactants to the system. In the last configuration (Figure 1d.), both the high pressure compressor and the vacuum pump are used. In all SOFC systems with the membrane reactor, the residue gas in the reaction gas mixture and the exhausted gas from the SOFC stacks are combusted in the burner similar to the case with the conventional reformer. Table 3 summarizes the standard condition of the SOFC system in this study.

2.6 Economic analysis

Economic analysis was carried out to compare the costs of the SOFC systems incorporated with palladium membrane reactors of different operation modes with that of the system with the conventional reformer. The total capital cost includes the costs of compressor, vacuum pump, SOFC stack (1500 \$/m^2) [21] and Pd membrane (746 \$/m^2) [22]. The compressor cost and vacuum pump cost (\$) were described by the following expressions, Eq.25 and Eq.26 [23].

$$\text{Cost of compressor}\,(\$) = 1.49 \cdot HP^{0.71} \times 10^3 \qquad (25)$$

where: $10 < HP < 800$

$$\text{Cost of vacuum pump (\$)} = 2.59 \cdot X^{1.03} \times 10^5 \quad (26)$$

where: $0.01 < X < 0.52$ (lbs H_2/h)/(suction Torr)

3. Results and Discussion

The study began with the model validation of the methane steam reforming in a conventional reformer. The calculations were based on the condition reported in the literature [19]; i.e., H_2O:CH_4 ratio = 3, GHSV = 1067 h^{-1} and reformer pressure = 1 atm. As shown in Figure 2, it is obvious that our calculation results are in good agreement with those reported earlier [19] for all temperature ranges (723-773 K). The deviations are in the range between 3-5%. Then, the SOFC model was verified. Figure 3 shows the relationship between the power density and current density at three temperature levels; i.e., 1023, 1073 and 1123 K. In the simulation, pure hydrogen was fed to the SOFC and the fuel utilization (U_f) was kept at 80%. Again, our calculations show good agreement with those reported in the previous literature [18].

In order to demonstrate the benefit from replacing of the conventional reformer with the membrane reactor, the plots of the power density and electrical efficiency against the current density of different systems are compared (Figure 4). The fuel utilization and operating temperature were kept at 80% and 1073 K, respectively. It is obvious that the SOFC system with the membrane reactor offers higher power density and electrical efficiency than that with the conventional reformer, particularly at higher values of hydrogen recovery (ξ). At ξ = 95%, the increase of the maximum power density of 25% can be achieved. However, when the membrane reactor is operated at too low hydrogen recovery (e.g., ξ = 80.6%), the use of the palladium membrane reactor can not compete the use of the conventional

reactor due to the fuel depletion in the anode of the SOFC. Therefore, the membrane reactor has to be operated at a sufficiently high hydrogen recovery (ξ).

According to the operation of membrane reactors, various operation modes are possible for enhancing the driving force of hydrogen permeation through the membrane. The selection of suitable operation mode and operating condition should be based on the consideration of the required membrane area and power consumption. Figure 5 shows the effect of the compressor pressure on the required palladium membrane area and the required power for the case of the membrane reactor with a high pressure compressor (MR-HPC). The pressure in the permeation side was always kept at 1 atm. The results indicate that when the compressor is operated at higher pressures, the membrane reactor requires less membrane area but higher compressor power. For the membrane reactor with a vacuum pump (MR-V), the results shown in Figure 6 indicate that when the vacuum pump pressure is reduced, the required membrane area decreases initially and then levels off but the overall power consumption for operating the vacuum pump and the low pressure compressor continuously increases. Comparison between the MR-HPC and the MR-V reveals that the MR-V generally requires less membrane area but higher power consumption. The other operation mode of the membrane reactor considered in this study is the combination of both high pressure compressor and vacuum pump (MR-HPC-V). Figure 7 shows the effects of the compressor pressure (between 2-5 atm) and the vacuum pump pressure (between 0.01-0.2 atm) on the required membrane area and the power consumption for ξ = 90%. Similar trends as the effects of the compressor pressure and the vacuum pump pressure on the required membrane area and the power consumption are observed. For comparison among the three operation modes, considering the case with the required membrane area of 25 m^3 and the hydrogen

recovery of 90%, it is obvious that within the range of pressure studied in the MR-HPC, even with the highest pressure (30 atm), the hydrogen recovery of 90% can not be achieved. For the MR-V, the required vacuum pump pressure and power consumption are about 0.035 atm and 50 kW, respectively. For the MR-HPC-V, the power consumption also depends on the choice of the operating pressure of the high pressure compressor. At P_R = 2, 3, 4 and 5 atm, the vacuum pump pressures are 0.088, 0.127, 0.162 and 0.198 atm, respectively while the required power consumptions are 50, 52.5, 54 and 55 kW, respectively. It is therefore obvious for the MR-HPC-V that the load of the vacuum pump can be reduced by using the high pressure compressor.

It is clear from the previous paragraph that the operation modes of the membrane reactor and the operating condition (pressure) play an important role on the membrane area and the power requirement. The economic analysis is essential for selecting a suitable operation mode of the membrane reactor for the SOFC system. Table 4 provides an example of the economic analysis of the SOFC systems with different operation modes. In all systems, the hydrogen recovery (ξ) and the fuel utilization (U_f) were set at 90% and 80%, respectively. The compressor was operated at 30 atm for the MR-HPC while the vacuum pump was operated at 0.035 atm for the MR-V. For the MR-HPC-V, the compressor and the vacuum pump were operated at 5 and 0.135 atm, respectively. The net electrical power was 371.4 kW corresponding to the overall electrical efficiency of 45.3%. However, the actual electrical power to be generated for the cases with the conventional reformer, MR-HPC, MR-V and MR-HPC-V are 373.7, 429.8, 426.8 and 427.5 kW, respectively. The additional powers are required to operate the compressor and/or vacuum pump in the systems. It should be noted that for all cases the heat obtained from the burner and the SOFC is sufficient to provide to all heat-demanding units in the systems. Regarding the required SOFC

area, it is clear that the uses of membrane reactors could reduce the requirement of the overall SOFC area; however, they require additional cost on the palladium membrane and the compressor and/or vacuum pump. The total capital cost of each system could be calculated. The values of the total capital cost followed the order: MR-HPC-V < MR-HP-C < MR-V < conventional. Obviously, based on the same net electrical power output, the total capital costs of the SOFC systems with the membrane reactors were lower than that of the conventional SOFC system. The MR-V was the most expensive among different operation modes due to the expensive vacuum pump. The MR-HPC-V was found to be the most attractive operation mode under this condition.

The economic analysis at various values of hydrogen recovery (85, 90 and 95%) and overall electrical efficiency (40.7, 45.3 and 47.7%) were considered and the corresponding values of the total capital cost/net electrical power were calculated for the cases with the conventional reformer, MR-HPC, MR-V and MR-HPC-V. As shown in Figure 8, the total capital cost/net electrical power is dependent on the hydrogen recovery, electrical efficiency and operation mode. In all systems, the values of the total capital cost/net electrical power increases with the increase of the electrical efficiency because the SOFC needs to operate at a lower power density to achieve the high electrical efficiency, resulting in the higher SOFC area and consequently the higher total capital cost. When the system is operated at a higher hydrogen recovery, the value of the total capital cost/net electrical power decreases due to the improved power density of the SOFC as demonstrated earlier in Figure 4. It is observed that for η = 40.7%, the replacement of the conventional reformer with the membrane reactor is not attractive at ξ = 85%. However, it becomes quite comparable at ξ = 90% and attractive at ξ = 95%. At high electrical efficiency, the use of membrane reactor offers lower total capital cost/net electrical power than the

use of the conventional reformer. Comparison between the different operation modes of the SOFC systems with membrane reactor reveals that the MR-HPC-V is the most attractive operation mode in all ranges of hydrogen recovery and electrical efficiency.

4. Conclusion

Performance of the SOFC systems fed by methane was analyzed to investigate the potential benefit from replacing the conventional reformer with the palladium membrane reactor. Obviously, the use of the palladium membrane reactor can improve the power density of the SOFC. Three operation modes of membrane reactors; i.e., MR-HPC, MR-V and MR-HPC-V were considered. The economic analysis of the different systems revealed that the total capital cost/net electrical power is dependent on hydrogen recovery, electrical efficiency and operation mode of the membrane reactor. The use of the palladium membrane reactor becomes attractive over the conventional reformer when the system is operated at high values of electrical efficiency and hydrogen recovery. Finally, it was demonstrated that the MR-HPC-V was the best operation mode for integration with the SOFC system.

Acknowledgment

The supports from The Thailand Research Fund and Commission on Higher Education are gratefully acknowledged.

References

[1] S.P. Yoon, J. Han, S.W. Nam, T.H. Lim, S.A. Hong, J. Power Sources 136 (2004) 30-36.

[2] S.D. Kim, S.H. Hyun, J. Moon, J.H. Kim, R.H. Song, J. Power Sources 139 (2005) 67-72.

[3] S.P. Simner, J.F. Bonnett, N.L. Canfield, K.D. Meinhardt, J.P. Shelton, V.L. Sprenkle, J.W. Stevenson, J. Power Sources 113 (2003) 1-10.

[4] P. Kuchonthara, S. Bhattacharya, A. Tsutsumi, J. Power Sources 124 (2003) 65-75.

[5] J. Palsson, A. Selimovic, L. Sjunnesson, J. Power Sources 86(2000) 442-448.

[6] B. Fredriksson Möller, J. Arriagada, M. Assadi, I. Potts, J. Power Sources 131 (2004) 320-326.

[7] Y. Inui, T. Matsumae, H. Koga, K. Nishiura, Energy Conversion and Management 46 (2005) 1837-1847.

[8] A. Selimovic, J. Palsson, J. Power Sources 106 (2002) 76-82.

[9] S.F. Au, N. Woudstra, K. Hemmes, J. Power Sources. 122 (2003) 28-36.

[10] S.M. Senn, D. Poulikakos, Electrochemistry Communications 7 (2005) 773-780.

[11] S. Vivanpatarakij, S. Assabumrungrat, N. Laosiripojana, J. Power Sources 167 (2007) 139-144,

[12] E. Kikuchi, Catalysis Today 56 (2000) 97-101.

[13] S.H. Chan, O.L. Ding, Int. J. Hydrogen Energy. 30 (2005) 167-179.

[14] W. Sangtongkitcharoen, S. Vivanpatarakij, N. Laosiripojana, A. Arpornwichanop, S. Assabumrungrat, Chemical Engineering Journal.2007, doi:10.1016/ j.cej.2007.06.021

[15] H.J. Renner, R. Marschner, Catalytic reforming of natural gas and other hydrocarbon, Ullmann's Encyclopedia of Industrial Chemistry fifth edition, VCH Verlagsgesellschaft, Weinheim, Germany. A2 (1985) 186–204.

[16] J. Xu, G.F. Froment, AICHE Journal 35 (1989) 88-96.

[17] M.A. Khaleel, Z. Lin, P. Singh, W. Surdoval, D. Collin, J. Power Sources 130 (2004) 136-148.

[18] E. Hernandez-Pacheco, M.D. Mann, P.N. Hutton, D. Singh, K.E. Martin, Inter J. Hydrogen Energy 30 (2005) 1221-1233.

[19] M. Pfafferodt, P. Heidebrecht, M. Stelter, K. Sundmacher, J. Power Sources 149 (2005) 53-62.

[20] J. Shu, B.P.A. Grandjean, S. Kaliaguine, Applied Catalysis A 119 (1994) 305-325.

[21] E. Riensche, U. Stimming, G. Unverzagt, J. Power Sources 73 (1998) 251-256.

[22] A. Criscuol, A. Basile, E. Drioli, O. Loiacono, J. Membr. Sci. 181 (2001) 21-27.

[23] S.M. Walas, Chemical Process Equipment Selection and Design. Butterworth, Inc. 1988 665-668.

Nomenclature

a	Constant in Eq.19	(Ω m)
A_{Pd}	Pd membrane area	(m^2)
b	Constant in Eq.19	(K)
E	Open circuit voltage (OCV)	(V)
E_0	Reversible potential	(V)
E_D	Activation energy for diffusion through membrane (1.57)	(kJ mol^{-1})
F	Faraday constant (96485.34)	(C mol^{-1})
$H_{2,permeate}$	Permeation hydrogen	(mol)
HP	Horse power in Eq.25	(HP)
i	Current density	(A m^{-2})
i_0	Exchange current density	(A m^{-2})
k	Adsorption parameters	(-)
K	Equilibrium constant	(-)
n_e	Electron transfer	(-)
N_{H_2}	Hydrogen flux	(mol s^{-1} m^{-2})
P_i	Partial pressure	(atm)
P_{com}, P_{vac}	Power requirement of compressor, vacuum pump	(kW)
P	Total pressure	(atm)
Q_0	Pre-exponential constant for membrane permeability (4.40×10^{-7})	(mol m^{-1} s^{-1} $Pa^{-0.5}$)
Q_{MR}	Heat of membrane reactor	(kW)
Q_R	Heat of reformer	(kW)
r_{ext}	External radius tube reactor	(m)

r_{int}	Internal radius tube reactor	(m)
R	Universal gas constant (8.31447×10^{-3})	(kJ mol^{-1} K^{-1})
T	Absolute temperature	(K)
U_f	Fuel utilization	(%)
W	Electrical work	(W)
X	Parameter in Eq.26	(lbs.H_2/h/suction Torr)
y_i^I	Mole faction of component *i* in bulk phase	(-)
z_{Pd}	Length of Pd membrane reactor	(m)

Greeks letters

α	electron transfer coefficient	(-)
η_i	Overpotential	(Ω m^2)
η	Electrical efficiency	(%)
δ	Thickness	(m)
ρ	Specific ohmic resistance	(Ω m)
ξ	Hydrogen recovery	(%)

Figure(s)

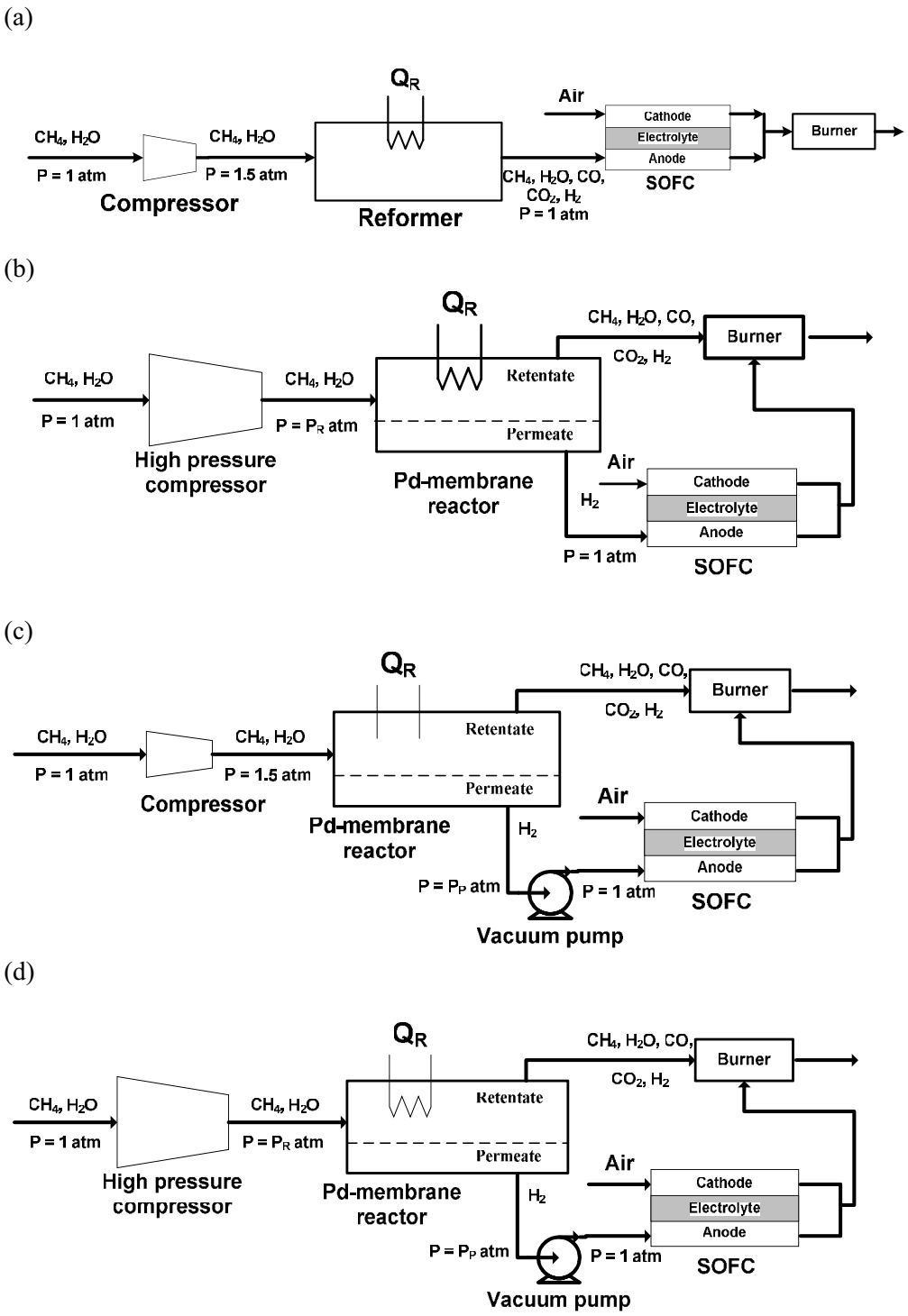

Fig. 1. Schematic diagrams of SOFC systems with different operation modes: (a) conventional reformer, (b) MR-HPC, (c) MR-V, (d) MR-HPC-V.

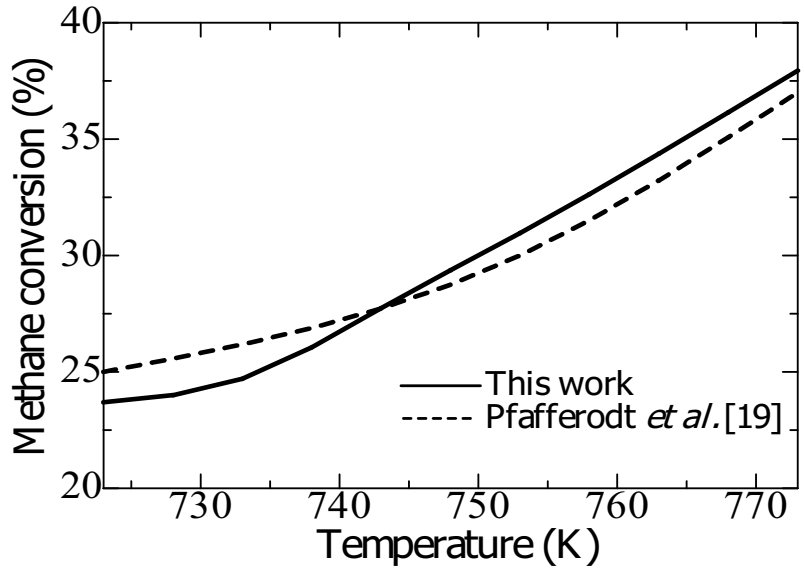

Fig. 2. Validation of the reformer model with experimental results from the literature [19] (P = 1 atm and H_2O:CH_4 = 3).

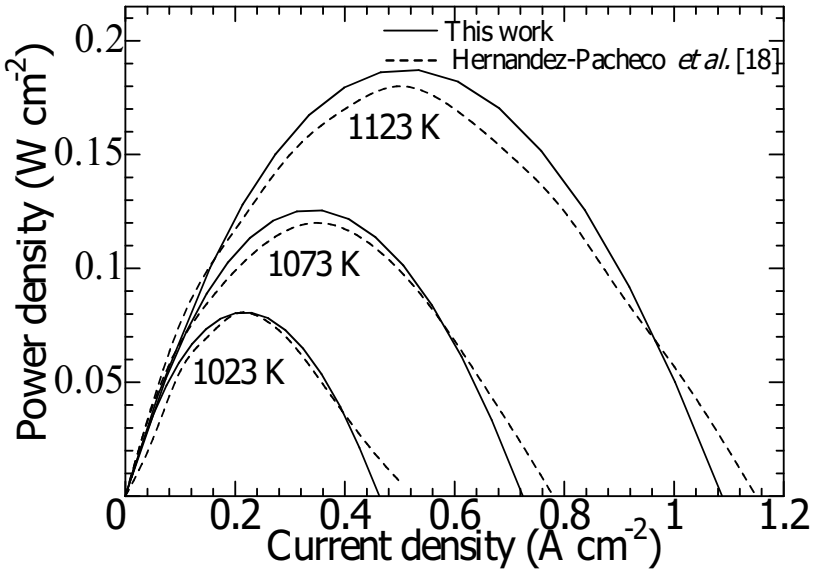

Fig. 3. Validation of SOFC model with results from the literature [18] (pure H_2 feed and U_f = 80%).

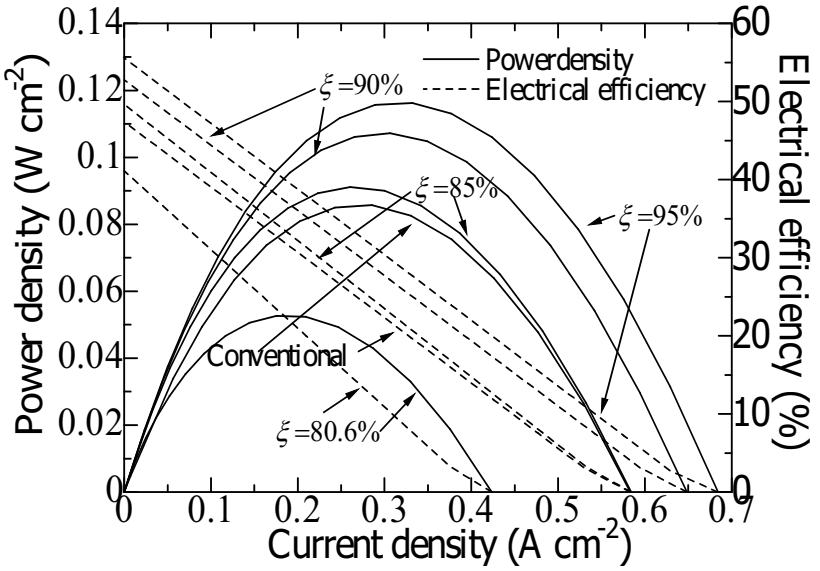

Fig. 4. Improvement of SOFC performance by using Pd membrane reactor (U_f =80% and T = 1073 K).

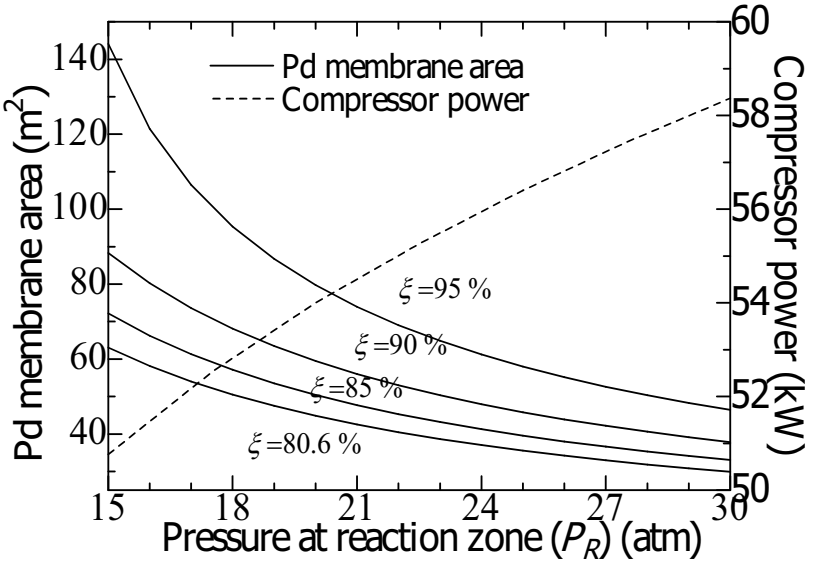

Fig. 5. Effect of reaction pressure on required Pd membrane area and compressor power (T = 773 K, P_R = 1 atm and H_2O:CH_4 = 3).

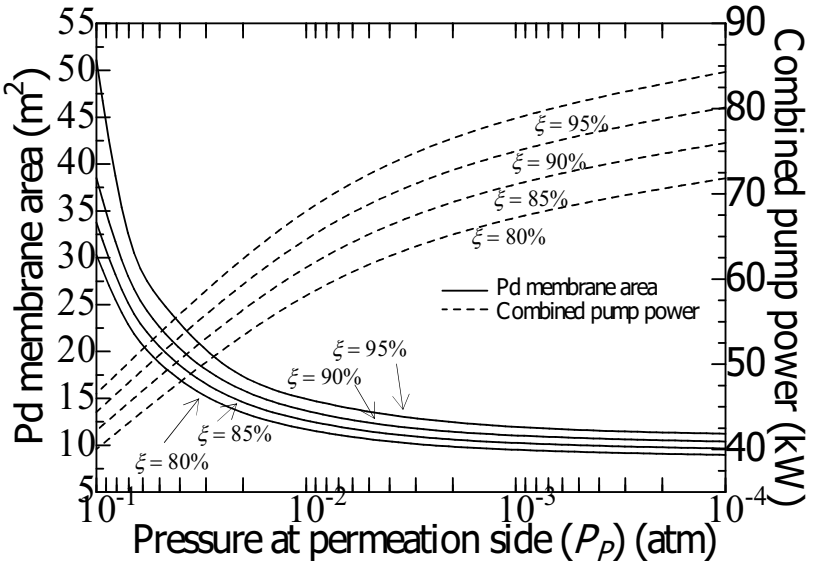

Fig. 6. Effect of permeation pressure on required Pd membrane area and vacuum pump power (T = 773 K, P_P = 1 atm and $H_2O:CH_4$ = 3).

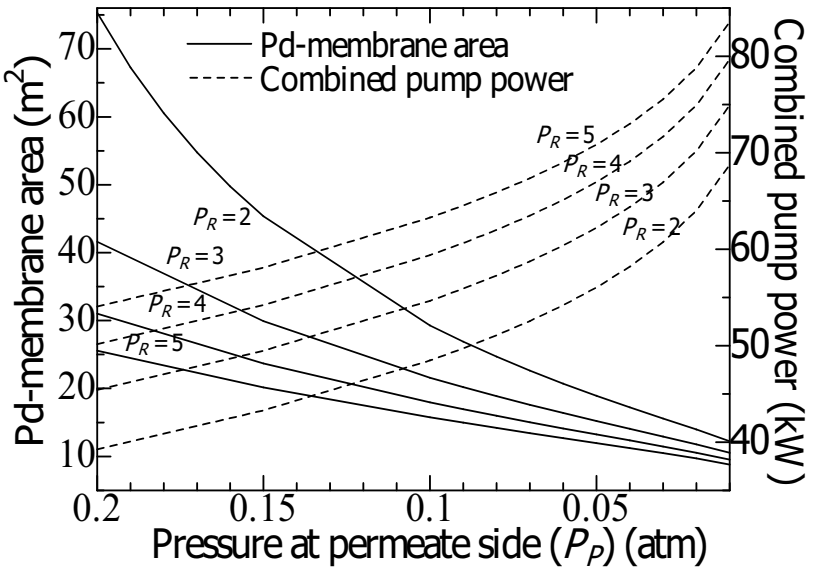

Fig. 7. Effect of reaction and permeation pressure on required Pd membrane area and power consumption (ξ = 90%, T = 773 K and $H_2O:CH_4$ = 3).

(a)

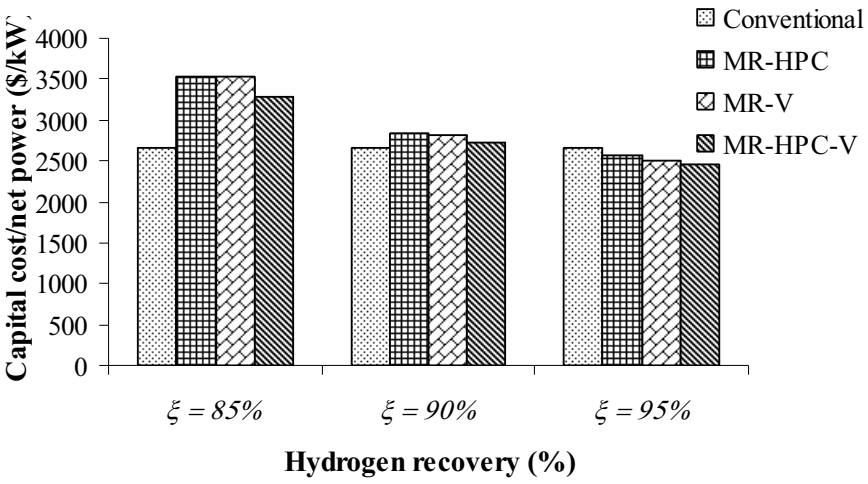
Capital cost/net power ($/kW)
4000
3500
3000
2500
2000
1500
1000
500
0
Conventional
MR-HPC
MR-V
MR-HPC-V
ξ = 85%
ξ = 90%
ξ = 95%
Hydrogen recovery (%)

(b)

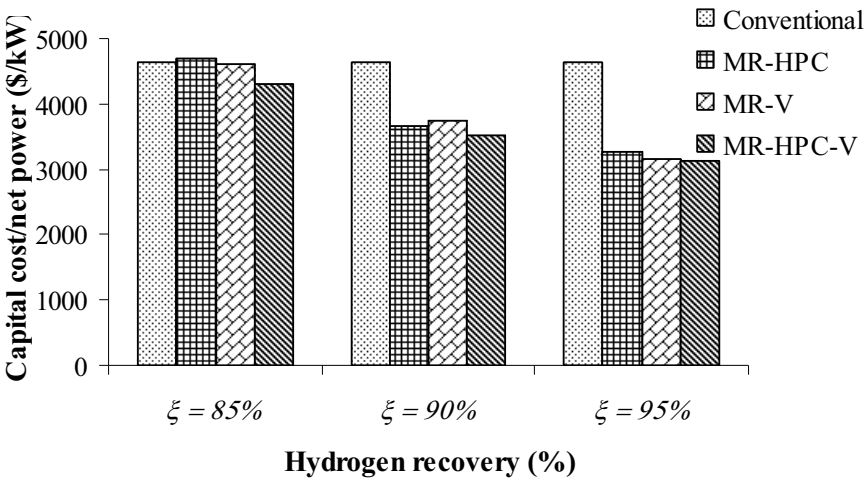
Capital cost/net power ($/kW)
5000
4000
3000
2000
1000
0
Conventional
MR-HPC
MR-V
MR-HPC-V
ξ = 85%
ξ = 90%
ξ = 95%
Hydrogen recovery (%)

(c)

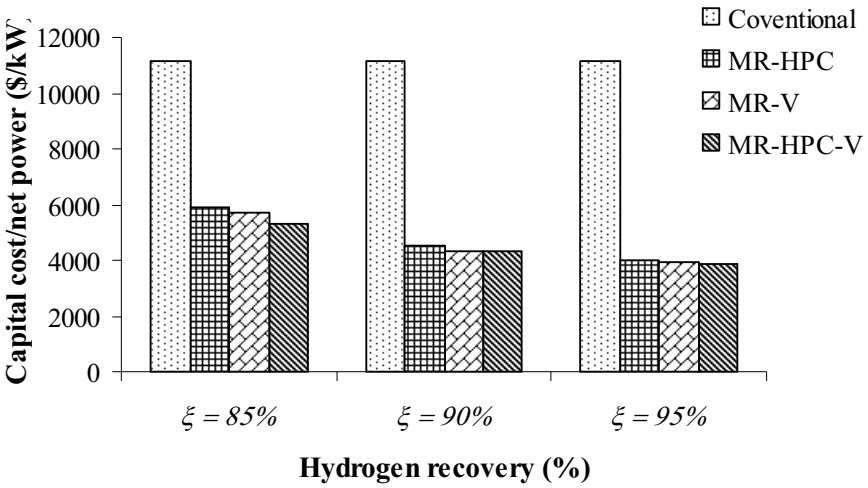

Fig. 8. Economic analysis of different SOFC systems: (a) $\eta = 40.7\%$, (b) $\eta = 45.3\%$ and (c) $\eta = 47.7\%$ (U_f= 80% and T = 1073 K).

Table(s)

Table 1 Kinetic parameters for methane steam reforming [16].

Parameter	Pre-exponential factor (A or B)	E or ΔH (kJ.mol^{-1})
k_1	4.225×10^{15} (mol atm$^{0.5}$ (g h)$^{-1}$)	240.10
k_2	1.955×10^{6} (mol (g h)$^{-1}$)	67.13
k_2	1.020×10^{15} (mol atm$^{0.5}$ (g h)$^{-1}$)	243.9
K_{CO}	6.65×10^{-4} (atm^{-1})	-38.28
K_{H2}	1.77×10^{5} (-)	88.68
K_{H2O}	6.12×10^{-9} (atm^{-1})	-82.90
K_{CH4}	8.23×10^{-5} (atm^{-1})	-70.65

Table 2 Ohmic polarization constants for Eqs.(18) and (19).

	a	b	δ (μm)
Anode	2.98×10^{-5}	-1392	50
Cathode	8.11×10^{-5}	600	50
Electrolyte	2.94×10^{-5}	10350	140

Table 3 Standard condition.

Parameter	Value
CH_4 input	1 (mol/s)
Reformer input H_2O:CH_4 ratio	3 (-)
U_f (fuel utilization)	80 (%)
Temperature of SOFC	1073 (K)
SOFC input Air:CH_4 ratio	15 (-)
Temperature of conventional reformer	973 (K)
Temperature of membrane reactor	773 (K)
Pressure of conventional reformer	1.5 (atm)
Pressure of SOFC	1 (atm)

Table 4 Economic analysis of the SOFC systems with different operation modes.

	Conventional	MR-HPC	MR-V	MR-HPC-V
Temperature of reformer (K)	923	773	773	773
Fuel utilization (U_f) (%)	80	80	80	80
H_2 Recovery (%)	-	90	90	90
Operating voltage (V)	0.610	0.696	0.691	0.692
Electrical power (kW)	376.7	429.9	426.8	427.5
Pressure at reaction side (P_R) (atm)	1.5	30	1.5	5
Compressor Power (kW)	5.3	58.4	5.3	20.3
Pressure at permeation side (P_P) (atm)	-	1.00	0.035	0.135
Vacuum pump power (kW)	-	-	50.	35.9
Net electrical power (kW)	371.4	371.4	371.4	371.4
Efficiency (%)	45.26	45.26	45.26	45.26
Pd membrane area (m^2)	-	38.17	19.12	18.76
SOFC area (m^2)	1143	866.72	877.86	843.34
Cost of Pd membrane (746 \$/m^2)	-	28,476	14,260	13,995
Cost of SOFC (1500 \$/m^2)	1,714,500	1,300,080	1,316,790	1,265,010
Saving cost on SOFC (\$)	-	414,420	397,710	449,490
Capital cost of compressor (\$)	5,979	32,194	5,979	17,200
Capital cost of vacuum pump (\$)	-	-	51,700	13,652
Saving cost of SOFC over Pd membrane (\$)	-	385,944	383,450	435,495
Total capital cost (\$)	1,720,479	1,360,750	1,388,729	1,309,857
Total capital cost/electrical energy (\$/kW)	4,568	3,166	3,254	3,064
Total Capital cost /net power (\$/kW)	4,633	3,664	3,739	3,527

Appendix 10

Elsevier Editorial System(tm) for Chemical Engineering and Processing: Process Intensification

Manuscript Draft

Manuscript Number:

Title: Performance of biogas-fed solid oxide fuel cell systems integrated with membrane module for CO2 removal

Article Type: Full Text Article

Keywords: Biogas; CO2-selective membrane; Solid oxide fuel cell; Thermodynamic analysis; Economic analysis

Corresponding Author: Professor Suttichai Assabumrungrat, Ph.D.

Corresponding Author's Institution: Chulalongkorn University

First Author: Pakorn Piroonlerkgul , B.Eng.

Order of Authors: Pakorn Piroonlerkgul , B.Eng.; Suttichai Assabumrungrat, Ph.D.; Navadol Laosiripojana , PhD; Adesoji A Adesina, PhD

Abstract: Two SOFC systems with CO2 capture, i.e., SOFC with CO2 capture from biogas feed (biogas-cap SOFC) and SOFC with CO2 capture from reformed gas (reformed gas-cap SOFC) have been investigated. Employing the sweep gas to increase the gas separation capability, both systems offered higher power density but lower electrical efficiency than those of the SOFC without CO2 capture (non-cap SOFC). The installation of a vacuum pump can improve the electrical efficiency of the biogas-cap SOFC but not for the reformed gas-cap SOFC. Economic analysis revealed that the biogas-cap SOFC with sweep gas is superior to the other SOFC systems.

Department of Chemical Engineering
Faculty of Engineering
Chulalongkorn University

Professor A. Górak
Technische Universität Dortmund, Chair of Fluid Separations,
Department of Biochemical and Chemical Engineering,
Emil-Figge-Strasse 70, D-44227 Dortmund,
Germany,
Email: Gorak.CEP@ct.uni-dortmund.de

April 2, 2008

Dear Professor Górak,

I would like to submit a research article entitled "Performance of biogas-fed solid oxide fuel cell system integrated with membrane module for CO_2 removal" for your consideration for inclusion in Chemical Engineering and Processing: Process Intensification. The article is original and unpublished and is not being considered for publication elsewhere.

The paper investigates improvement in the performance of SOFC system by incorporation of a CO_2-selective membrane separation unit via engineering and economic analyses. Different integration configurations have been considered in order to explore an appropriate choice and benefits of the integration.

If you have any query, please do not hesitate to contact me. I am looking forward to hearing from you.

Sincerely yours,

(Professor Suttichai Assabumrungrat)
Department of Chemical Engineering, Faculty of Engineering,
Chulalongkorn University, Bangkok 10330, Thailand
Tel: 662-2186878-82; fax:662-2186877
E-mail: Suttichai.A@chula.ac.th

List of Suggested Reviewers

1. Professor You, H.-X.; Chemical Engineering College, Dalian University of Technology, Dalian 116012, China; email:youhx@sina.com

2. Professor Diwekar, U.M.; Vishwamitra Research Institute, Center for Uncertain Systems, Tools for Optimization and Management, 34, N.Cass Ave., Westmont, IL 60607, United States; email:urmila@vri-custom.org

Submitted to Chemical Engineering and Processing: Process Intensification

Type of contribution: Full text article

Performance of biogas-fed solid oxide fuel cell systems integrated with membrane module for CO_2 removal

P. Piroonlerkgul [a], S. Assabumrungrat [a,*], N. Laosiripojana [b] and A.A. Adesina [c]

[a] Center of Excellence in Catalysis and Catalytic Reaction Engineering,
Department of Chemical Engineering, Faculty of Engineering, Chulalongkorn University,
Bangkok 10330, THAILAND

[b] The Joint Graduate School of Energy and Environment,
King Mongkut's University of Technology Thonburi, Bangkok 10140, THAILAND

[c] Reactor Engineering & Technology Group,
School of Chemical Sciences & Engineering, University of New South Wales,
Sydney, NSW, Australia 2052

Corresponding author (FAX: 662-218-6877, Email: Suttichai.A@chula.ac.th)

Abstract

Two SOFC systems with CO_2 capture, i.e., SOFC with CO_2 capture from biogas feed (biogas-cap SOFC) and SOFC with CO_2 capture from reformed gas (reformed gas-cap SOFC) have been investigated. Employing the sweep gas to increase the gas separation capability, both systems offered higher power density but lower electrical efficiency than those of the SOFC without CO_2 capture (non-cap SOFC). The installation of a vacuum pump can improve the electrical efficiency of the biogas-cap SOFC but not for the reformed gas-cap SOFC. Economic analysis revealed that the biogas-cap SOFC with sweep gas is superior to the other SOFC systems.

Key words: Biogas; CO_2-selective membrane; Solid oxide fuel cell; Thermodynamic analysis; Economic analysis

1. Introduction

In view of current and foreseeable energy shortage and environmental scenario, the exploitation of a renewable energy sources has attracted much attention in recent literature. Biogas is one of the renewable energy sources derived from the processing of the waste streams with variable nature, e.g. farm residues, industrial effluents and landfill. Compared to fossil fuel, biogas offers advantages of being renewable and free of non-methane hydrocarbon. A general problem found in the utilization of biogas for electricity generation is that most of biogas is derived from small-scale sources, e.g. farm and municipal wastes, therefore, biogas can only be employed in a small size power generator (5-100 kW) [1]. Furthermore, the biogas composition fluctuates markedly depending on its sources [2]; it generally contains methane (40-65%) and carbon dioxide (30-40%) with small amount of H_2S as an impurity.

The solid oxide fuel cell (SOFC) is a promising electricity generation technology owing to its high performance and environmentally-friendly operation. SOFC fuelled by biogas can offer high efficiency (30-40%) even in small size power generations (< 20 kW) [1]. Additionally, it can achieve reasonable performance even at low methane contents in biogas. Laboratory tests suggest that, the SOFC electrical efficiency drops only 5% when the methane contents in biogas diminish from 70 mol% to 30 mol% [3]. Moreover, biogas can be internally-reformed in SOFC stack due to the typical high stack temperature (1073-1273 K). However, if biogas is directly fed into the SOFC stack, carbon deposition can easily occur [4], in addition, a large temperature gradient is also a major problem for the SOFC stack fed directly by biogas due to a strong cooling effect caused by the fast reforming reaction [5, 6]. A fuel processor is normally installed in the biogas-fuelled SOFC system to relieve these problems. Our recent work has shown that the addition of excess steam, CO_2 or air can inhibit the carbon formation in the fuel

processor [7]. The use of steam as the reforming agent in the fuel processor (steam reforming) offers higher performance for SOFC system compared with the use of air (partial oxidation) [8]. Nevertheless, with an increase in CO_2 content in biogas, the H_2 yield of the pre-reformer reduces due to the reaction between CO_2 and H_2 generated from the steam reforming reaction via Reverse water gas shift reaction, RWGS. The decrease in H_2 concentration in the reformed gas can diminish the power density and the investment cost also increase due to the enlargement in the SOFC stack size [9]. Furthermore, the presence of large amounts of CO_2 in the pre-reforming product can decrease the cell potential. Suwanwarangkul et al. [10] studied the performance of SOFC fuelled by the mixture of H_2 and CO_2 gases with several H_2/CO_2 ratios. They reported that when H_2 concentration decreases from 100% to 20%, the SOFC cell potential decreases by 20% due to the impact of the RWGS reaction. Hence, the separation of CO_2 from the biogas feed or from the reformed gas is the interesting way to increase the biogas-fuelled SOFC system performance.

Currently, there are various available CO_2 separation technologies e.g. chemical absorption, adsorption and membrane technology. Membrane technology has been widely tested and presently applicable in the capture of CO_2 in natural gas [11]. Compared with CO_2 absorption technology which is conventionally used, membrane technology offers the advantages of operational flexibility in handling feed streams with variable flow rates and compositions. Polymeric membrane is one of the interesting choices due to its low capital investment costs compared with other types of membrane [12]. Moreover, the process equipment for the polymeric membrane operation is also simple and easy to handle. Selection of polymeric membrane for gas separation is based on two parameters; permeability and permselectivity. Polyimide membrane is the more attractive gas separator because it offers higher permselectivity and permeability

compared to membranes derived from other polymers [13]. The use of capillary module with polyimide membrane for the CH_4 enrichment in biogas mixtures (CH_4, CO_2 and H_2S) was also investigated and the results showed that CH_4 concentration in biogas increases from 55-85% up to 91-94.4% [14]. Poly(dimethylsiloxane) (PDMS) and poly(1-trimethylsilyl-1-propyne) (PTMSP) can be utilized in the separation of acid gases (CO_2 and H_2S) from syngas at room temperature due to their high CO_2/H_2 selectivity. Nonetheless, H_2 permeance increases at elevated temperature [15]. It should be noted that a common problem arising from the use of these polymeric membranes is the instability of the membranes at high operating temperature [16].

In the present study, an integration of a biogas-fuelled SOFC system and CO_2-selective membrane technology was investigated. The improvement in the SOFC power density following to the installation of CO_2-selective membrane was considered. Two configurations are applied in this study: 1) SOFC with the capture of CO_2 from the biogas feed (biogas-cap SOFC) and 2) SOFC with the capture of CO_2 from the reformed gas (reformed gas-cap SOFC). Furthermore, two available operation modes in the permeation side of membrane i.e. the exploitation of sweep gas and the exploitation of vacuum pump were also investigated. Thermodynamic analysis was performed to evaluate the performance indicators (overall electrical efficiency and power density) of these configurations and operations and to compare them with those of the SOFC system without CO_2-selective membrane installation. Lastly, an economic analysis was employed to identify whether the CO_2-selective membrane should be installed into the SOFC system.

2. Modeling

2.1 Fuel processor

The key steps are the dry reforming (Eq.(1)) and the steam reforming (Eq.(2)) reactions.

$$CH_4 + CO_2 \leftrightarrow 2H_2 + 2CO \quad (1)$$

$$CH_4 + H_2O \leftrightarrow 3H_2 + CO \quad (2)$$

Due to the high CO_2 concentration in biogas feed, the mildly endothermic reverse water gas shift reaction (RWGS) (Eq.(3)) also takes place in the fuel processor inhibiting the generation of hydrogen.

$$CO_2 + H_2 \leftrightarrow H_2O + CO \quad (3)$$

To simplify the calculations, the fuel processor is assumed to operate isothermally with the exit gas reaching equilibrium composition. The relevant thermodynamic equilibrium constants for the dry reforming, steam reforming and RWGS are provided in Eqs. (4), (5) and (6), respectively.

$$K_{eq,dry} = \frac{P_{H_2}^2 P_{CO}^2}{P_{CH_4} P_{CO_2}} \quad (4)$$

$$K_{eq,steam} = \frac{P_{H_2}^3 P_{CO}}{P_{CH_4} P_{H_2O}} \quad (5)$$

$$K_{eq,RWGS} = \frac{P_{H_2O} P_{CO}}{P_{H_2} P_{CO_2}} \quad (6)$$

where $K_{eq,i}$ is the equilibrium constant of reaction i and may be calculated from:

$$K_{eq,i} = e^{-\frac{\Delta G_i}{RT}} \quad (7)$$

2.2 SOFC stack model

Electrochemical reactions taking place in the SOFC stack convert the chemical energy of the fuel directly to electricity. At the cathode section, oxygen is reduced to oxygen ions (Eq.(8)) which migrates through the solid electrolyte to react with the fuel (Eq.(9)) at the anode section. Only hydrogen is assumed to react electrochemically with oxygen ions since the H_2 electro-oxidation is much faster than the CO electro-oxidation [17] and the rate of WGS reaction is fast at high temperatures [18-20]. It is also assumed that methane remaining from the fuel processor is consumed via the steam reforming and that the anode gas compositions are always at their equilibrium along the cell length due to the fast kinetics particularly at high temperature of SOFC. It is noted that Ni-YSZ, YSZ and LSM-YSZ are chosen as the materials for the anode, electrolyte and cathode of the SOFC stack, respectively.

$$\frac{1}{2}O_2 + 2e^- \longrightarrow O^{2-} \quad (8)$$

$$H_2 + 2O^{2-} \longrightarrow H_2O + 2e^- \quad (9)$$

The open circuit voltage (E) of the cell can be calculated from the following Nernst equation:

$$E = E^0 + \frac{RT}{2F}\ln\left(\frac{P_{H_2}P_{O_2}^{\frac{1}{2}}}{P_{H_2O}}\right) \quad (10)$$

The actual cell potential (V) (Eq. (11)) is always less than the open circuit voltage (E) due to the existence of various overpotentials; i.e., ohmic overpotential (η_{ohm}), activation overpotential (η_{act}) and concentration overpotential (η_{conc}).

$$V = E - \eta_{ohm} - \eta_{act} - \eta_{conc} \quad (11)$$

2.2.1 Ohmic overpotential (η_{Ohm})

The ohmic overpotential is the resistance to flow of electron through the electrodes and the interconnectors as well as resistance to the flow of ions through electrolyte. This voltage drop is the vital one in all types of cells and is linearly proportional to current density (*i*). Due to the higher electronic conductivity of the electrodes and interconnectors compared to the electrolyte, only ohmic overpotential in the electrolyte is considered. The ohmic overpotential of SOFC may be expressed as [21]:

$$\eta_{ohmic} = 2.99 \times 10^{-11} iL \exp\left(\frac{10300}{T}\right) \quad (12)$$

2.2.2 Activation overpotential (η_{Act})

Activation overpotential is controlled by the kinetics at the electrode surface. It is directly related to the activation barrier and to be overcome by the reacting species in order to conduct the electrochemical reaction. For SOFC, due to the high temperature, the electrode reaction rate is fast, resulting in low activation polarization. The activation overpotentials in electrodes can be expressed by the Butler-Volmer equation,

$$i = i_0\left[\exp\left(\frac{\alpha z F \eta_{act}}{RT}\right) - \exp\left(-\frac{(1-\alpha) z F \eta_{act}}{RT}\right)\right] \quad (13)$$

In case of SOFC, α and *z* are set to 0.5 and 2 [22]. Therefore, the activation potential at the anode and cathode can be explicitly written as:

$$\eta_{act,j} = \frac{RT}{F} \sinh^{-1}\left(\frac{i}{2i_0}\right), \qquad j = a, c \quad (14)$$

It should be noted that the exchange current density (i_0) for the cathode side depends on partial pressure of both hydrogen and water as well as the operating temperature [23, 24]. For the anode side, i_0 depends on oxygen partial pressure and operating temperature as expressed in Eqs. (15)-(16) [25].

$$i_{0,a} = \gamma_a \left(\frac{P_{H_2}}{P_{ref}}\right)\left(\frac{P_{H_2O}}{P_{ref}}\right)\exp\left(-\frac{E_{act,a}}{RT}\right) \quad (15)$$

$$i_{0,c} = \gamma_c \left(\frac{P_{O_2}}{P_{ref}}\right)^{0.25}\exp\left(-\frac{E_{act,c}}{RT}\right) \quad (16)$$

2.2.3 Concentration overpotential (η_{Conc})

The concentration overpotential is the electrical loss arising from the difference between the reactant concentration on the reaction site and that in the bulk of the gas stream. It may be calculated from Eqs. (17) and (18):

$$\eta_{Conc,a} = \frac{RT}{2F}\ln\left[\frac{\left(1+\left(\frac{RT}{2F}\right)\left(\frac{l_a}{D_{a(eff)}p^I_{H_2O}}\right)i\right)}{\left(1-\left(\frac{RT}{2F}\right)\left(\frac{l_a}{D_{a(eff)}p^I_{H_2}}\right)i\right)}\right] \quad (17)$$

$$\eta_{Conc,c} = \frac{RT}{4F}\ln\left[\frac{p^I_{O_2}}{\left(p_c-\delta_{O_2}\right)-\left(\left(p_c-\delta_{O_2}\right)-p^I_{O_2}\right)\exp\left[\left(\frac{RT}{4F}\right)\left(\frac{\delta_{O_2}l_c}{D_{c(eff)}p_c}\right)i\right]}\right] \quad (18)$$

where δ_{O_2}, $D_{a(eff)}$ and $D_{c(eff)}$ are given as:

$$\delta_{O_2} = \frac{D_{O_2,k(eff)}}{D_{O_2,k(eff)}+D_{O_2-N_2(eff)}} \quad (19)$$

$$\frac{1}{D_{c(eff)}} = \frac{\xi}{n}\left(\frac{1}{D_{O_2,k}}+\frac{1}{D_{O_2-N_2}}\right) \quad (20)$$

$$D_{a(eff)} = \left(\frac{p_{H_2O}}{p_a}\right) D_{H_2(eff)} + \left(\frac{p_{H_2}}{p_a}\right) D_{H_2O(eff)} \quad (21)$$

$$\frac{1}{D_{H_2(eff)}} = \frac{\xi}{n}\left(\frac{1}{D_{H_2,k}} + \frac{1}{D_{H_2-H_2O}}\right) \quad (22)$$

$$\frac{1}{D_{H_2O(eff)}} = \frac{\xi}{n}\left(\frac{1}{D_{H_2O,k}} + \frac{1}{D_{H_2-H_2O}}\right) \quad (23)$$

The relationship between the effective diffusivity and the molecular diffusivity, $D_{A\text{-}B}$, is:

$$D_{(eff)} = \frac{n}{\xi} D_{A-B} \quad (24)$$

Knudsen diffusivity, $D_{A,K}$, may be estimated from:

$$D_{A,K} = 9700 r_p \sqrt{\frac{T}{M_A}} \quad (25)$$

The molecular diffusivity may be obtained from Chapman-Enskog equation (Eq. (26)) [26]:

$$D_{A-B} = 1.8583 \times 10^{-3} \left(\frac{T^{\frac{3}{2}} \left(\frac{1}{M_A} + \frac{1}{M_B}\right)^{\frac{1}{2}}}{P \sigma_{AB}^2 \Omega_D} \right) \quad (26)$$

where σ_{AB} is the collision diameter (Å) which is equal to $\frac{\sigma_A + \sigma_B}{2}$. Ω_D is computed from Eq. (27) below [27]:

$$\Omega_D = \frac{A}{T_k^B} + \frac{C}{\exp(D \cdot T_k)} + \frac{E}{\exp(F \cdot T_k)} + \frac{G}{\exp(H \cdot T_k)} \quad (27)$$

where T_k is equal to $\frac{T}{\varepsilon_{AB}}$ and A, C, E and G are constants for each gas.

2.3 Membrane Module

A membrane module for CO_2 removal is installed in the SOFC system. Fig. 1 shows the configuration of the membrane tube. Feed gas containing CO_2 is introduced to the inner side of the membrane, where pressure is maintained at 1.5 atm and negligible axial pressure gradient is assumed. To enhance the rate of CO_2 removal, the partial pressure of CO_2 was reduced by introducing a sweep gas (air) or using a vacuum pump at the shell side of the membrane. Steady-state mass balances in both tube and shell sides of the membrane provide:

$$\frac{dR_i}{dA} = -\frac{p_i}{\delta}\left(P_R x_i - P_P y_i\right) \quad (28)$$

$$\frac{dPe_i}{dA} = \frac{p_i}{\delta}\left(P_R x_i - P_P y_i\right) \quad (29)$$

In this study, 6FDA-DAT polyimide is chosen for the separation of CO_2 from the biogas feed due to its high CO_2/CH_4 selectivity [28], whereas PDMS (polydimethylsiloxane) membrane is employed to separate CO_2 from the reformed gas due to its high CO_2/H_2 selectivity [29]. According to the high-temperature instability of membrane, the operating temperature of 298 K is assumed for these membrane modules. The values of parameter used in the calculation for the membrane module are summarized in Table 1.

2.4 Afterburner and heat exchanger

At the outlets of the SOFC stack, the anode and cathode exhaust gases are mixed for the post combustion. Total combustion is presumed in the afterburner; hence methane, carbon monoxide and hydrogen contents in the flue gas are assumed to be zero. The heat obtained is then supplied to several heat-demanding units in the SOFC system such as

feed preheaters and fuel processor. All the heat exchangers are assumed to operate without heat loss in this study.

2.5 Vacuum pump and compressor

For the calculations of vacuum pump and compressor, the outlet gas temperature (T_{out}) and power consumption ($\dot{W}_{comp}$) can be estimated by employing Eqs. (30) and (31), respectively [30]. The efficiency (η_c) of 75% is assumed in this study.

$$T_{out} = T_{in}\left(1+\frac{1}{\eta_c}\left(\left(\frac{P_{out}}{P_{in}}\right)^{\frac{\gamma-1}{\gamma}}-1\right)\right) \tag{30}$$

$$\dot{W}_{comp} = -\dot{m}\int_{T_{in}}^{T_{out}} C_p dT \tag{31}$$

where $$\gamma = \frac{C_p}{C_p - R}. \tag{32}$$

2.6 Calculation procedure for determining SOFC stack performance

For the SOFC operation, a constant operating voltage (V) along the cell length is assumed due to the high electrical conductivity of the current collector. The operating voltage is kept at 0.7 V in this study. The quantity of air fed as the oxidant into the SOFC cathode is 4 times that of theoretical amount required to combust the biogas fuel. Due to the changes in gas compositions along the cathode and anode sections, the open circuit voltage and consequently the current density vary with the distance from the stack entrance. In this work, the calculation takes place for each small fuel utilization region employing the mathematical model presented in Section 2.2. The thermodynamic equilibrium is assumed for the anode gas in each region because the anode material is also active for the reactions and the operating temperature of the SOFC stack is high. In each region, the open circuit voltage, overpotentials, equilibrium composition of anode fuel, stack area and current density are calculated. The stack areas calculated in each region are added up to yield the total stack area. Finally, the current calculated from the fuel utilized in the stack is divided by the total stack area to obtain the average current density, and the average power density can be then determined. The electrical efficiency and the fuel utilization are computed from Eqs. (33) and (34), respectively.

$$SOFC\ plant\ efficiency = \frac{net\ electricity\ generated}{LHV\ of\ biogas\ feed} \quad (33)$$

$$Fuel\ utilization = \frac{total\ H_2\ consumed\ in\ SOFC\ stack}{Inlet\ molar\ flow\ rate\ of\ H_2\ and\ CO} \quad (34)$$

2.7 SOFC system configurations

Two biogas-fed SOFC systems with CO_2 capture unit are proposed in this study, i.e. the SOFC system with the CO_2 capture from the biogas (biogas-cap SOFC) and the SOFC system with the CO_2 capture from the reformed gas (reformed gas-cap SOFC). The SOFC system without CO_2 capture unit (non-cap SOFC) is also considered as a base case for comparison. Fig. 2 shows the plant configuration of the non-cap SOFC. Several unit operations such as pre-reformer, SOFC stack, an afterburner, a mixer, a vaporizer and preheaters are included in this configuration. Steam is generated in the vaporizer, preheated and then mixed with biogas. The gas mixture is fed into the fuel processor where the steam reforming, dry reforming and WGS take place. The obtained H_2-rich gas is then fed into the SOFC stack where the electrical energy is generated. The isothermal condition is assumed for the SOFC stack to simplify the computation. The heat generated in the SOFC stack from the irreversibility is utilized for air and H_2-rich gas preheating. To achieve a desired temperature of the SOFC stack, an oxidizing agent (air) temperature is tuned up, employing the energy balance of the SOFC stack. The residue fuel gas released from the SOFC stack is burned up in the afterburner in order to supply heat to the pre-heaters, fuel processor and vaporizer. The flue gas is set to be released from the system at 473 K. The total heat requirement for the SOFC system is computed and a trial-and-error is performed by tuning the fuel utilization until the total heat requirement for the system is equal to the total heat generation from the system ($\sum_i Q_{endo,i} = \sum_j Q_{exo,j}$).

Considering the SOFC systems with CO_2 capture unit, their configurations are almost identical to that of the non-cap SOFC system. However, for the biogas-cap SOFC (Fig. 3), biogas is compressed and then fed into the polyimide membrane module where CO_2 is captured. The sweep gas (air) is also fed into the permeate side in order to decrease the gas partial pressure. The retentate gas is preheated and then fed into the fuel

processor whereas the permeate gas is fed into the selective oxidation unit prior to being released into the environment. For the reformed gas-cap SOFC (Fig. 4), biogas is compressed and fed into the fuel processor. The reformed gas is cooled down to the membrane operating temperature (298 K) at which water is condensed and removed from the gas stream. In the membrane module, CO_2 is captured and the retentate gas is heated and then fed into the SOFC stack, while the permeate gas (CO_2-rich gas) is burned in selective oxidation unit (this unit is not considered in this study) before being released into the environment.

The exploitation of a vacuum pump as another alternative for improving driving force of CO_2 removal is also investigated and its basic working is illustrated in Fig. 5. The high temperature permeate gas released from the vacuum pump can be fed directly into the afterburner, while the retentate gas is fed into the SOFC stack. The advantage of this operation mode is that the permeate gas can be subsequently utilized to generate heat in the afterburner regardless of the dilution effect of the sweep gas.

3. Results and Discussion

In the present work, all models of the SOFC systems are written in Visual Basic. The values of all parameters used in the calculations are given in Table 2. The study starts with the model validation of the SOFC stack. Our previous work [8] demonstrated that the model is a good predictor of the performance curves of the SOFC stack fed by a mixture of hydrogen (97%) and water (3%). In this work, the model is further verified with the simulation results for the case with a lower concentration of hydrogen. Based on the condition listed in Table 3, the results shown in Table 4 indicate that the calculation results from our model are in good agreement with those from the literature [31]. This strengthens confidence in the reliability of the model for SOFC. Then, the model of CO_2

separation by membrane is verified. The feed conditions and the parameters used in the model are summarized in Table 5. Again, our results show good agreement with those reported in the literature [29] as illustrated in Fig. 6.

Prior to the SOFC system investigation, the performance of membrane modules for CO_2 separation was examined. The flow rates and compositions of the feed gases are summarized in Table 6. The feed gas composition for the polyimide membrane is based on a raw biogas, whereas that for the PDMS membrane is based on a reformed gas after water removal. The $\%CO_2$ removal and $\%CH_4$ or H_2 loss at different membrane areas and sweep gas to feed gas ratios are summarized in Fig. 7. It is obvious that the increases in membrane area and sweep gas to feed gas ratio can raise the extent of CO_2 removal. At membrane area of 50 m^2 and sweep gas to feed gas ratio of 4, polyimide and PDMS membranes can remove 80 and 90% of CO_2 in the feed gases, respectively. However, some CH_4 (4%) and a large extent of H_2 (55%) also permeate together with CO_2 through polyimide and PDMS membrane, respectively, into the permeate side. It should be noted that the permeate gases cannot be fed into the afterburner for heat utilization due to the dilution of sweep gas (air); and a selective oxidation unit is required before releasing the gas to the environment. Subsequently, the sweep gas to feed gas ratio was fixed at 4.

Following these preliminary runs, the performance of the biogas-fed SOFC systems is then investigated. Figs. 8(a) and 8(b) show the electrical efficiency and power density of the biogas-cap SOFC system and reformed gas-cap SOFC system, respectively. It is clear that the electrical efficiency decreases with increasing membrane area due to the high loss of CH_4 or H_2 in the permeate gas. However, it is evident that the increase in membrane area for CO_2 removal can improve the power density of the SOFC stack since higher H_2 concentration in the SOFC feed gas is achieved. Compared to the non-cap SOFC system (dashed lines), both biogas-cap SOFC and reformed gas-cap

SOFC offer lower electrical efficiency due to the CH_4 or H_2 loss; however, their power densities are always higher. The electrical efficiency of the reformed gas-cap SOFC is lower than that of the biogas-cap SOFC because the CO_2/H_2 selectivity of PDMS membrane is much lower than the CH_4/H_2 selectivity of the polyimide membrane, resulting in higher loss of fuel in the SOFC feed for the reformed gas-cap SOFC.

To improve the electrical efficiency of the biogas-cap SOFC and reformed gas-cap SOFC, the benefit from the installation of vacuum pump is then studied in order to reduce the operating pressure at the membrane permeate side. The basic working scheme of the membrane module with a vacuum pump is shown in Fig. 5. Under this operation mode, the sweep gas is not required because the partial pressure of each gas component is sufficiently low. Hence, without the dilution by the sweep gas, the permeate gas can be fed into the afterburner and produced more heating energy for the system. It should be noted that as described earlier in Section 2.7, the fuel utilized in the SOFC stack is adjusted to meet the condition at which the endothermic heat required in the system is satisfied by the exothermic heat obtained from the afterburner. Therefore, it is expected that the use of the vacuum pump would offer a higher electrical efficiency. Nevertheless, large amount of electrical energy consumption for operating with the vacuum pump needs to be taken into account.

Fig. 9 shows the $\%CO_2$ removal and $\%CH_4$ or H_2 loss for different membrane areas and different pressures at the permeate side. The lowering of pressure at the permeate side offers similar effect as the increase of the sweep gas to feed gas ratio. Compared with Fig. 7, it is observed that when operated with the vacuum pump at 0.1 bar, the values of $\%CO_2$ removal and $\%CH_4$ or H_2 loss are similar to those of the case with the sweep gas to feed gas ratio of 4 for the same membrane area. Considering the biogas-cap SOFC with vacuum pump installation, the increase in membrane area and

decrease in membrane permeate side pressure can improve the electrical efficiency as illustrated in Fig. 10. This result is in good agreement with that of our recent work [8] indicating that the split of a part of biogas feed from the fuel processor for direct feeding to the afterburner can improve the electrical efficiency by reducing the heat load in the SOFC system. The results also reveal that within some operating ranges, the electrical efficiency of the biogas-cap SOFC operating with high membrane area becomes higher than that of the non-cap SOFC. The power density of the biogas-cap SOFC with vacuum pump installation is always higher than that of the non-cap SOFC. The increase in membrane area diminishes the power density at high values of permeate side pressure (> 0.3 bar) since the effect of methane loss overshadows the benefit of CO_2 removal. An optimum membrane area which provides a maximum power density is observed at low permeate side pressure due to competing effects between the increase in the methane loss and the promotion in CO_2 removal. With the identical membrane area, the biogas-cap SOFC offers the lowest power density when the permeate side pressure is at 0.7 bar. As membrane permeate side pressure is lower than 0.7, the decrease in permeate side pressure can improve the power density due to the significant increase in CO_2 removal.

Considering the reformed gas-cap SOFC with vacuum pump installation, the operation at which the endothermic energy is equal to the exothermic energy cannot be achieved at high membrane area and low membrane permeate side pressure because the heating energy generated is higher than the heat load in SOFC system as shown in Fig. 11a. It should be noted that the fuel utilization is always controlled to be lower than 95% to achieve reasonable power density. The maximum electrical efficiency that the reformed gas-cap SOFC can achieve is 49.37% which is lower than that of the non-cap SOFC. Considering only the condition that the optimal operation can be achieved, the increase in membrane area and the decrease in permeate side pressure do not improve the

power density, implying that the effect of H_2 loss always overshadows the effects of CO_2 removal. However, it still offers higher power density than the non-cap SOFC; probably due to the effect of water removal which increases the H_2 concentration in the SOFC feed gas.

In summary, the operation of the reformed gas-cap SOFC offers extremely lower electrical efficiency (less than 40%) compared with that of the non-cap SOFC. Moreover, large heat exchanger area is also required to cool down the reformed product to the membrane operating temperature and reheat to the SOFC operating temperature. In addition, there is no benefit obtained from the installation of vacuum pump in the reformed gas-cap SOFC system. These clearly indicate that the reformed gas-cap SOFC is not a good choice for the SOFC system. For the biogas-cap SOFC, even if it can offer higher power density compared with the non-fed SOFC, its electrical efficiency is lower than that of the non-fed SOFC when operating with the sweep gas mode. The installation of the vacuum pump to the biogas-cap SOFC can offer comparable or even higher electrical efficiency compared to that of the non-cap SOFC; however, the improvement of the power density over that of the non-cap SOFC becomes smaller compared to the case with the sweep gas mode. Therefore, it is difficult to identify which operation mode can provide utmost performance for the SOFC system among non-cap SOFC, biogas-cap SOFC with sweep gas and biogas-cap SOFC with vacuum pump installation.

In order to determine a suitable SOFC system, the economic analysis called "incremental analysis" is employed for the investigation. This method considers only the cost difference between the base case and the interested case. The non-cap SOFC is considered as the base case in this study. There are five costs considered in this study: SOFC stack cost, membrane module and replacement cost, compressor cost, vacuum pump cost and biogas fuel cost. Other costs of the interested case are assumed to be

similar to those of base case. The parameters utilized in the economic analysis and the costing models for each unit operation are summarized in Tables 7 and 8, respectively. The incremental net present value (INPV) (Eq. 35) for each operation is computed as the indicator. A positive value of INPV represents that the interested case is more economically feasible than the non-cap SOFC.

$$INPV = -(capital\cos t - capital\cos t_{base}) - (annual\cos t - annual\cos t_{base})\frac{\left(1-\left(\frac{1}{1+r}\right)^{y}\right)}{r} \quad (35)$$

As shown in Fig. 12, the biogas-cap SOFC system offers the optimum INPV at a membrane area of 4 m^2 and is superior to the non-cap SOFC system when the area of polyimide membrane is less than 30 m^2 even if it can offer high power density (low SOFC active area) at high membrane area. This is due to the effect of the electrical efficiency drop and more biogas feed required for maintaining identical electrical power. Moreover, high capital cost for compressor and membrane module also reduce the possibility of the biogas-cap SOFC for operation at high membrane area. Considering the biogas-cap SOFC with vacuum pump installation, the effect of the increase in biogas feed and additional investment on the compressor, vacuum pump and membrane modules also overshadow the decrease in SOFC stack size at high polyimide membrane area. Moreover, it is not feasible to operate at very low pressure of membrane permeate side as illustrated in Fig. 13. The biogas-cap SOFC with vacuum pump installation is more feasible than the non-cap SOFC at the membrane area less than 12 m^2 for the permeate side pressure between 0.3-0.9 bar. At extremely low permeate side pressure (< 0.1 bar), the biogas-cap SOFC with vacuum pump installation is not feasible to operate at

membrane area higher than 6 m^2. This can be explained by the fact that the decrease in permeate side pressure increases the vacuum pump load and also the investment cost of vacuum pump. The economic comparison between the biogas-cap SOFC and that with vacuum pump installation is shown in Table 9. The optimum condition of each operation mode is chosen for this comparison. Both of these cases offer INPV higher than 0, indicating that they are more attractive to operate compared with the non-cap SOFC. The biogas-cap SOFC with sweep gas offers higher INPV ($5,320.21) than the biogas-cap SOFC with vacuum pump installation ($4,359.18). Even if the biogas-cap SOFC with vacuum pump installation can offer higher electrical efficiency compared with the biogas-cap SOFC, the cost of vacuum pump suppresses this effect. It therefore seems that the biogas-cap SOFC is a preferred economic option to the biogas-cap SOFC with vacuum pump installation.

4. Conclusion

Performance of biogas-fed SOFC system was analyzed to investigate the benefit of CO_2-selective membrane installation. The two configurations, namely; biogas-cap SOFC and reformed gas-cap SOFC were examined in terms of both engineering and economic models. It was observed that the power density improves when the SOFC was integrated with a CO_2-selective membrane. However, due to low CO_2/H_2 or CO_2/CH_4 selectivity of membrane separator, there was significant H_2 (or CH_4) loss and electrical efficiency also dropped especially in case of reformed gas-cap SOFC. In particular, it was found that the installation of vacuum pump (replacing the use of sweep gas) to the biogas-cap SOFC can offer comparable electrical efficiency to the non-cap SOFC. Unfortunately, this advantage has detrimental effect on the power density. For the reformed gas-cap SOFC, although the installation of vacuum pump can improve the

electrical efficiency, the increase in membrane area and the decrease in membrane permeate pressure did not improve the power density. This implies that there is no benefit in the installation of vacuum pump for the reformed gas-cap SOFC. It may therefore be concluded that the reformed gas-cap SOFC is not a good alternative for the SOFC system owing to its extremely low efficiency (less than 40 percent) and the large heat exchanger area required. Economic assessment via the "incremental analysis" method was then employed to evaluate the feasibility study of biogas-cap SOFC operation. The results showed that the biogas-cap SOFC with sweep gas and that with vacuum pump installation were more superior to the non-cap SOFC at low membrane area. The biogas-cap SOFC with vacuum pump installation is, however, economically less attractive than the biogas-cap SOFC with sweep gas due to high vacuum pump cost.

Acknowledgement

This research is financially supported by the Thailand Research Fund and Commission on Higher Education.

References

[1] J. Van herle, Y. Membrez, O. Bucheli, Biogas as a fuel source for SOFC co-generators, Journal of Power Sources 127 (2004) 300-312.

[2] D.C. Dayton, Fuel cell integration-a study of the impacts of gas quality and impurities, NREL final report, 2001.

[3] M. Jenne, T. Dörk, A. Schuler, Proceedings of the Fifth European Solid Oxide Fuel Cell Forum, Lucerne, Switzerland, European Forum Secretariat, CH 5442-Oberrohrdorf, Switzerland, 2002, pp. 460-466.

[4] K. Kendall, C.M. Finnerty, G. Saunders, J.T. Chung, Effects of dilution on methane entering an SOFC anode, Journal of Power Sources 106 (2002) 323-327.

[5] E. Achenbach, E. Riensche, Methane/steam reforming kinetics for solid oxide fuel cells, Journal of Power Sources 52 (1994) 283-288.

[6] J. Meusinger, E. Riensche, U. Stimming, Reforming of natural gas in solid oxide fuel cell systems, Journal of Power Sources 71 (1998) 315-320.

[7] S. Assabumrungrat, N. Laosiripojana, P. Piroonlerkgul, Determination of the boundary of carbon formation for dry reforming of methane in a solid oxide fuel cell, Journal of Power Sources 159 (2006) 1274-1282.

[8] P. Piroonlerkgul, S. Assabumrungrat, N. Laosiripojana, A.A. Adesina, Selection of appropriate fuel processor for biogas-fuelled SOFC system, Chemical Engineering Journal In Press, Corrected Proof.

[9] W. Sangtongkitcharoen, S.Vivanpatarakij, N. Laosiripojana, A. Arpornwichanop, S. Assabumrungrat, Performance analysis of methanol-fueled solid oxide fuel cell system incorporated with palladium membrane reactor, Chemical Engineering Journal 138 (2008) 436-441.

[10] R. Suwanwarangkul, E. Croiset, E. Entchev, S. Charojrochkul, M.D. Pritzker, M.W. Fowler, P.L. Douglas, S. Chewathanakup, H. Mahaudom, Experimental and modeling study of solid oxide fuel cell operating with syngas fuel, Journal of Power Sources 161 (2006) 308-322.

[11] E.J. Granite, T. O'Brien, Review of novel methods for carbon dioxide separation from flue and fuel gases, Fuel Processing Technology 86 (2005) 1423-1434.

[12] S. Alexander Stern, Polymers for gas separations: the next decade, Journal of Membrane Science 94 (1994) 1-65.

[13] D. Shekhawat, D.R. Luebke, H. Pennline, A review of carbon dioxide selective membranes; U.S. Department of Energy Topical Report, DOE/NETL-2003/1200., 2003.

[14] M. Harasimowicz, P. Orluk, G. Zakrzewska-Trznadel, A.G. Chmielewski, Application of polyimide membranes for biogas purification and enrichment, Journal of Hazardous Materials 144 (2007) 698-702.

[15] T.C. Merkel, R.P. Gupta, B.S. Turk, B.D. Freeman, Mixed-gas permeation of syngas components in poly(dimethylsiloxane) and poly(1-trimethylsilyl-1-propyne) at elevated temperatures, Journal of Membrane Science 191 (2001) 85-94.

[16] M. Amelio, P. Morrone, F. Gallucci, A. Basile, Integrated gasification gas combined cycle plant with membrane reactors: Technological and economical analysis, Energy Conversion and Management 48 (2007) 2680-2693.

[17] M.A. Khaleel, Z. Lin, P. Singh, W. Surdoval, D. Collin, A finite element analysis modeling tool for solid oxide fuel cell development: coupled electrochemistry, thermal and flow analysis in MARC(R), Journal of Power Sources 130 (2004) 136-148.

[18] R. Blom, I.M. Dahl, A. Slagtem, B. Sortland, A. Spjelkavik, E. Tangstad, Carbon dioxide reforming of methane over lanthanum-modified catalysts in a fluidized-bed reactor, Catalysis Today 21 (1994) 535-543.

[19] M.C.J. Bradford, M.A. Vannice, Catalytic reforming of methane with carbon dioxide over nickel catalysts II. Reaction kinetics, Applied Catalysis A: General 142 (1996) 97-122.

[20] H.M. Swaan, V.C.H. Kroll, G.A. Martin, C. Mirodatos, Deactivation of supported nickel catalysts during the reforming of methane by carbon dioxide, Catalysis Today 21 (1994) 571-578.

[21] J.R. Ferguson, J.M. Fiard, R. Herbin, Three-dimensional numerical simulation for various geometries of solid oxide fuel cells, Journal of Power Sources 58 (1996) 109-122.

[22] S.H. Chan, K.A. Khor, Z.T. Xia, A complete polarization model of a solid oxide fuel cell and its sensitivity to the change of cell component thickness, Journal of Power Sources 93 (2001) 130-140.

[23] S.P. Jiang, S.P.S. Badwal, Hydrogen oxidation at the nickel and platinum electrodes on yttria-tetragonal zirconia electrolyte, Journal of the Electrochemical Society 144 (1997) 3777-3784.

[24] S.P. Jiang, S.P.S. Badwal, An electrode kinetics study of H2 oxidation on Ni/Y2O3-ZrO2 cermet electrode of the solid oxide fuel cell, Solid State Ionics 123 (1999) 209-224.

[25] J. Fleig, Solid Oxide Fuel Cell Cathodes: Polarization Mechanisms and Modeling of the Electrochemical Performance, Annual Review of Materials Research 33 (2003) 361-382.

[26] W.J. Massman, A review of the molecular diffusivities of H2O, CO2, CH4, CO, O3, SO2, NH3, N2O, NO, and NO2 in air, O2 and N2 near STP, Atmospheric Environment 32 (1998) 1111-1127.

[27] H. Yakabe, M. Hishinuma, M. Uratani, Y. Matsuzaki, I. Yasuda, Evaluation and modeling of performance of anode-supported solid oxide fuel cell, Journal of Power Sources 86 (2000) 423-431.

[28] L. Wang, Y. Cao, M. Zhou, S.J. Zhou, Q. Yuan, Novel copolyimide membranes for gas separation, Journal of Membrane Science 305 (2007) 338-346.

[29] A. Corti, D. Fiaschi, L. Lombardi, Carbon dioxide removal in power generation using membrane technology, Energy 29 (2004) 2025-2043.

[30] T. Kaneko, J. Brouwer, G.S. Samuelsen, Power and temperature control of fluctuating biomass gas fueled solid oxide fuel cell and micro gas turbine hybrid system, Journal of Power Sources 160 (2006) 316-325.

[31] L. Petruzzi, S. Cocchi, F. Fineschi, A global thermo-electrochemical model for SOFC systems design and engineering, Journal of Power Sources 118 (2003) 96-107.

[32] M. Ni, M.K.H. Leung, D.Y.C. Leung, Parametric study of solid oxide fuel cell performance, Energy Conversion and Management 48 (2007) 1525-1535.

[33] F. Palazzi, N. Autissier, F.M.A. Marechal, D. Favrat, A methodology for thermo-economic modeling and optimization of solid oxide fuel cell systems, Applied Thermal Engineering 27 (2007) 2703-2712.

[34] S.M. Walas, Chemical Process Equipment Selection and Design. Butterworth, Inc., 665-668, 1988.

[35] A.K. Datta, P.K. Sen, Optimization of membrane unit for removing carbon dioxide from natural gas, Journal of Membrane Science 283 (2006) 291-300.

Nomenclature

A	membrane area, m^2
A_{cell}	SOFC stack active area, m^2
C_p	specific heat capacity, J mol^{-1} K^{-1}
C_{cell}	cost of one SOFC cell, $
$C_{compressor}$	cost of compressor, $
C_{stack}	cost of SOFC stack, $
$C_{Vacuum\ pump}$	cost of vacuum pump, $
$D_{i(eff)}$	effective diffusion coefficient of species i (i = anode, cathode), cm^2 s^{-1}
$D_{A,k(eff)}$	effective Knudsen diffusivity of gas A, cm^2 s^{-1}
$D_{A-B(eff)}$	ordinary diffusivity of gas A versus gas B, cm^2 s^{-1}
$D_{A,k}$	Knudsen diffusivity of gas A, cm^2 s^{-1}

D_{A-B}	ordinary diffusivity of gas A versus gas B, $cm^2\ s^{-1}$
D_p	catalyst pore diameter, μm
E	open circuit voltage, V
$E_{act,a}$	activation energy at anode, $J\ mol^{-1}$
$E_{act,c}$	activation energy at cathode, $J\ mol^{-1}$
F	Faraday constant (9.6495×10^4), $C\ mol^{-1}$
ΔG_i	Gibb's free energy of reaction i, $J\ mol^{-1}$
i	current density, $A\ cm^{-2}$
$i_{0,i}$	exchange current density (i = anode, cathode), $A\ cm^{-2}$
$K_{eq,dry}$	equilibrium constant of dry reforming reaction, Pa^2
$K_{eq,steam}$	equilibrium constant of steam reforming reaction, Pa^2
$K_{eq,pox}$	equilibrium constant of partial oxidation reaction, $Pa^{3/2}$
$K_{eq,RWGS}$	equilibrium constant of reverse water gas shift reaction, dimensionless
l_a	thickness of anode, μm
l_c	thickness of cathode, μm
L	thickness of electrolyte, μm
$\dot{m}$	total gas molar flow rate, $mol\ s^{-1}$
M_A	molecular weight of gas A, g
n	electrode porosity, dimensionless
N_{cell}	number of cells, dimensionless
N_{stack}	number of stack, dimensionless
p_i	permeability of component i, barrer
p_a	operating pressure at the SOFC anode, Pa
p_c	operating pressure at the SOFC cathode, Pa

p_i^I	inlet pressure of species *i*, Pa
P	operating pressure, Pa
P_i	partial pressure of species *i*, Pa
P_P	operating pressure at permeate side of membrane, Pa
P_{ref}	reference pressure (10^5), Pa
P_R	operating pressure at retentate side of membrane, Pa
Pe_i	molar flow rate of component *i* at permeate side of membrane, mol s^{-1}
Q_{endo}	heat demand in the SOFC system, kW
Q_{exo}	heat generated in the SOFC system, kW
r_p	average radius of the catalyst pore, μm
R	gas constant (8.3145), J $mol^{-1}K^{-1}$
R_i	molar flow rate of component *i* at retentate side of membrane, mol s^{-1}
r	interest rate, dimensionless
T	operating temperature, K
V	cell voltage, V
$\dot{W}_{comp}$	electricity consumed in the compressor, kW
x_i	mole fraction of component *i* at retentate side of membrane, dimensionless
y_i	mole fraction of component *i* at permeate side of membrane, dimensionless
y	plant life time, year
z	the number of electrons involved per reaction, dimensionless

Greek letters

α	symmetrical factor, dimensionless
δ	membrane thickness, μm

ξ	electrode tortuosity, dimensionless
$\eta_{act,a}$	activation overpotential at anode, V
$\eta_{act,c}$	activation overpotential at cathode, V
$\eta_{Conc,a}$	concentration overpotential at anode, V
$\eta_{Conc,c}$	concentration overpotential at cathode, V
η_c	compressor or pump efficiency, dimensionless
η_{ohmic}	ohmic overpotential, V
σ_{AB}	collision diameter, Å
Ω_D	collision integral, dimensionless
ε_{AB}	Lennard-Jones energy interaction parameter scaled with respect to the Boltzman constant, dimensionless
γ_a	pre-exponential factor for anode exchange current density, A m^{-2}
γ_c	pre-exponential factor for cathode exchange current density, A m^{-2}

Figure Caption

Fig. 1. The configuration of membrane module.

Fig. 2. The plant configuration of non-cap SOFC system.

Fig. 3. The plant configuration of biogas-cap SOFC system.

Fig. 4. The plant configuration of the reformed gas-cap SOFC system.

Fig. 5. The basic working of membrane module with vacuum pump installation.

Fig. 6. Verification of the membrane separation model.

Fig. 7. The percentage of CO_2 removal and the percentage of CH_4 or H_2 loss at different membrane area and sweep gas to feed gas ratio: (a) polyimide membrane and (b) PDMS membrane.

Fig. 8. The electrical efficiency and power density at different membrane area: (a) biogas-cap SOFC and (b) reformed gas-cap SOFC.

Fig. 9. The percentage of CO_2 removal and the percentage of CH_4 or H_2 loss at different membrane area and permeate side pressure: (a) polyimide membrane with vacuum pump installation and (b) PDMS membrane with vacuum pump installation.

Fig. 10. The electrical efficiency and power density of biogas-cap SOFC with vacuum pump installation at different membrane area and permeate side pressure.

Fig. 11. Performance of the reformed gas-cap SOFC with vacuum pump installation at different membrane areas and membrane permeate side pressures: (a) Excess energy released to the environment, (b) electrical efficiency and (c) power density.

Fig. 12. Incremental net present value of biogas-cap SOFC operated at different membrane areas (sweep gas to feed gas ratio = 4).

Fig. 13. Incremental net present value of the biogas-cap SOFC with vacuum pump installation operated at different membrane areas and permeate side pressure.

List of Table

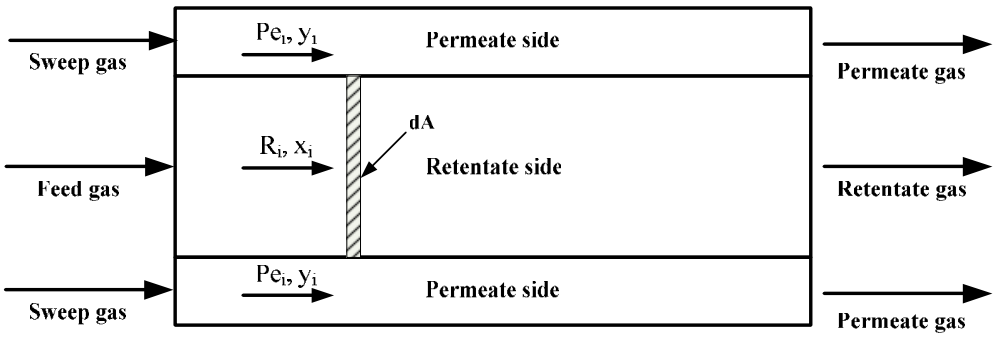

Fig. 1. The configuration of membrane module.

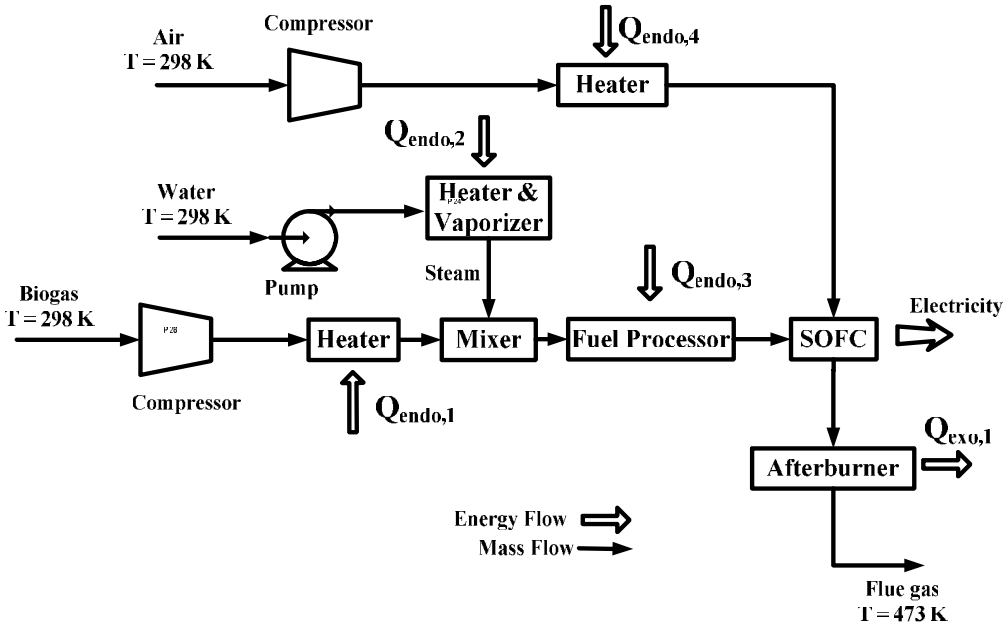

Fig. 2. The plant configuration of the non-cap SOFC system.

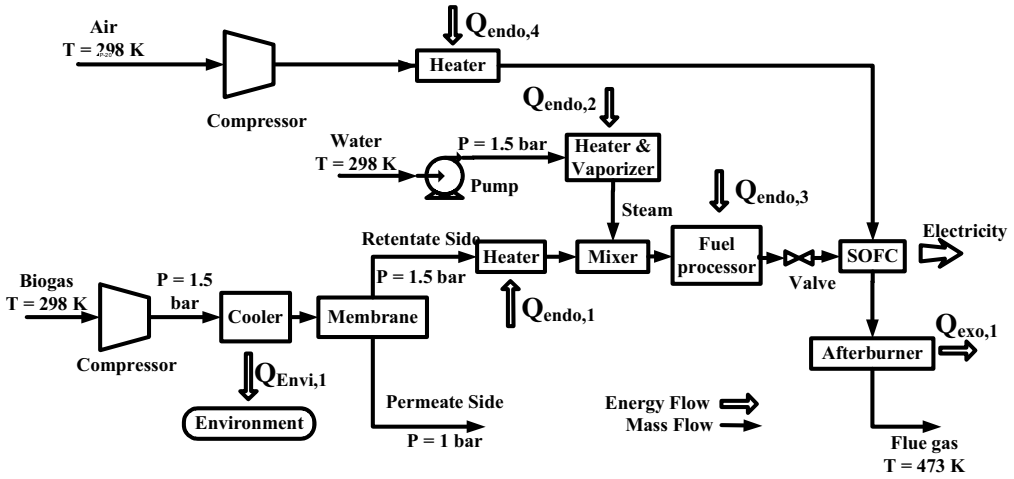

Fig. 3. The plant configuration of biogas-cap SOFC system.

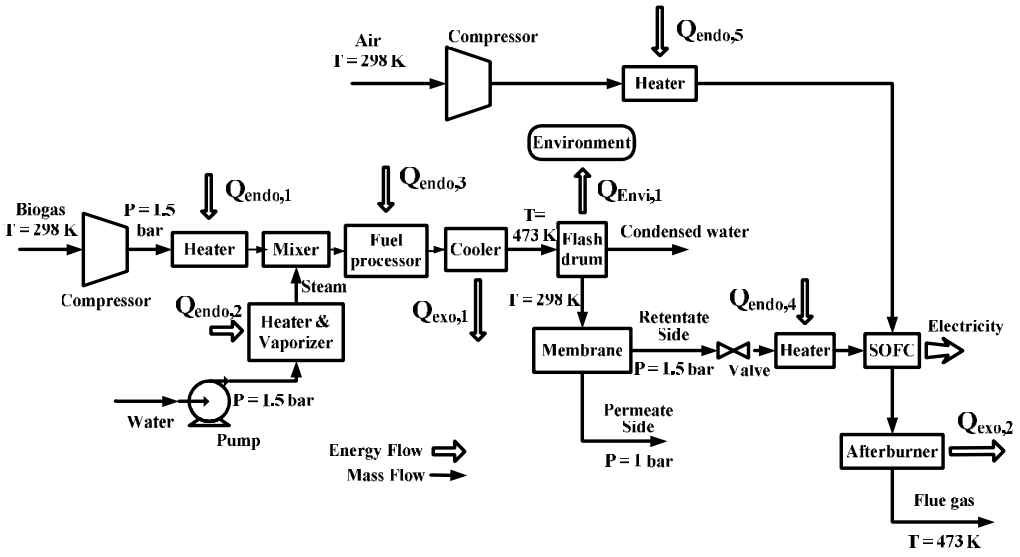

Fig. 4. The plant configuration of the reformed gas-cap SOFC system.

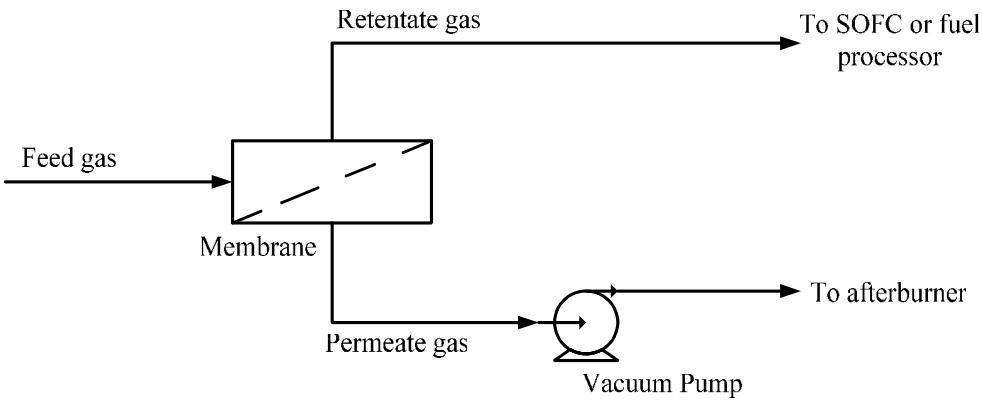

Fig. 5. The basic working of membrane module with vacuum pump installation.

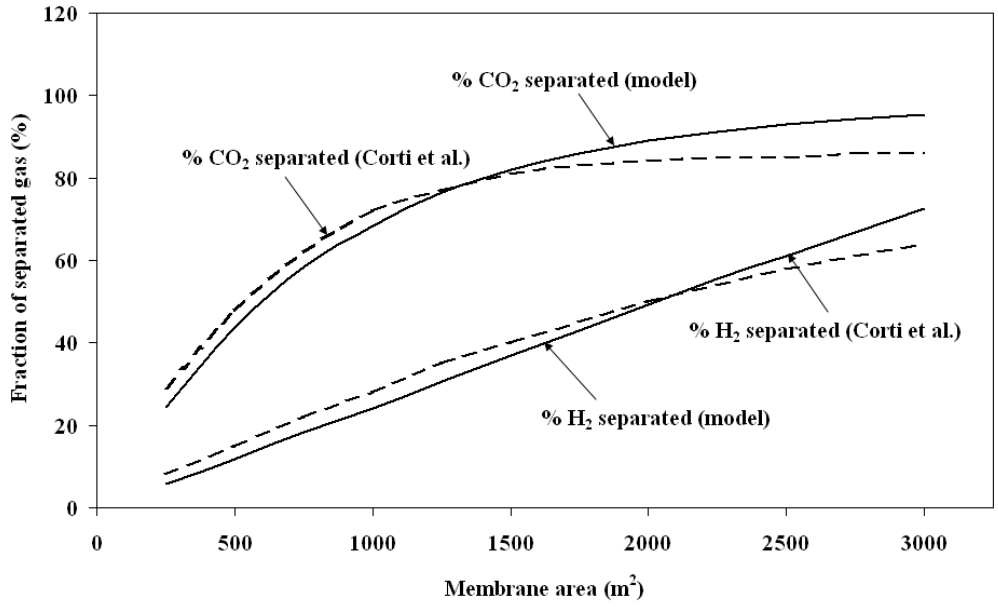

Fig. 6. Verification of the membrane separation model.

a

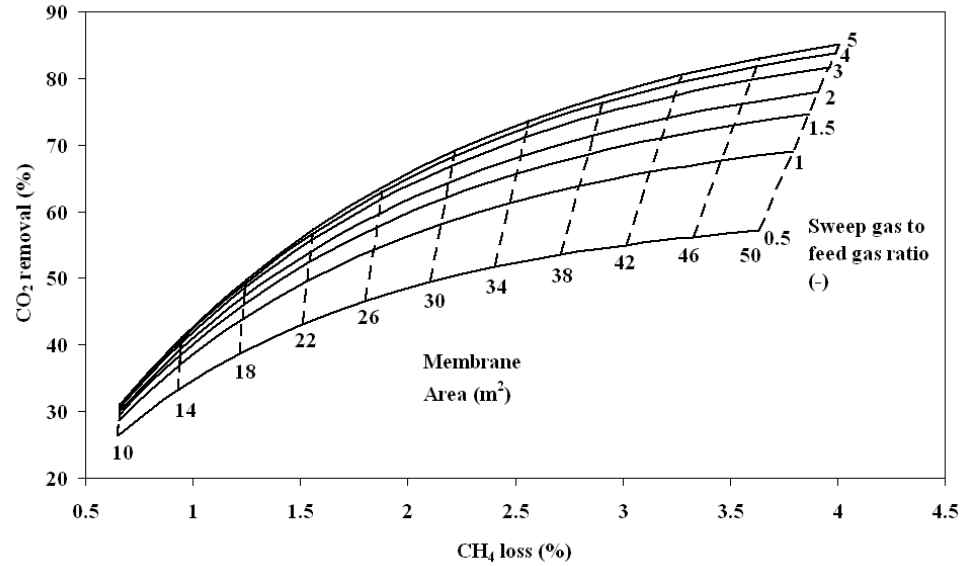

b

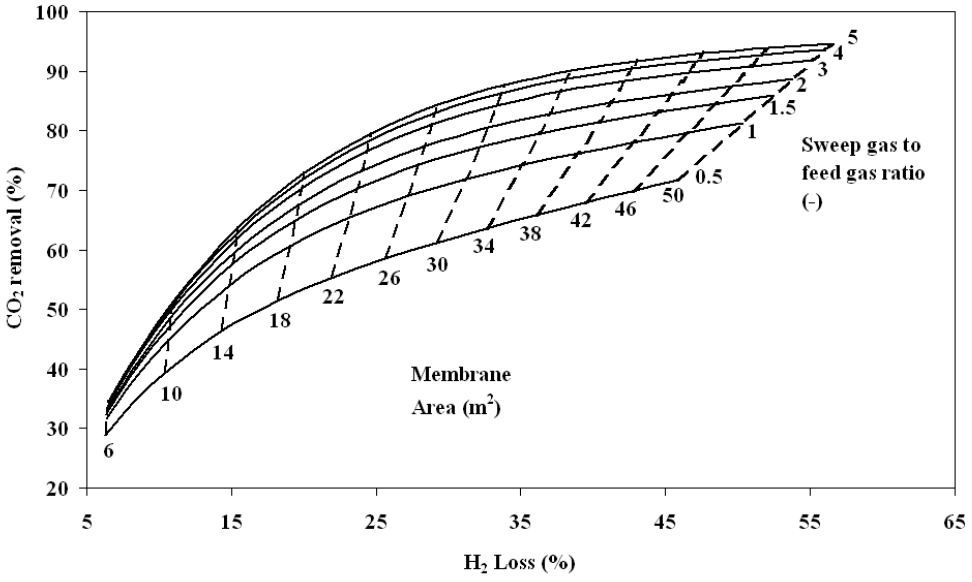

Fig. 7. The percentage of CO_2 removal and the percentage of CH_4 or H_2 loss at different membrane area and sweep gas to feed gas ratio: (a) polyimide membrane and (b) PDMS membrane.

a

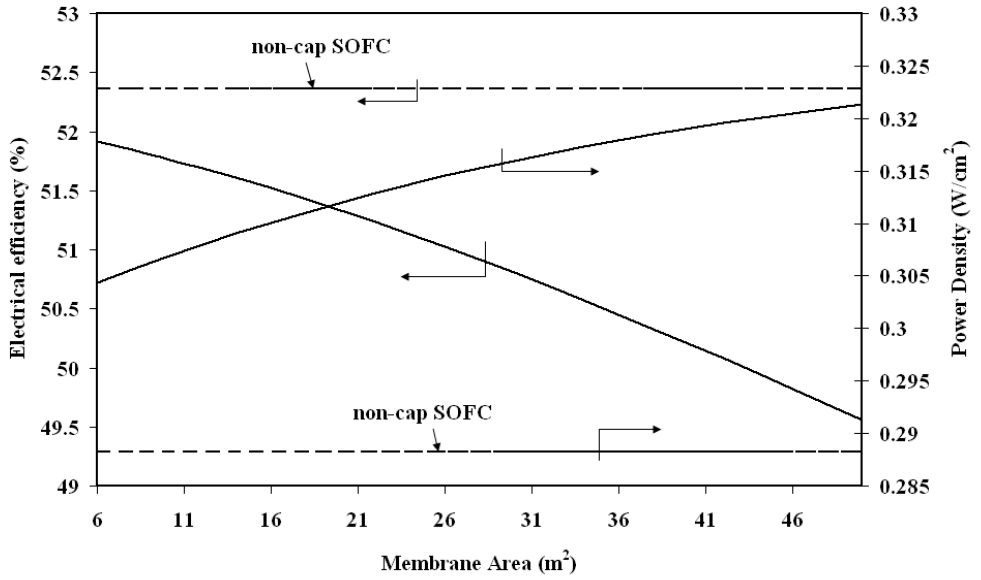

b

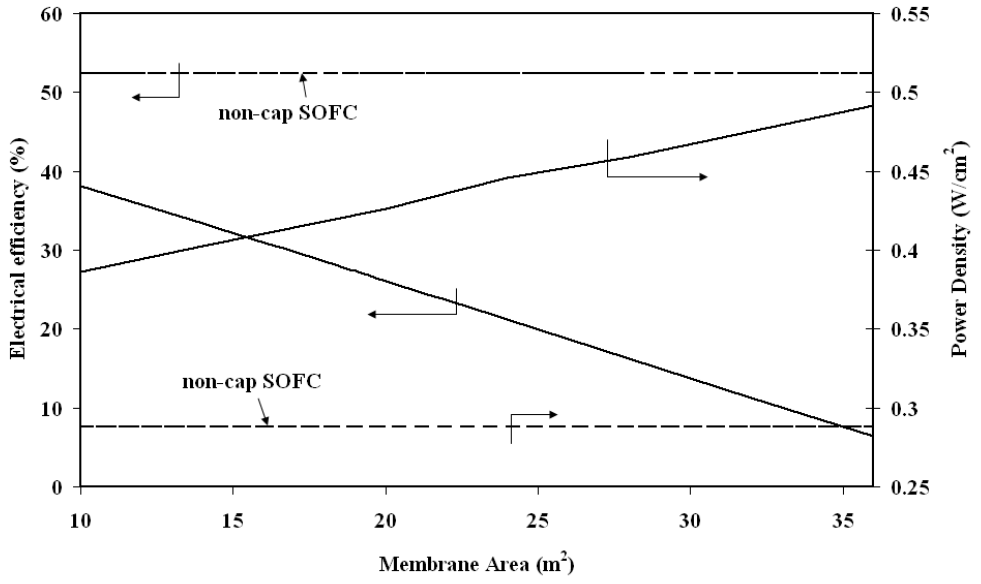

Fig. 8. The electrical efficiency and power density at different membrane area: (a) biogas-cap SOFC and (b) reformed gas-cap SOFC.

a

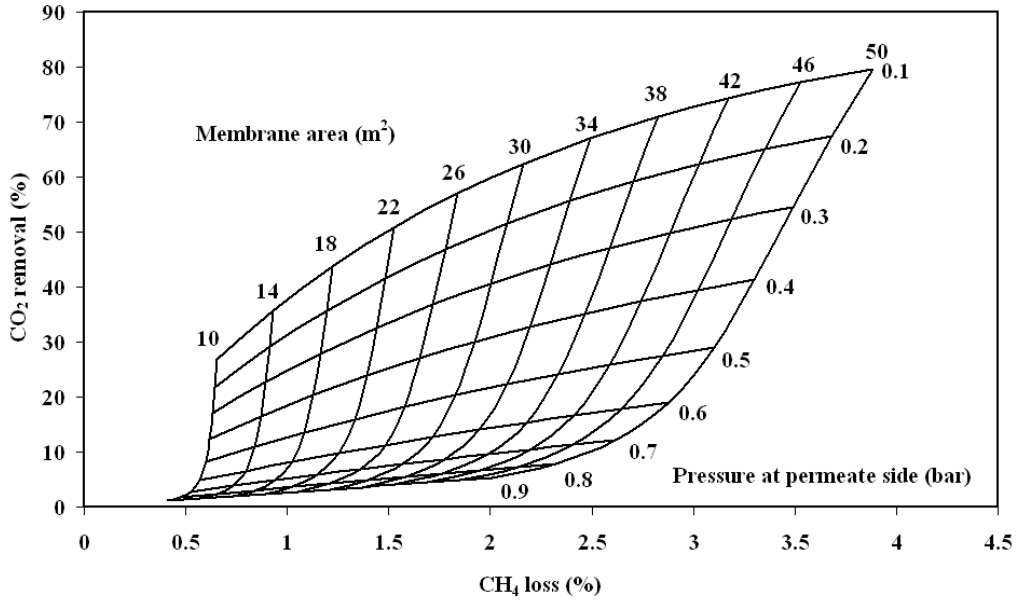

b

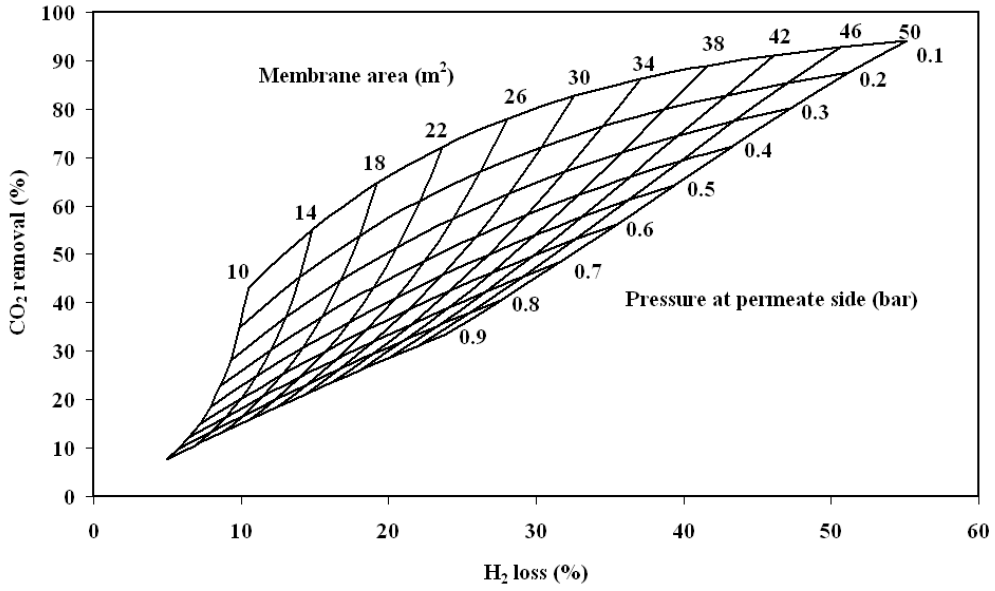

Fig. 9. The percentage of CO_2 removal and the percentage of CH_4 or H_2 loss at different membrane area and permeate side pressure: (a) polyimide membrane with vacuum pump installation and (b) PDMS membrane with vacuum pump installation.

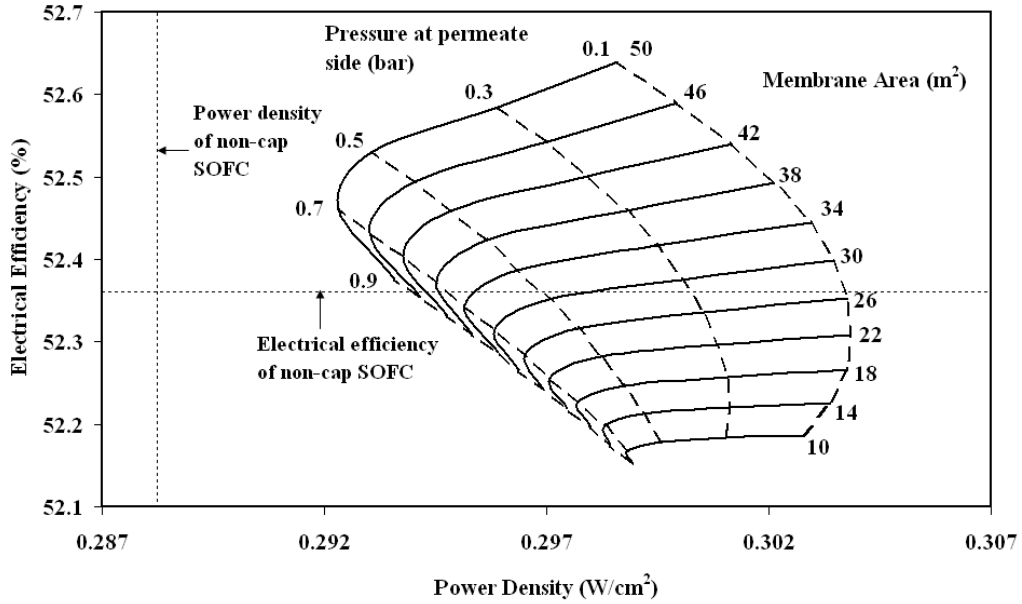

Fig. 10. The electrical efficiency and power density of biogas-cap SOFC with vacuum pump installation at different membrane area and permeate side pressure.

a

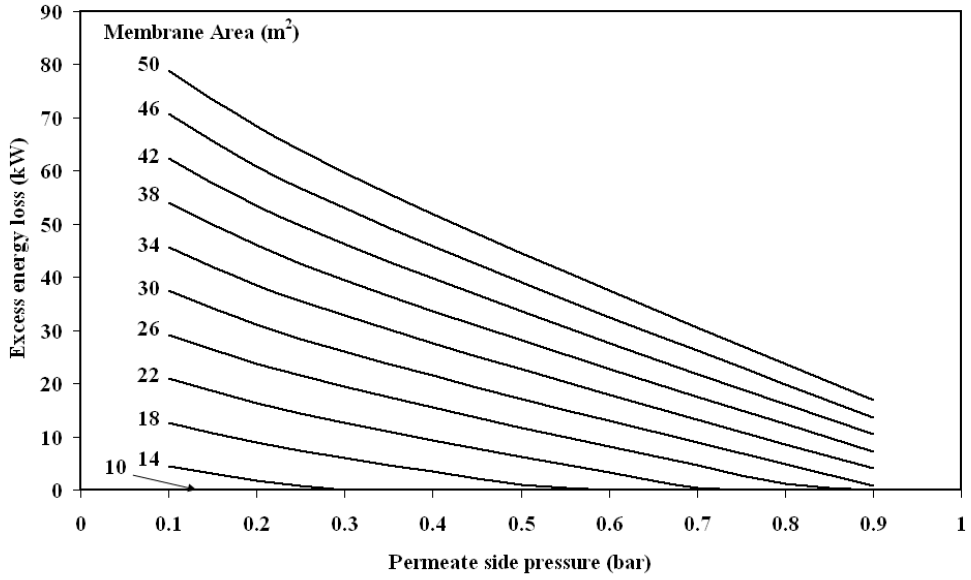

b

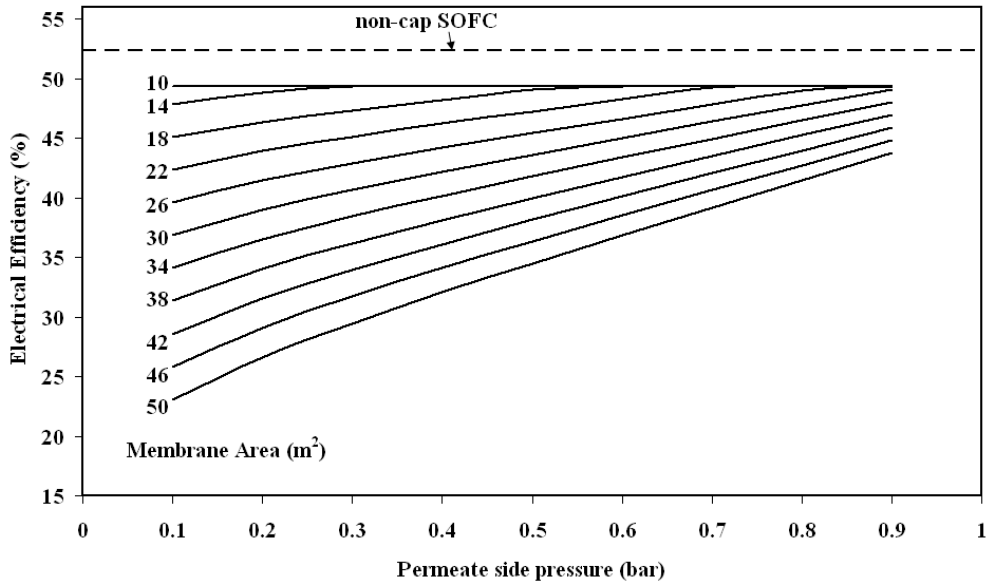

c

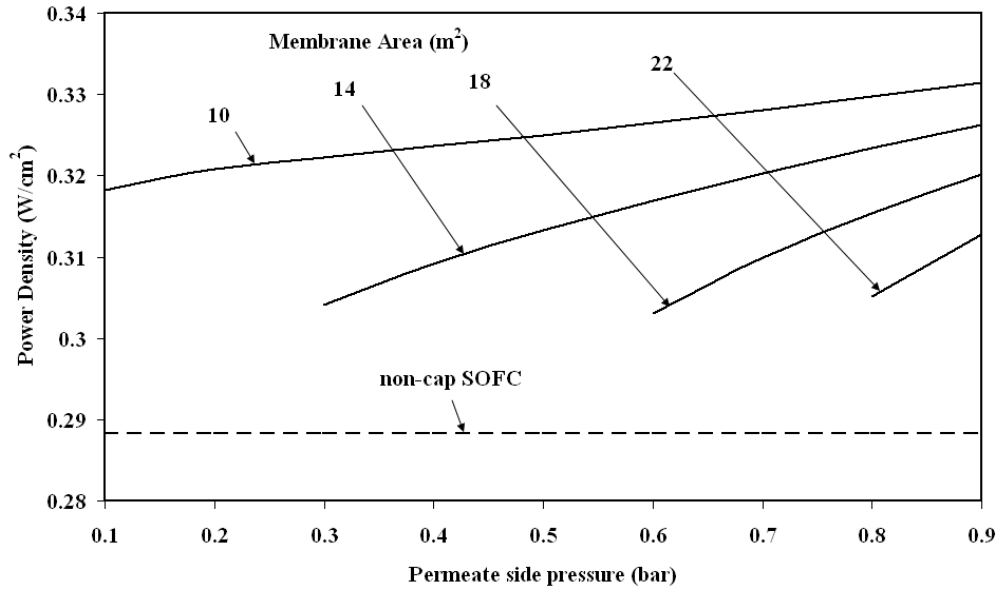

Fig. 11. Performance of the reformed gas-cap SOFC with vacuum pump installation at different membrane areas and membrane permeate side pressures: (a) Excess energy released to the environment, (b) electrical efficiency and (c) power density.

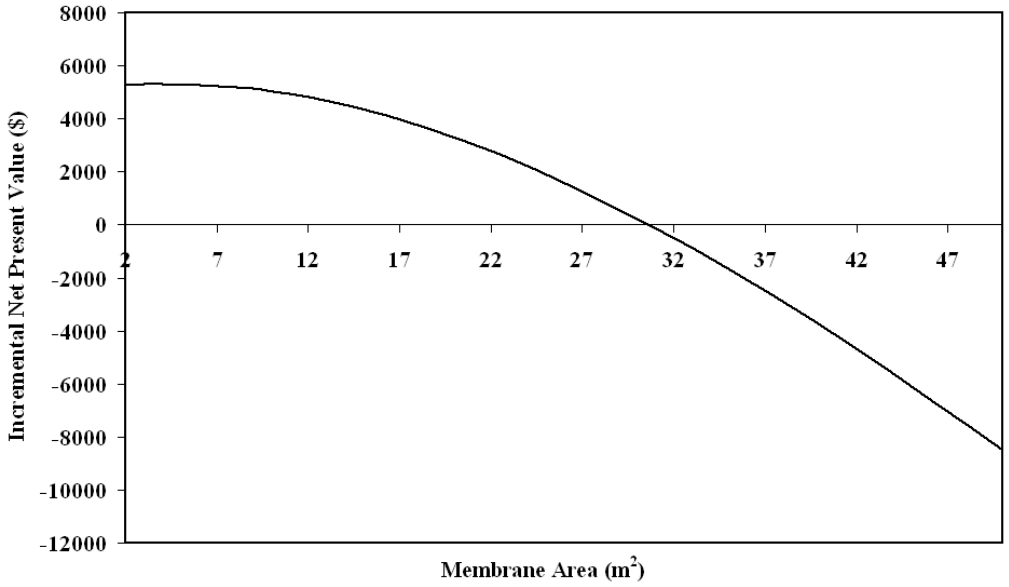

Fig. 12. Incremental net present value of biogas-cap SOFC operated at different membrane areas (sweep gas to feed gas ratio = 4).

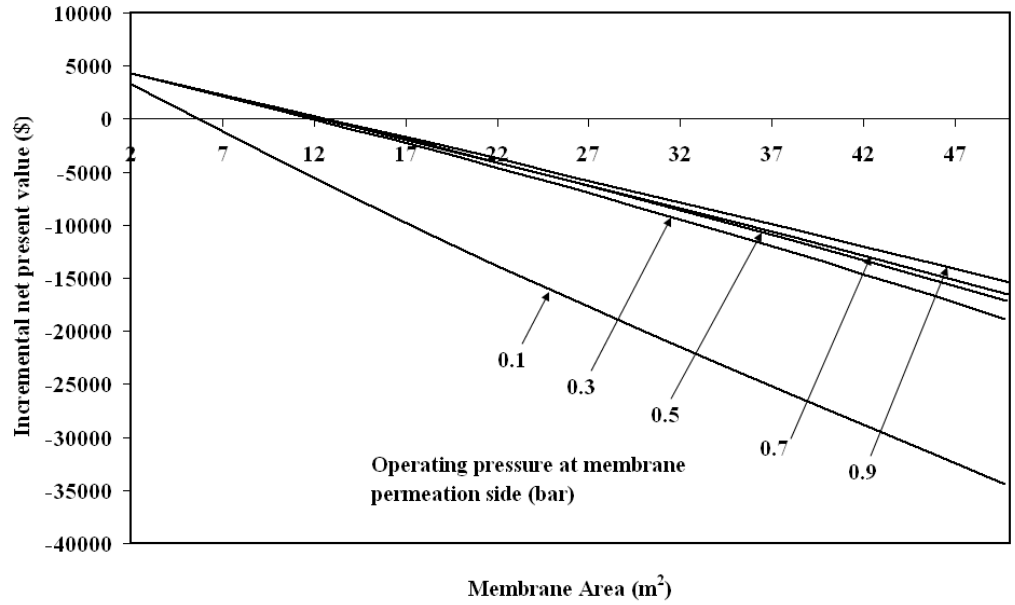

Fig. 13. Incremental net present value of the biogas-cap SOFC with vacuum pump installation operated at different membrane areas and permeate side pressure.

Table 1

Membrane thickness and permeability of each gas component

	Polyimide membrane [28]	PDMS membrane [29]
Membrane Thickness (μm)	0.1	1.5
Permeability (barrer)		
CH_4	0.69	940
CO_2	39.59	3200
CO	-	400
H_2O	-	10
H_2	-	500

1 barrer = [10^{-10} cm^3 (STP) cm]/[cm^2 s cmHg]

Table 2

Summary of model parameters [32].

Parameters	*Value*
γ_a	1.344×10^{10} A/m^2
γ_c	2.051×10^{9} A/m^2
$E_{act,a}$	1.0×10^{5} J/mol
$E_{act,c}$	1.2×10^{5} J/mol
n	0.48
ξ	5.4
D_p	3 μm
l_a	750 μm
l_c	50 μm
L	50 μm
V	0.7 V
T_{SOFC}	1073 K
Operating pressure (SOFC)	1 bar
$T_{fuel\ processor}$	973 K

Table 3

Feed compositions and SOFC stack dimensions used in model validation.

Parameters	Values [31]
Fuel compositions (Mole fraction):	
CH_4	-
H_2	0.26
CO	0.24
CO_2	0.025
N_2	0.46
H_2O	0.015
Stack dimensions:	
Type of cell	Planar SOFC with 225 cm^2 active surface area
n	0.48
ξ	5.4
D_p	3 μm
l_a	40 μm
l_c	40 μm
L	70 μm
Stack average temperature	1073 K

Table 4

Model validation of the SOFC model.

T = 1073 K	Petruzzi et al., 2003	Model	Error (%)	Petruzzi et al., 2003	Model	Error (%)
Cell Voltage (V)	0.8	0.8	0	0.75	0.77	2.67
Electrical Power (W)	62.9	63	0.16	70	71.6	2.29
Fuel Utilization (%)	70	70	-	80	80	-

Table 5

Summary of feed characteristics and parameters used in the model verification of membrane separation.

Parameters	*Values*
Fuel mass flow rate (kg/s)	5.89
Fuel compositions (Mole fraction):	
CH_4	0.068
H_2	0.6714
CO	0.0068
CO_2	0.1627
N_2	-
H_2O	0.0911
Membrane parameters:	
Material used	PDMS
Membrane thickness (μm)	1.3
Operating pressure (bar):	
Permeate side	1
Retentate side	10
Permeability (barrer) at 298 K:	
CH_4	940
CO	400
CO_2	3200
H_2	500
H_2O	10

1 barrer = $[10^{-10}$ cm^3 (STP) cm] / [cm^2 s cmHg].

Table 6

Flow rates and compositions of the membrane feed gases.

	Polyimide membrane	PDMS membrane
Molar flow rate (mol/s)	0.56028	0.56028
Pressure (bar)	1.5	1.5
Temperature (K)	298	298
Mole Fraction		
CH_4	0.6	0.0035
CO_2	0.4	0.1563
CO	0	0.1961
H_2O	0	0
H_2	0	0.6441

Table 7

Economic parameters used in the calculations.

Parameter	Value
Biogas price ($/MMBTU)	7.85 (Natural gas price is assumed.)
Membrane module cost ($/m^2)	108 [35]
Membrane replacement cost ($/m^2)	54 [35]
Interest rate (%)	7
Plant load time (h/a)	7,000
Plant life time (year)	5

Table 8

Costing models of SOFC [33], compressor and vacuum pump [34].

Costing model	
Cell cost ($)	$C_{cell} = A_{cell} \times 0.1442$
Number of cells	$N_{cell} = A_{cell}/200$
Number of stacks	$N_{stack} = N_{cell}/100$
Fuel cell stacks cost ($)	$C_{stack} = 2.7 \times (C_{cell} \times N_{cell} + 2 \times N_{stack} \times A_{cell} \times 0.46425)$
Compressor ($)	$C_{compressor} = 1.49 \times HP^{0.71} \times 10^3$
Vacuum pump ($)	$C_{Vacuum\ pump} = 2.59 \times X^{1.03} \times 10^5$ where: $0.01 < X < 0.52$ (lbs/h)/(suction Torr)

Table 9

The economic comparison between the biogas-cap SOFC with different modes.

	Biogas-cap SOFC (Sweep gas)	Biogas-cap SOFC (Vacuum pump)
Power produced (kW)	156.72	156.72
Membrane area (m^2)	4.03	2
Operating pressure at permeate side (bar)	1	0.5
Sweep gas to feed gas ratio	4	0
Feed rate of biogas (mol/s)	0.5644	0.5629
Electrical efficiency (%)	51.98	52.11
Power density (W/cm^2)	0.303	0.3
SOFC area (m^2)	51.98	52.5
Decrease in capital cost from base case ($)	7,903.48	5,901.02
Increase in operating and fuel cost from base case ($/year)	630.04	376.04
Incremental net present value ($)	5,320.21	4,359.18

Appendix 11

Fe(III), Cu(II), V(V)/TiO_2 for Hydroxylation of Benzene to Phenol with Hydrogen Peroxide at Room Temperature

Garun TANARUNGSUN[1], Worapon KIATKITTIPONG[2], Suttichai ASSABUMRUNGRAT[1], Hiroshi YAMADA[3], Tomohiko TAGAWA[3] and Piyasan PRASERTHDAM[1]

[1]*Center of Excellence in Catalysis and Catalytic Reaction Engineering, Department of Chemical Engineering, Faculty of Engineering, Chulalongkorn University, Bangkok 10330, Thailand*

[2]*Department of Chemical Engineering, Faculty of Engineering and Industrial Technology, Silpakorn University, Nakhon Pathom 73000, Thailand*

[3]*Department of Chemical Engineering, Nagoya University, Chikusa-ku, Nagoya-shi, Aichi 464-8603, Japan*

Keywords: Hydroxylation, Benzene, Hydrogen Peroxide, Phenol, TiO_2

The hydroxylation of benzene to phenol with hydrogen peroxide catalyzed by transition metal (Fe(III), Cu(II), and V(V)) on a TiO_2 support was performed at room temperature. The Fe(III) catalyst gave the highest conversion and yield but showed the lowest selectivity. At room temperature, the phenol yield was quite low and therefore modifying the system by solvent addition or operation under UV light was examined. Among the various solvents studied, i.e., acetone, acetronitrile and pyridine, acetone gave the highest conversion and yield; however, the selectivity was low. Acetonitrile is a suitable solvent in terms of improved selectivity and yield. Operation under UV light significantly improved the yield with comparatively high selectivity. Ascorbic acid, as a reducing agent, was able to improve the phenol yield. In some solvent systems, an optimum amount of ascorbic acid was observed.

Introduction

Phenol is an important intermediate for the synthesis of various petrochemical and agrochemical products. More than 90% of the world's phenol production is produced from the cumene process (Schmidt, 2005). The process is composed of three steps and produces acetone as a co-product, which will be an oversupplied product in the future. In addition, the cumene hydroperoxide intermediate can decompose aggressively. Therefore, an alternative process could be developed.

The direct oxidation of benzene to phenol is one of the alternative routes. There are two main pathways for the direct oxidation of benzene to phenol; i.e., gas and liquid phase reactions.

Gas phase hydroxylation of benzene with nitrous oxide has been conducted in a pilot facility (Uriarte *et al.*, 1998). However, it is efficient only when the supply of nitrous oxide is available, for example, as a by-product from the adipic acid synthesis. Major problems of an industrial application are deactivation of the catalyst by heavy coke formation and the low phenol selectivity of nitrous oxide (Uriarte *et al.*, 1998; Lemke *et al.*, 2003). The other disadvantages are that it is operated at an elevated temperature of higher than 573 K and yields marginal conversion, resulting in an unduly high cost.

Liquid phase hydroxylation of benzene to phenol is operated at room temperature or normally not higher than 353 K. H_2O_2 or O_2 is employed as an oxidant. High selectivity can be obtained at a lower oxidant cost compared with the gas phase operation using N_2O as an oxidant. Therefore many researchers have focused on this route and aimed at developing a suitable catalyst for the reaction. Several kinds of metals such as Fe, Cu and V were loaded on supports such as SiO_2, Al_2O_3, HZSM-5, MCM-41, and TiO_2 (Seo *et al.*, 1995; Okamura *et al.*, 1998; Chen and Lu 1999; Kanzaki *et al.*, 2004).

The solvent is usually added to the reaction system for dissolving hydrogen peroxide and benzene into one phase for the oxidation of benzene to phenol. Several solvents such as acetone, acetonitrile, acetic acid, pyridine and dichloromethane have been employed (Stockmann *et al.*, 2001; Xiao *et al.*, 2001; Miyake *et al.*, 2002; Choi *et al.*, 2005; Dubey and Kannan 2005; Liu *et al.*, 2005; Zhang *et al.*, 2005). However, there are only a few works comparing the effect of solvent types. Stockmann *et al.* (2001) studied the oxidation

Received on June 6, 2006; accepted on January 16, 2007.
Correspondence concerning this article should be addressed to S. Assabumrungrat (E-mail address: Suttichai.A@chula.ac.th).

Table 1 Materials and chemicals

Metal source	Iron (III) acetylacetonate 97% (Sigma-Aldrich Co.) Cupric (II) nitrate 99% (Sigma-Aldrich Co.) Ammonium metavanadate (V) 99.5% (Carlo Erba reagenti Co.)
Support	TiO_2 (JRC-TIO1) (Catalysis Society of Japan)
Solvent	99.8% Acetone (Carlo Erba Reagenti Co.) 99.8% Acetonitrile (Merck Co.) 99.7% Pyridine (Merck Co.)
Reducing agent	99.7% Ascorbic acid (Polskic Odczynniki Chemiczne S.A. Co.)
Substrate	99.7% Benzene (Merck Co.)
Oxidant	30 wt% Hydrogen peroxide (Merck Co.)
By product	99.9% Biphenyl (Sigma-Aldrich Co.)
Reference	98% Catechol (Sigma-Aldrich Co.) 99% Phenol (Panreac Sintesis Co.) 99.8% Quinol (APS Co.) 98% 1,4-Benzoquinone (ACROS Co.)

of benzene to phenol using amorphous microporous mixed oxides catalyst. The acetonitrile solvent showed the highest yield among several solvents; i.e., 2-propanol, dimethyl glycol, and propylene glycol. On the other hand, there are some researchers, who study a solvent free system from the environmental viewpoint but low conversion and yield are usually obtained. The liquid-phase oxidation of benzene to phenol in a benzene–water bi-phase system was studied (Mizuno *et al.*, 2005). The catalyst was dissolved in water that was saturated with benzene. Therefore benzene was oxidized to phenol in the water phase. By extracting the produced phenol into the organic phase, products were easily separated from the catalyst, preventing the consecutive oxidation of phenol.

It is widely accepted that OH• radicals can also be generated on photo-irradiated TiO_2 surfaces (Park and Choi, 2005). TiO_2 photocatalyst has been applied to the hydroxylation of benzene to phenol but the conversion efficiency in photocatalysis was lower than that of the Fenton process. Therefore, surface modifications of TiO_2 should be performed. The presence of electron acceptors, i.e., Fe(III), Ag(I) and O_2, enhanced the photocatalytic reaction (Park and Choi, 2005). In the addition, the recent works found that Cu-, Fe-, and V-containing catalysts gave high yield of phenol (Choi *et al.*, 2005; Liu *et al.*, 2005). It should be noted that the comparison of reaction performance of different systems published in the literature is rather difficult due to the differences in various parameters such as types and amounts of catalyst, support, oxidant and solvent and also the differences in operating condition such as the operating temperature and pressure.

In this study, we have mainly investigated the catalytic behavior of Fe(III), Cu(II) and V(V) catalysts impregnated with a TiO_2 commercial support for the hydroxylation of benzene to phenol at room temperature. Various reaction systems such as solvent free systems with and without UV for photooxidation and a system with a solvent were investigated. In addition, the influences of the solvent type and the amount of ascorbic acid as a reducing agent have also been studied.

1. Experimental

1.1 Materials and chemicals

The details of materials and chemicals employed in this work were summarized in **Table 1**. All chemicals were used without prior purification.

1.2 Catalyst preparation

Metal oxide/TiO_2 catalyst was prepared by impregnation of support powder in an aqueous solution of a metal salt at 353 K followed by evaporation and drying over night. The dry catalysts were calcined in an air stream with a heating rate of 10 K/min from room temperature to 773 K and left for 5 h to remove the organic template. After calcination, the catalysts were stored in a dessicator.

1.3 Characterization

XRD patterns of the TiO_2 support and metal supported catalysts were obtained by using X-ray diffractrometer, D 5000 (Siemens AG) using Cu Kα radiation equipped with Ni filter with a range of detection of 2θ 20–80 and a resolution of 0.04.

BET surface area and porosity of the catalysts were measured by Micromeritics ASAP 2020 (Micromeritics Instrument Corp.). The sample of 0.3 g was degassed at 573 K for 3 h and the amount of N_2 adsorption was observed.

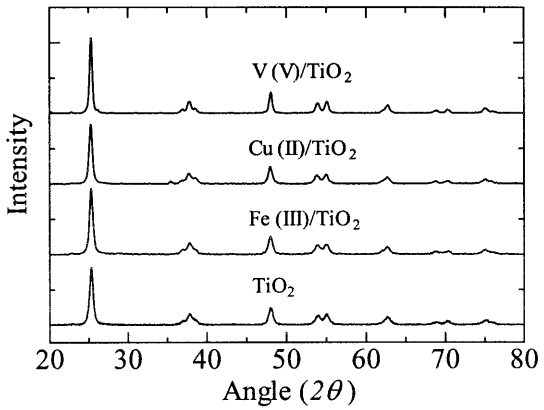

Fig. 1 XRD patterns of the TiO_2 support and supported metal catalysts

XPS surface analysis was performed using a Kratos Amicus X-ray photoelectron spectroscope (Shimadzu Corp.). The XPS spectra were measured using the following conditions: Mg Ka X-ray source at the current of 20 mA and 12 keV, resolution of 0.1 eV/step, and pass energy of 75 eV. The operating pressure was approximately 1×10^{-6} Pa. A wide-scan survey spectrum was collected for each sample in order to determine the elements present on the surface. All the binding energies were calibrated internally with the carbon C 1s photoemission peak at 285.0 eV. Photoemission peak areas were determined after smoothing and background subtraction using a linear routine. Deconvolution of complex spectra were done by fitting with Gaussian (70%)–Lorentzian (30%) shapes using the VISION 2 software equipped with the XPS system (Shimadzu Corp.).

1.4 Experimental setup and product analysis

The oxidation of benzene by H_2O_2 was carried out in a 125-cm^3 round flat bottomed flask at 303 K and 1 atm with a high speed stirrer. The reaction system consisted of two liquid phases: an organic phase containing a substrate and a solvent, and an aqueous phase containing acetone and 30% H_2O_2.

In a typical experiment, 0.2 g of catalyst (metal loading 5 wt%) in a metal oxide form was added in a liquid mixture containing 40 cm^3 of solvent, 30 cm^3 of H_2O_2 (0.32 mol) and 11 cm^3 of benzene (0.16 mol). For the photooxidation system, the ultraviolet light source is a black light blue fluorescent bulb (8 W).

The feed and products were analyzed by a gas chromatogragh (GC 9A, Shimazu Corp.) with a packed column of GP 10% SP-2100. The operating conditions of GC are as follows: the injection temperature of 523 K, detector temperature of 523 K, initial column temperature of 383 K, final column temperature of 443 K and temperature programmed rate of 10 K/min. The products were also analyzed by GC-MS especially for some product species which cannot be detected by the FID detector. The metal loading of catalyst was calculated as (the weight of metal)/(the weight of TiO_2 added metal).

Table 2 BET surface area and pore volume of support and synthesized catalysts and metal/Ti atomic ratio on surface analyzed by XPS

Catalyst	BET surface [m^2/g]	Pore volume [cm^3/g]	Metal/Ti atomic ratio on surface
TiO_2 (JRC-TIO-1)	76.56	0.29	—
V/TiO_2 5%	60.62	0.24	0.31
Cu/TiO_2 5%	62.33	0.23	0.32
Fe/TiO_2 5%	68.52	0.25	0.35

2. Results and Discussion

2.1 Catalyst characterization

From our preliminary study, metal loading at 5 wt% was selected for this study because it showed the optimum value for obtaining a reasonable yield and turnover number. The characteristics of the catalyst were investigated to identify its crystal structure, surface area and pore size volume and metal loading on the surface which were analyzed by XRD, BET and XPS, respectively. Due to a low loading, no obvious peaks of V, Cu and Fe metal were observed, similar XRD patterns with a blank TiO_2 anatase phase were obtained as shown in **Figure 1**. However, it should be noted that from the other sets of our data, the metal oxide peaks were observed obviously at metal loadings of higher than 10 wt% (not shown). The XPS results shown in **Table 2** suggest that the metal species were deposited at least on the surface of the support.

The BET surface area and pore volume of various metal-supported catalysts were shown in Table 2. As metals were loaded on the TiO_2 support, the surface area and pore volume decreased compared with those of the blank TiO_2 support.

2.2 Effect of metal species on the reaction performance in the solvent free system

The byproducts from the reactions were CO_2, hydroquinone, cresol, biphenyl and catechol. However, CO_2 went out from our open system, the analysis of sampled exit gas showed a neglected amount of CO_2 and, therefore, the amount of CO_2 was not measured in the routine experiments. As for the oxidation of the solvent, a blank test was done in the system consisting of an only solvent, TiO_2 and H_2O_2 without benzene. As an example, only a small amount of acetic acid and CO_2 were detected from the blank test with the acetone solvent. Because the system was operated at room temperature, only a small amount of solvent could be oxidized. Therefore, this effect could be negligible.

The effect of metal species on the reaction performance in the solvent free system was summarized

Table 3 Catalytic performances for hydroxylation of benzene to phenol of Fe(III), Cu(II), V(V)/TiO_2 catalysts under a solvent free condition

Catalyst	Conversion[a] [%]	Selectivity[b] [%]	Yield[c] [%]	TOF[d] [h^{-1}]	TON[e]
Fe/TiO_2 5%	0.5	46	0.23	0.53	2.14
Cu/TiO_2 5%	0.29	80	0.23	0.61	2.44
V/TiO_2 5%	0.21	90	0.19	0.4	1.62

[a]Conversion [%] = (moles of benzene reacted)/(initial moles of benzene) × 100
[b]Selectivity [%] = (moles of phenol)/(moles of benzene reacted) × 100
[c]Yield [%] = (moles of phenol)/(initial moles of benzene) × 100
[d]Turnover frequency = (moles of phenol)/(moles of metal × h)
[e]Turnover number = (moles of phenol)/(moles of metal)

in **Table 3**. The operating condition and the terms of reaction performance were shown below the table. The activity of metal catalysts was ordered as Fe(III) > Cu(II) > V(V), however, the phenol selectivity was in the reverse order. It should be noted that the differences of surface area and pore volume among three metal species were insignificant (as shown in Table 2). In addition, the impregnation method does not usually change the structure or morphology of the support. The characterization study of Navio *et al.* (1996) showed that the structure of TiO_2 was similar to that of TiO_2 impregnated with Fe(III) from Iron(III) acetylacetonate. Therefore, the differences in catalytic activity should be mainly affected by the difference in type of metal ion species. The formation of phenol proceeds through a similar mechanism as that of Fenton chemistry by replacing the redox of Fe(III)/Fe(II) to that of Cu(II)/Cu(I) (Sasaki *et al.*, 1983; Ito *et al.*, 1988; Yamanaka *et al.*, 2002) as well as V(V)/V(IV). Even though the solvent free system is environmental friendly, the obtained yields are very low. In this case Cu/TiO_2 was highest of TON and TOF. The system should be modified in several ways such as by adding solvent or operating in photooxidation with a UV light as studied in the following sections.

2.3 Effect of solvent on the reaction performance

A solvent was used to reduce the mass transfer resistance for dissolving H_2O_2 into the benzene phase. It should be noted that 40 cm^3 of various solvents were added. In this amount, the system stills consisted of three phases (i.e., organic, aqueous and catalyst). Using a high-speed stirrer for well mixing was preferable than adding more solvent for obtaining two-phase mixture to avoid the dilution effect. The effects of several solvent species, i.e., acetone, acetronitrile and pyridine, on the reaction performance in various metal catalysts were summarized in **Table 4**.

The effect of the operation with a UV light was also provided in the table and will be described in the next section.

In the case of acetone and acetonotrile solvents, the addition of a solvent obviously improved conversion, the yield and also turnover number and turnover frequency for all metal catalysts. The Fe(III) show the highest of TON and TOF in the solvent system. These solvents are effective to prevent the decomposition of H_2O_2, which leads to an increase of TON (total activity). On the other hand, in the case of the pyridine solvent, conversion and the yield decreased when adding solvent.

These agree with the necessity of the acidic environment around the catalyst (Seo *et al.*, 1993). Acetone gave the highest conversion in all metal catalysts but, unfortunately, the selectivity was low. The acetonitrile showed a good alternative, offering a slightly lower yield with significantly higher phenol selectivity.

2.4 Effect of UV light on the reaction performance

Comparison of the results shown in Tables 3 and 4 for the cases of solvent free with and without UV light indicated that higher conversion and yield can be obtained by applying the UV light. Selectivity slightly increased in the case of an Fe catalyst while slightly decreased in the cases of Cu and V catalysts.

It should be noted that the activity of metal catalyst was ordered as Fe(III) > Cu(II) > V(V) and in the reverse order of the selectivity, which is the same trend as the cases of solvent free and solvent added both in the previous sections.

In the case of using acetone as a solvent, UV light improved the conversion but with an insignificant effect on selectivity for all metal catalysts.

In this study only a simple comparison was done on the photocatalytic oxidation of benzene. No apparent change on the selectivity was observed but strong promotion in conversion.

The primary and principal step of the UV/H_2O_2 degradation has been postulated as the initial attack by photon to hydrogen peroxide and the formation of hydroxyl free radicals (OH•) (De *et al.*, 1999).

$$H_2O_2 + h\nu \rightarrow 2OH\bullet$$

The UV light enhances the decomposition of H_2O_2 to increase the hydroxyl radicals for the reaction to phenol. However, if the amount of the hydroxyl radicals was excessive, it can convert phenol to hydroquinone and benzoquinone.

In the UV light system, TiO_2 enhanced the decomposition of H_2O_2 to hydroxyl free radicals and hydroxyl ions by generating electrons (Hong and Kang, 2006).

$$TiO_2 + h\nu \rightarrow h^+ + e^-$$

$$H_2O_2 + e^- \rightarrow OH\bullet + OH^-$$

Table 4 Catalytic performances for hydroxylation of benzene to phenol of Fe(III), Cu(II), $V(V)/TiO_2$ catalysts in a solvent-added systems and solvent free system with UV

Catalyst	Solvent	Conversion[a] [%]	Selectivity[b] [%]	Yield[c] [%]	TOF[d] [h^{-1}]	TON[e]
Fe	Acetone	4.5	32	1.44	3.35	13.39
	Acetronitrile	1.2	90	1.08	2.51	10.04
	Pyridine	0.2	95	0.19	0.44	1.77
	Solvent free with UV	2.4	51	1.22	2.85	11.35
	Acetone with UV	5.6	30	1.68	3.91	15.62
Cu	Acetone	3.1	32	0.99	2.62	10.48
	Acetronitrile	1	88	0.88	2.33	9.31
	Pyridine	0.2	92	0.18	0.49	1.91
	Solvent free with UV	1.5	72	1.08	2.86	11.43
	Acetone with UV	4.5	32	1.44	3.81	15.24
V	Acetone	2.1	39	0.82	1.74	6.97
	Acetronitrile	0.9	84	0.76	1.61	6.46
	Pyridine	0.1	100	0.1	0.21	0.85
	Solvent free with UV	1.2	82	0.98	2.09	8.33
	Acetone with UV	3.9	37	1.44	3.06	12.27

(Benzene, 11 cm^3; catalyst weight, 0.2 g; benzene/H_2O_2 mole ratio, 0.5; solvent, 40 cm^3; temperature, 303 K; pressure, 1 atm; reaction time, 4 h)
[a]Conversion [%] = (moles of benzene reacted)/(initial moles of benzene) × 100
[b]Selectivity [%] = (moles of phenol)/(moles of benzene reacted) × 100
[c]Yield [%] = (moles of phenol)/(initial moles of benzene) × 100
[d]Turnover frequency = (moles of phenol)/(moles of metal × h)
[e]Turnover number = (moles of phenol)/(moles of metal)

The hydroxyl radical reacts directly with benzene to produce a hydroxycyclohexadienyl (CHD) radical, which subsequently undergoes an H^+ abstraction by metal catalyst as follows (Bremmer *et al.*, 2000; Gao and Hua, 2004).

$$OH\bullet + \text{benzene} \rightarrow \text{CHD}$$

$$\text{CHD} + Fe(III) \rightarrow \text{phenol} + Fe(II) + H^+$$

However, the CHD radical intermediate can react with H^+ and collapse to benzene as follows.

$$\text{CHD} + Fe(II) + H^+ \rightarrow \text{benzene} + Fe(III) + \text{water}$$

Although photocatalytic activity could be modified by adding metal species rather than the promotion of OH radicals, Park and Choi (2005) suggested the effect of Fe species to oxidize CHD radicals. They have also suggested the "photo-Fenton reaction" in the presence of $Fe^{3+} + H_2O_2 + h\nu$. On the other hand, Shimizu *et al.* (2002) reported that Fe^{3+} and Cu^{2+} were selective for dihydroxybenzene while TiO_2 was likely to oxidize dihydroxybenzene to CO_2. Thus, further studies are needed on the photocatalytic promotion of added metal ions.

The side reaction of hydroxyl radicals reacted with H_2O_2 to water can occur and therefore, the concentration of H_2O_2 possibly decreased faster than the system without UV light (De *et al.*, 1999).

$$H_2O_2 + OH\bullet \rightarrow HO_2\bullet + H_2O$$

$$OH\bullet + H_2O_2 \rightarrow O_2\bullet + H + H_2O$$

$$HO_2\bullet + H_2O_2 \rightarrow OH\bullet + O_2 + H_2O$$

The species of hydrogen oxidant compound affected the generation of phenol and other aromatic compounds. Moreover, when increasing the temperature, the hydrogen oxidant compound can be decomposed faster than the decomposition at room temperature.

Comparing with the case of using acetone as a solvent, the obtained yields are similar while phenol selectivities are significantly higher in the case of solvent-free with UV light.

2.5 Effect of reducing agent

The ascorbic acid was used as a reducing agent for changing the metal ion state, such as Fe(III) to Fe(II), V(V) to V(IV) and Cu(II) to Cu(I) (Seo *et al.*, 1997). **Figure 2** shows the effects of the amount of ascorbic acid and types of solvent on the phenol yield and selectivity of the $Fe(III)/TiO_2$ catalyst.

In the case of a solvent added system, the phenol yield increased while selectivity slightly decreased with

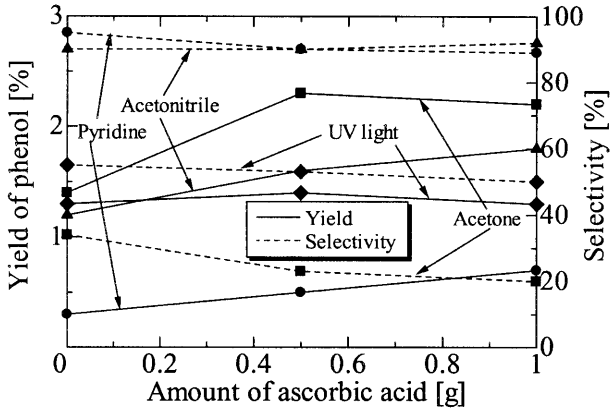

Fig. 2 Effect of the amount of ascorbic acid on the phenol yield and selectivity for different systems catalyzed by the Fe(III)/TiO_2 catalyst

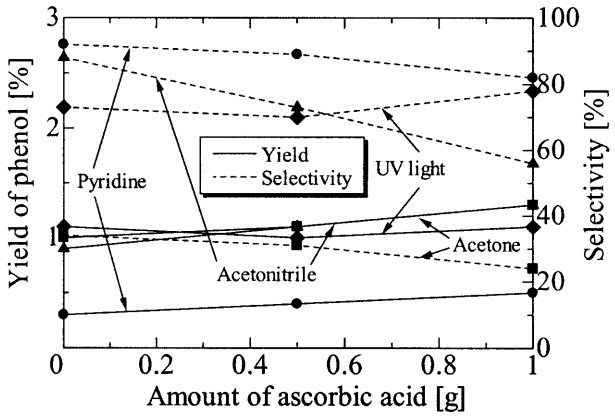

Fig. 3 Effect of the amount of ascorbic acid on the phenol yield and selectivity for different systems catalyzed by the Cu(II)/TiO_2 catalyst

an increasing amount of ascorbic acid for all solvent types. A similar tendency can be obtained for the systems catalyzed by Cu(II) and V(V) metal catalysts as shown in **Figures 3** and **4**, respectively.

The mechanism of Fenton's method is widely accepted as follows.

$$Fe(II) + H_2O_2 \rightarrow Fe(III) + OH\bullet + OH^-$$

The ascorbic acid is well known as a good reducing agent. It changes the state of metal catalyst from Fe(III) to Fe (II).

$$2Fe(III) + \text{ascorbic acid} + 0.5O_2 \rightarrow 2Fe(II) + \text{dehydroascorbic acid} + H_2O$$

$$2Fe(II) + O_2 + 2H^+ \rightarrow 2Fe(III) + H_2O_2$$

$$Fe(III) + H_2O_2 + H^+ \rightarrow Fe(II) + OH\bullet + H_2O$$

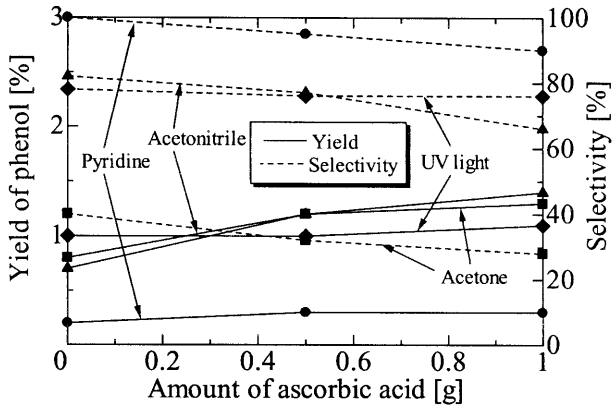

Fig. 4 Effect of the amount of ascorbic acid on the phenol yield and selectivity for different systems catalyzed by the V(V)/TiO_2 catalyst

Both Fe(III) and Fe(II) play important roles in the reaction system. Fe(III) reacts with a CHD radical intermediate to form phenol while Fe(II) promotes the decomposition of hydrogen peroxide to a hydroxyl free radical. The amount of generated hydroxyl radicals which affects the phenol formation could be controlled by the amounts of ascorbic acid and metal catalyst added.

It is worthwhile to note that the formation of phenol proceeds through the similar mechanism of that of Fenton chemistry by replacing the redox of Fe(III)/Fe(II) to that of Cu(II)/Cu(I) and V(V)/V(IV).

However, as shown in Figures 2–4, further addition of ascorbic acid caused a lower effect on the yield enhancement. In some cases, a drop of the yield was observed. It can be explained that too the much ascorbic acid, which functions as a reducing agent, suppressed the formation of Fe(III) which resulted in a decrease in the formation of phenol via the H^+ abstraction of CHD. It should be noted that phenol can be produced even though no ascorbic acid was added. These results were not the same as those reported by Miyahara *et al.* (2001) that no phenol was produced in the absence of ascorbic acid.

In the case of a solvent-free with UV light condition, the increase in the amount of ascorbic acid insignificantly affected the conversion and selectivity for all metal catalysts as shown in Figures 2–4. As the formation of active OH• species in the photocatalytic reactions does not include the oxidation of metal ions, only a retardation effect of ascorbic acid might be observed.

Conclusions

The hydroxylation of benzene to phenol with hydrogen peroxide was performed at room temperature using various transition metals, Fe(III), Cu(II) and

V(V) impregnated on TiO_2 support. The activity was ordered as follows: Fe(III) > Cu(II) > V(V); however, the phenol selectivity was in the reverse order. Among various solvents studied, i.e., acetone, acetronitrile and pyridine, acetone showed the highest conversion and yield but low in selectivity. However, acetronitrile may be an attractive solvent because of its high selectivity. Operation with UV light can significantly the improve the yield and selectivity. Addition of ascorbic acid can enhance the phenol yield; however, too much ascorbic acid can retard the yield improvement.

Acknowledgments

Financial supports from the Thailand Research Fund and Commission on Higher Education are gratefully acknowledged. The authors also would like to thank Assistant Professor Okorn Mekasuwandamrong and Assistant Professor Varong Pavarajarn for useful discussion.

Literature Cited

Bremmer, D. H., A. E. Burgess and F. B. Li; "Coupling of Chemical, Electrochemical and Ultrasonic Energies for Controlled Generation of Hydroxyl Radicals Direct Synthesis of Phenol by Benzene Hydroxylation," *Appl. Catal. A*, **203**, 111–120 (2000)

Chen, Y. W. and Y. H. Lu; "Characteristics of V-MCM-41 and Its Catalytic Properties in Oxidation of Benzene," *Ind. Eng. Chem. Res.*, **38**, 1893–1903 (1999)

Choi, J. S., T. H. Kim, K. Y. Choo, J. S. Sung, M. B. Saidutta, S. O. Ryu, S. D. Song, B. Ramachandra and Y. W. Rhee; "Direct Synthesis of Phenol from Benzene on Iron-Impregnated Activated Carbon Catalysts," *Appl. Catal. A*, **290**, 1–8 (2005)

De, A. K., B. Chaudhuri, S. Bhattacharjee and B. K. Dutta; "Estimation of (·)OH Radical Reaction Rate Constants for Phenol and Chlorinated Phenols Using UV/H_2O_2 Photo-Oxidation," *J. Hazard Mater.*, **64**, 91–104 (1999)

Dubey, A. and S. Kannan; "Liquid Phase Hydroxylation of Benzene over Cu-Containing Ternary Hydrotalcites," *Catal. Commum.*, **6**, 394–398 (2005)

Gao, F. and R. Hua; "Highly Efficient K7NiV13O38-Catalyzed Hydroxylation of Aromatics with Aqueous Hydrogen Peroxide (30%)," *Appl. Catal. A*, **270**, 223–226 (2004)

Hong, W. J. and M. Kang; "The Super-Hydrophilicities of Bi-TiO_2, V-TiO_2, and Bi-V-TiO_2 Nano-Sized Particles and Their Benzene Photodecompositions with H_2O Addition," *Mater. Lett.*, **60**, 1296–1305 (2006)

Ito, S., H. Okada, R. Katayama, A. Kunai and K. Sasaki; "Direct Conversion of Benzene to Hydroquinone Mediated with Cu(I)/Cu(II) Redox System," *J. Electrochem. Soc.*, **135**, 2996–3000 (1988)

Kanzaki, H., T. Kitamura, R. Hamada, S. Nishiyama and S. Tsuruya; "Activities for Phenol Formation Using Cu Catalysts Supported on Al_2O_3 in the Liquid-Phase Oxidation of Benzene in Aqueous Solvent with High Acetic Acid Concentration," *J. Mol. Catal. A: Chem.*, **208**, 203–211 (2004)

Lemke, K., H. Ehrich, U. Lohse, H. Berndt and K. Jahnisch; "Selective Hydroxylation of Benzene to Phenol over Supported Vanadium Oxide Catalysts," *Appl. Catal. A*, **243**, 41–51 (2003)

Liu, Y., K. Murata and M. Inaba; "Liquid-Phase Oxidation of Benzene to Phenol by Molecular Oxygen over Transition Metal Substituted Polyoxometalate Compounds," *Catal. Commun.*, **6**, 679–683 (2005)

Miyahara, T., H. Kanzaki, R. Hamada, S. Kuroiwa, S. Nishiyama and S. Tsuruya; "Liquid-Phase Oxidation of Benzene to Phenol by CuO–Al_2O_3 Catalysts Prepared by Co-Precipitation Method," *J. Mol. Catal. A: Chem.*, **176**, 141–150 (2001)

Miyake, T., M. Hamada, H. Niwa, M. Nishizuka and M. Oguri; "Effect of Vanadium Compound on the Synthesis of Phenol by Hydroxylation of Benzene with Oxygen and Hydrogen on Platinum Catalyst," *J. Mol. Catal. A: Chem.*, **178**, 199–204 (2002)

Mizuno, T., H. Yamada, T. Tagawa and S. Goto; "Partial Oxidation Benzene in Benzene–Water Bi-Phase System," *J. Chem. Eng. Japan*, **38**, 849–853 (2005)

Navio, J. A., G. Colon, M. I. Litter and G. N. Bianco; "Synthesis, Characterization and Photocatalytic Properties of Iron-Doped Titania Semiconductors Prepared from TiO_2 and Iron(III) Acetylacetonate," *J. Mol. Catal. A: Chem.*, **106**, 267–276 (1996)

Okamura, J., S. Nishiyama, S. Tsuruya and M. Masai; "Formation of Cu-Supported Mesoporous Silicates and Aluminosilicates and Liquid-Phase Oxidation of Benzene Catalyzed by the Cu-Mesoporous Silicates and Aluminosilicates," *J. Mol. Catal. A: Chem.*, **135**, 133–142 (1998)

Park, H. and W. Choi; "Photocatalylytic Conversion of Benzene to Phenol Using Midified TiO_2 and Polyoxometalates," *Catal. Today*, **101**, 291–297 (2005)

Sasaki, K., A. Kunai, J. Harada and S. Nakabori; "Electrolytic Hydrogenation of Phenols in Aqueous Acid Solutions," *Electrochimica. Acta*, **28**, 671–674 (1983)

Schmidt, R. J.; "Industrial Catalytic Processes-Phenol Production," *Appl. Catal. A*, **280**, 89–103 (2005)

Seo, Y. J., T. Tagawa and S. Goto; "Liquid Phase Oxidation of Benzene to Phenol over Supported $FeCl_3$ Catalyst," *J. Mol. Catal.*, **78**, 201–210 (1993)

Seo, Y. J., T. Tagawa and S. Goto; "Effect of Supports for the Direct Cxidation of Benzene to Phenol over Supported $FeCl_3$ Catalyst," *React. Kinet. Catal. Lett.*, **54**, 265–271 (1995)

Shimizu, K., T. Kaneko, T. Fujishima, T. Kodama, H. Yoshida and Y. Kitayama; "Selective Oxidation of Liquid Hydrocarbons over Photoirradiated TiO_2 Pillared Clays," *Appl. Catal. A*, **225**, 185–191 (2002)

Stockmann, M., F. Konietzni and J. U. Notheis; "Selective Oxidation of Benzene to Phenol in Liquid Phase with Amorphous Microporous Mixed Oxides," *Appl. Catal. A*, **225**, 343–358 (2001)

Uriarte, A. K., M. A. Rodkin, M. J. Gross, A. S. Kharitonov and G. I. Panov; "Direct Hydroxylation of Benzene to Phenol by Nitrous Oxide," *Stud. Surf. Sci. Catal.*, **110**, 857–864 (1998)

Xiao, F. S., J. Sun, X. Meng and R. Yu; "A Novel Catalyst of Copper Hydroxyphosphate with High Activity in Wet Oxidation of Aromatics," *Appl. Catal. A*, **207**, 267–271 (2001)

Yamanaka, H., R. Hamada, H. Nibuta, S. Nishiyama and S. Tsuruya; "Gas-Phase Catalytic Oxidation of Benzene over Cu-Supported ZSM-5 Catalysts: An Attempt of One-Step Production of Phenol," *J. Mol. Catal. A: Chem.*, **178**, 89–95 (2002)

Zhang, J., Y. Tang, G. Li and C. Hu; "Room Temperature Direct Oxidation of Benzene to Phenol Using Hydrogen Peroxide in the Presence of Vanadium-Substituted Heteropolymolybdates," *Appl. Catal. A*, **278**, 251–261 (2005)

Appendix 12

J. Ind. Eng. Chem., **Vol. 13**, No. 3, (2007) 444-451

Liquid Phase Hydroxylation of Benzene to Phenol with Hydrogen Peroxide Catalyzed by Fe(III)/TiO_2 Catalysts at Room Temperature

Garun Tanarungsun, Worapon Kiatkittipong*, Suttichai Assabumrungrat†, Hiroshi Yamada, Tomohiko Tagawa**, and Piyasan Praserthdam**

Center of Excellence in Catalysis and Catalytic Reaction Engineering, Department of Chemical Engineering, Faculty of Engineering, Chulalongkorn University, Bangkok 10330, Thailand
**Department of Chemical Engineering, Faculty of Engineering and Industrial Technology, Silpakorn University, Nakhon Pathom 73000, Thailand*
***Department of Chemical Engineering, Nagoya University, Chikusa, Nagoya, 464-8603, Japan*

Received November 15, 2006; Accepted February 2, 2007

Abstract: Liquid phase hydroxylation of benzene to phenol with hydrogen peroxide on Fe(III)/TiO_2 catalysts was examined at room temperature. The catalytic performances of various TiO_2 supports were tested. The TiO_2 (JRC-TIO-1, anatase) having the highest surface area and pore volume appeared to be the most suitable support because it offered the highest activity and selectivity. The effects of the Fe(III) precursor and Fe(III) loading were investigated. The catalyst prepared from iron(III) acetylacetonate with 5 wt% Fe(III) loading was selected as a suitable catalyst. From tests of seven solvents, it was found that acetone gave the highest conversion and yield; however, acetonitrile may also be attractive because it offered high selectivity. Biphasic operation, introduced by adding more amount of solvent, did not show a potential improvement because the dilution effect seemed to play an important role in the reaction system. Finally, it was revealed that increasing the amount of ascorbic acid helped increase the conversion by enhancing the decomposition of H_2O_2 to hydroxyl radicals. However, it suppressed the formation of Fe(III), which resulted in a decrease in the degree of phenol formation. In addition, phenol can be further reacted with excess hydroxyl radicals to yield hydroquinone, benzoquinone, and catechol, resulting in a decreased selectivity.

Keywords: *hydroxylation of benzene, phenol production, hydrogen peroxide, Fe(III), TiO_2*

Introduction

Phenol is an important intermediate for the synthesis of various petrochemical and agrochemical products. Commercial phenol production is mainly based on the cumene process [1]. Because this process produces acetone as a co-product, which will be oversupplied in the future, and the cumene hydroperoxide intermediate can decompose violently, the development of an alternative process is desired. A number of studies have been focused on the direct oxidation of benzene to phenol.

There are two main pathways for the direct oxidation of benzene to phenol; i.e., gas phase and liquid phase reactions. Gas phase hydroxylation of benzene with nitrous oxide has been conducted in a pilot facility [2]. However, this process is suitable only when a supply of nitrous oxide is available, for example, as a by-product from adipic acid synthesis. Major problems arise when adapting this process to industrial applications because of catalyst deactivation by heavy coke formation and the low phenol selectivity of nitrous oxide [2]. In addition, the process is operated at an elevated temperature (higher than 573 K) and results in marginal conversion, resulting in undue high costs. Liquid phase hydroxylation of benzene to phenol is operated at room temperature or temperatures normally not higher than 353 K. H_2O_2 or O_2 is employed as an oxidant. High selectivity can be obtained with lower oxidant cost when compared with the gas phase operation. Therefore, many researchers have focused on this route and have aimed to develop suitable catalysts for the reaction.

† To whom all correspondence should be addressed.
(e-mail: suttichai.A@chula.ac.th)

Table 1. Materials and Chemicals

Metal source	Iron(III) acetylacetonate, 97 % (Aldrich)
	Iron(III) nitrate monohydrate, 98 % (SIGMA)
	Iron(III) chloride hexahydrate, 99 % (MERCK)
Support	TiO_2 (JRC-TIO1, JRC-TIO4) (Catalysis Society of Japan)
	TiO_2, 99 % (Fluka)
	Titanium(IV) dioxide, powder, 99.8 % (Aldrich)
Solvent	Acetone, 99.8 % (Carlo Erba)
	Acetonitrile, 99.8 % (MERCK)
	1- Butyl alcohol, 99 % (Fluka)
	tert-Butyl alcohol, 99 % (Fluka)
	Dichloromethane, 99 % (Carol Erba reagenti)
	Ethyl alcohol, 99.9 % (Carol Erba reagenti)
	Pyridine, 99.7 % (MERCK)
Reducing agent	Ascorbic acid, 99.7 % (Polskic Odczynniki Chemiczne S.A.)
Substrate	Benzene, 99.7 % (MERCK)
Oxidant	Hydrogen peroxide, 30 % wt. (MERCK)
By-product reference	Biphenyl, 99.9 % (Fluka)
	Catechol, 98 % (Fluka)
	Phenol, 99 % (Panreac Sintesis)
	Quinol, 99.8 % (APS)
	1,4 Benzoquinone, 98 % (ACROS)

Several kinds of metal, such as Fe, Cu, and V, were loaded on various supports, such as SiO_2, Al_2O_3, HZSM-5, MCM-41, and TiO_2 [3-6]. Fe-containing catalysts have drawn some attention from researchers for the hydroxylation of benzene to phenol because of its low cost and acceptable yield. Seo and coworkers [3,7] studied the use of Fe(II) and Fe(III) on SiO_2. Various Fe precursors, i.e., $FeCl_3$, $FeCl_2$, and $Fe(NO_3)_3$, were investigated. Fe(III) from $FeCl_3$ as precursor showed good performance for the hydroxylation of benzene to phenol; the addition of acidic compounds strongly affected the catalytic performance.

The solvent is usually added to the reaction system to dissolvs hydrogen peroxide and benzene into one phase for the oxidation of benzene to phenol. Several solvents, such as acetone, acetonitrile, acetic acid, pyridine and, dichloromethane, have been employed [8-14]. However, there are only a few studies that have compared the effects of various solvent types. Stockmann and coworkers [10] studied the oxidation of benzene to phenol using amorphous microporous mixed-oxide catalyst. Acetonitrile showed the highest yield among several solvents; i.e., 2-propanol, dimethyl glycol, and propylene glycol. On the other hand, some researchers have studied solvent-free systems from an environmental viewpoint. Low conversion and yield are usually reported.

TiO_2 has been used extensively as a catalyst and support for oxidation and photooxidation reactions [15-19]. It is widely accepted that OH^o radicals can also be generated on illuminated TiO_2 surfaces [20]. TiO_2 photocatalysis has been applied to the hydroxylation of benzene to phenol, but the conversion efficiency in this photocatalysis was lower than that of the Fenton process. Therefore, surface modifications of TiO_2 should be performed. The presence of electron acceptors, i.e., Fe and O_2, enhanced the photocatalytic reaction [20]. In addition, recent studies have found that Cu-, Fe-, and V-containing catalysts gave high yields of phenol [12,13]. It should be noted that comparison of the reaction performance of different systems published in the open literature is rather difficult because of differences in various parameters, such as the types and amounts of catalysts, supports, oxidants, and solvents and also differences in operating conditions such as the operating temperature and pressure.

In this study, the liquid phase hydroxylation of benzene to phenol with hydrogen peroxide on various Fe(III)/TiO_2 catalysts at room temperature was investigated. Several TiO_2 supports were tested. TiO_2 has been used as a support for many oxidation reactions. It was also reported to offer high performance for the oxidation of benzene to phenol [20]. The effects of the type of Fe(III) precursor and the Fe(III) loading were studied to find a suitable catalyst. The catalytic performances of the systems with different types of solvent and under biphasic/triphasic operations were compared. In addition, the influence of the amount of ascorbic acid as a reducing agent was considered.

Experimental

Materials and Chemicals

Table 1 summarizes the materials and chemicals employed in this work. All chemicals were used without prior purification. Four types of TiO_2 supports, i.e., TiO_2 (JRC-TIO-1), TiO_2 (JRC-TIO-4), TiO_2 (Fluka), and TiO_2 (Aldrich), and three types of Fe(III) precursors, i.e., iron(III) acetylacetonate, iron(III) chloride hexahydrate, and iron(III) nitrate monohydrate, were used in the study.

Catalyst Preparation

Fe(III)/TiO_2 catalysts were prepared by impregnation of TiO_2 support powder in a solution of Fe(III) precursor at 353 K, followed by evaporation and drying overnight. The catalysts obtained were calcined in a furnace continuously fed with air (flow: 60 cm^3/min). The temperature was increased from room temperature to 773 K at a heating rate of 10 K/min and then held for 5 h to remove organic residues. After calcination, the catalysts were stored in a dessicator.

Table 2. Catalytic Performance of Commercial TiO_2 Supports

Catalyst	Conversion [a] (%)	Selectivity [b] (%)	BET surface area (m^2/g)	Pore volume (cm^3/g)
TiO_2 (JRC-TIO1, anatase)	0.8	100	76.6	0.29
TiO_2 (JRC-TIO4, anatase)	0.2	72	51.8	0.11
TiO_2 (Fluka, anatase)	0.4	100	16.5	0.03
TiO_2 (Aldrich, anatase)	0.1	70	8.0	0.02
TiO_2 (JRC-TIO1, rutile)	0.03	100	1.8	0.003
TiO_2 (Fluka, rutile)	0.01	100	1.7	0.002

(Benzene = 11 cm^3; catalyst weight = 0.2 g; benzene/H_2O_2 mole ratio = 0.5; temperature = 303 K; pressure = 1 atm; reaction time = 4 h)
[a] Conversion calculated as moles of benzene reacted per initial moles of benzene*100 %
[b] Selectivity calculated as moles of phenol per mole of benzene reacted*100 %

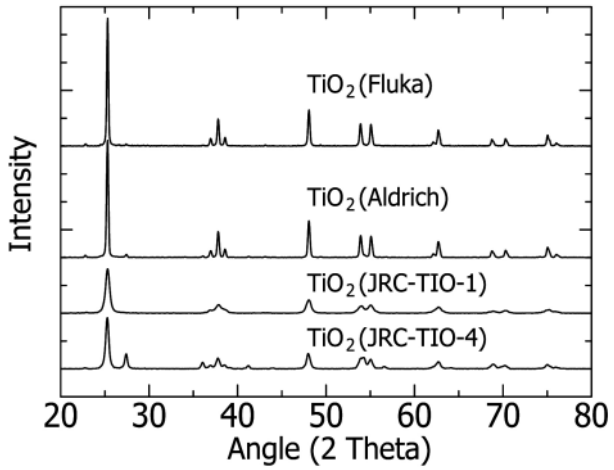

Figure 1. XRD patterns of TiO_2 supports.

Characterization

XRD patterns of the TiO_2 supports and Fe(III)/TiO_2 catalysts were obtained by using a SIEMENS D 5000 X-ray diffractrometer, with Cu Ka radiation and equipped with a Ni filter; range of detection (2θ): 20 ~ 80; resolution 0.04.

The BET surface areas and porosities of the catalysts were measured by a Micromeritics ASAP 2020 instrument. A sample of 0.3 g was degassed at 573 K for 3 h and the amount of N_2 adsorbed was observed.

XPS surface analysis was performed using Kratos Amicus X-ray photoelectron spectroscopy. The XPS spectra were measured using the following conditions: Mg Ka X-ray source at current of 20 mA and 12 keV, resolution of 0.1 eV/step, and pass energy of 75 eV. The operating pressure was ca. 1×10^{-6} Pa. A wide-scan survey spectrum was collected for each sample to determine the elements present on the surface. All the binding energies were calibrated internally with the carbon C 1s photoemission peak at 285.0 eV. Photoemission peak areas were determined after smoothing and background subtraction using a linear routine. Deconvolution of complex spectra was done by fitting with Gaussian (70 %)-Lorentzian (30 %) shapes using the VISION 2 software that came with the XPS system.

Experimental Setup and Product Analysis

The hydroxylation of benzene by H_2O_2 was carried out in a 125-cm^3 round-flat-bottomed flask at 303 K and 1 atm with high-speed stirring at 600 rpm. In a typical experiment, 0.5 g of ascorbic acid (2.8 mmol) was added in a liquid mixture containing 40 cm^3 of solvent, 30 cm^3 of H_2O_2 (0.32 mol), and 11 cm^3 of benzene (0.16 mol). It should be noted that the typical experiment was operated in a triphasic system consisting of solid catalyst, solvent phase, and aqueous phase. When more solvent was added to the system, the reaction might have occurre in the biphasic system comprising the solid catalyst and solvent phase.

The feed and products were analyzed by a gas chromatogragh (SHIMADZU 9A) equipped with a packed column of GP 10 % SP-2100. The operating conditions of the GC were as follows: injection temperature of 523 K, detector temperature of 523 K, initial column temperature of 383 K, final column temperature of 443 K, and temperature programmed rate of 10 K/min. The products were also analyzed by GC-MS, especially for some product species that could not be detected by the FID detector. The benzene conversion is defined as the number of moles of benzene consumed by the reaction divided by the initial unmber of moles of benzene, while the phenol selectivity is defined as the nuber of moles of generated phenol divided by the number of moles of benzene consumed.

Results and Discussion

Selection of TiO_2 Supports

TiO_2 was used as a catalyst support for the hydroxylation of benzene to phenol. TiO_2 supports were characterized by XRD. The similar XRD patterns shown in Figure 1 indicate that all of the supports were of the anatase phase [21]. The blank reaction tests of the TiO_2 supports were performed under solvent-free conditions. The results shown in Table 2 reveal that TiO_2 (JRC-TIO-1) offered the highest conversion, which corresponded with it also having the highest BET surface area and pore

Table 3. Effects of %Fe(III) Loading and Type of Fe(III) Precursor on Catalytic Performance

Precursor	Fe loading (%)	Conversion[a]	Selectivity[b]	Yield[c]	TOF[d]	TON[e]	BET[f]	Pore volume [g]
Fe(III) aca	1	4.7	25	1.19	13.83	55.34	74.4	0.26
	5	10.8	21	2.29	5.32	21.30	68.5	0.25
	10	13.2	20	2.65	3.08	12.32	64.3	0.22
	20	14.8	18	2.63	1.53	6.11	57.9	0.19
Fe(III) Cl	1	4.2	29	1.23	14.26	57.03	72.4	0.27
	5	9.2	23	2.16	5.02	20.09	69.1	0.24
	10	11.2	20	2.21	2.57	10.28	64.8	0.23
	20	12.8	18	2.24	1.30	5.21	58.5	0.2
Fe(III) N	1	5.1	24	1.23	14.29	57.15	70.1	0.26
	5	11.2	19	2.13	4.95	19.81	65.4	0.23
	10	13.7	16	2.16	2.51	10.04	59.9	0.22
	20	16.1	14	2.20	1.28	5.12	54.2	0.18

(Benzene = 11 cm^3; catalyst weight = 0.2 g; benzene/H_2O_2 mole ratio = 0.5; acetone solvent = 40 cm^3; ascorbic acid = 0.5 g; temperature = 303 K; pressure = 1 atm; reaction time = 4 h)

[a] Conversion calculated as moles of benzene reacted per initial moles of benzene*100 %

[b] Selectivity calculated as moles of phenol per mole of benzene reacted*100 %

[c] Yield calculated as moles of phenol per initial moles of benzene*100 %

[d] Turnover frequency calculated as moles of phenol per mole of Fe per h

[e] Turnover number calculated as moles of phenol per mole of Fe

[f] BET surface area (m^2/g)

[g] Pore size volume (cm^3/g)

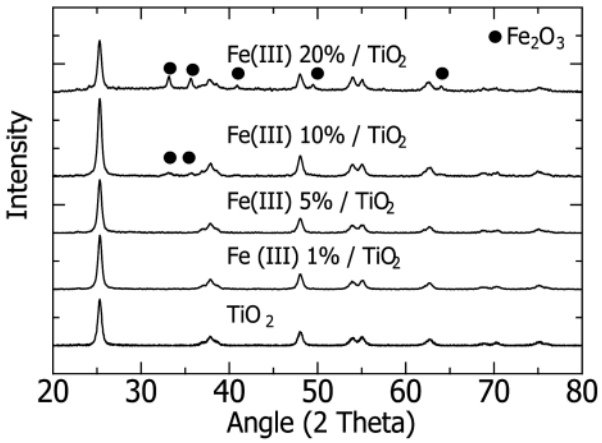

Figure 2. XRD patterns of Fe(III)/TiO_2 at various % loading (Fe(III) acetylacetonate as precursor).

volume. TiO_2 (JRC- TIO-1) and TiO_2 (Fluka) were further converted to the rutile phase by calcination at 773 K for 20 h. The reaction tests reveal that although TiO_2 in the rutile phase still maintained high selectivity (100 %), the conversion became much lower, which corresponded with the significant reduction of its BET surface area and pore volume. It should be noted that the obtained conversion was significantly low and, therefore, loading with metal catalyst was needed. Thus, TiO_2 (JRC-TIO-1) in the anatase phase was selected as a support for all of the following experiments.

Effects of Fe(III) Precursor and Fe(III) Loading

Fe(III)/TiO_2 catalysts were prepared from three precursors: Fe(III) acetylacetonate, Fe(III) chloride hexahydrate, and Fe(III) nitrate monohydrate, abbreviated as Fe (III) acac, Fe(III) Cl, and Fe(III) N, respectively. Because the TiO_2 surface is hydrophilic, the precursors in hydrate form or having water as a solvent should allow the uniform distribution of Fe metal in the catalysts. The XRD patterns of samples with various percentages of Fe(III) loadings (in the case of Fe(III) acac as precursor) are shown in Figure 2. The obvious peaks of Fe(III) in Fe_2O_3 crystallize were observed only at a Fe(III) loading of 20 %. The relationship between the Fe(III) loading at surface determined by XPS and the Fe(III) loading is shown in Figure 3. The results indicate that the metal was located more at the surface of TiO_2 than in the pores. In addition, it is clear that the type of precursor influenced the metal distribution in the catalysts. The accessibility of Fe(III) into the catalyst pores followed the order Fe(III) Cl > Fe(III) acac $\approx$ Fe(III) N.

The effects of the Fe(III) loading on the benzene conversion, phenol selectivitiy, and yield for different catalysts are summarized in Table 3. The values of the turnover frequency, turnover number, BET surface area, and pore volume are also provided. The byproducts from the reaction system were hydroquinone, benzoquinone, and catechol. The experimental results indicated that the conversion increased with increasing Fe(III) loading, while the selectivity decreased, thus an optimum yield was ob-

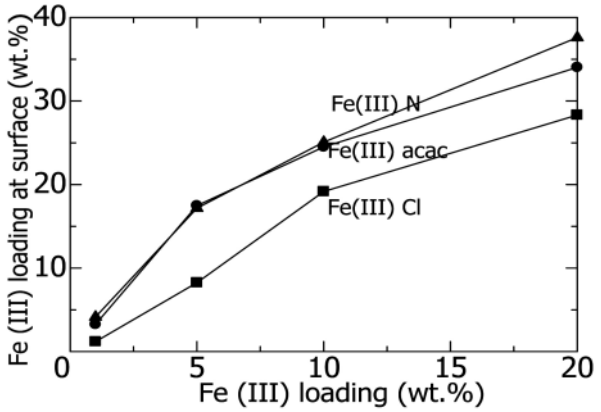

Figure 3. Relationship between %Fe on surface and %Fe(III) loading for different Fe precursors.

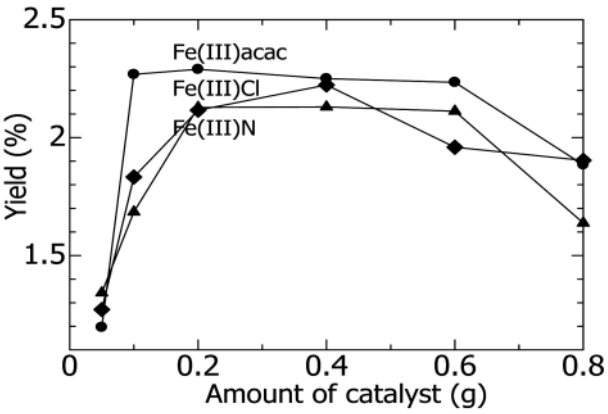

Figure 5. Effect of catalyst weight on phenol yield for different Fe(III) precursors.

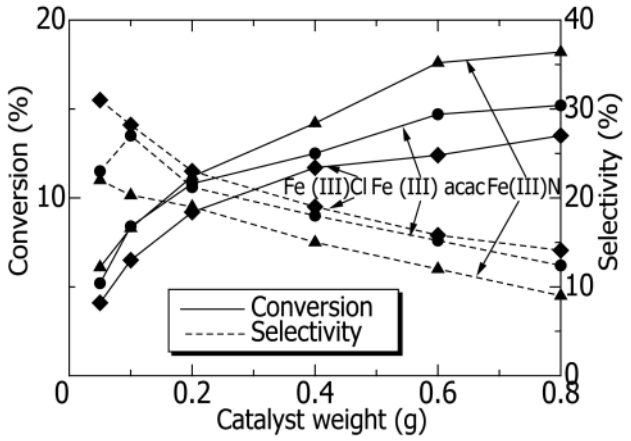

Figure 4. Effect of catalyst weight on benzene conversion and phenol selectivity for different Fe(III) precursors.

served. The increases in conversion were obtained as a result of the increased amount of metal active species. However, when considering the values of TOF and TON, it is noticed that the metal active sites were utilized less efficiently at high Fe(III) loadings. This situation is likely to be due to the reduced BET surface area and pore volume. The increase in yield was less pronounced when the Fe(III) loading was higher than 5 wt%. Therefore, this value was selected as an optimum Fe(III) loading for all precursors.

Figure 4 shows the catalytic performances of Fe(III)/TiO_2 catalysts prepared from the three precursors at different catalyst weights. The Fe(III) loading of the catalysts was 5 wt%. The benzene conversion increased, but the phenol selectivity decreased, upon increasing the amount of catalyst. This situation because phenol can be further reacted to give catechol, benzoquinone, and hydroquinone, which are undesirable by products. The catalytic activity followed the order Fe(III) N > Fe(III) acac > Fe(III) Cl; however, the selectivity followed the opposite order. From the corresponding yields (Figure 5), the most suitable precursor and catalyst weight were Fe(III) acac and 0.2 g, respectively.

It should be noted that the type of Fe(III) precursor influenced the metal distribution of the catalyst and its catalytic performance. It is likely that the reaction took place mainly at the catalyst surface because the rank of the catalytic activity observed from the benzene conversion in Table 3 followed the same trend as that shown in Figure 3 for all values of catalyst loading. In addition, the type of catalyst precursor may not significantly govern the selectivity. As shown in Figure 4, for example, when the conversion was ca. 12.5 %, the corresponding values of selectivity of Fe(III) N, Fe(III) acac, and Fe(III) Cl were ca. 15.5, 17, and 15 %, respectively, i.e., the were essentially equivalent. However, further studies are required to consider this situation in more detail.

Effect of Type of Solvent and Biphasic/Triphasic Operation

Solvent was used to reduce the mass transfer resistance by helping dissolve H_2O_2 into the benzene phase. Under the standard conditions with a solvent volume of 40 cm^3, the reaction was performed in a triphasic system comprising the solid catalyst, organic phase, and aqueous phase. The oxidation performances of the system with different solvents are summarized in Table 4. High yields were obtained for acetone, dichloromethane, and acetonitrile, respectively. Acetone offered the highest benzene conversion and phenol yield, but low selectivity. Acetonitrile might be a good alternative solvent because it provided very high selectivity with a yield as high as that obtained when using dichloromethane as solvent. From these observations, acetone and acetonitrile were further considered to compare the catalytic performance in biphasic and triphasic operations.

Figure 6 shows the catalytic performance of the reaction system using different amounts of solvent; i.e., 40, 60, and 80 cm^3. In the case of acetone, the system changed

Table 4. Effect of Solvent Type on the Catalytic Performance of Fe(III)/TiO_2 Catalysts

Solvent	Conversion[a] (%)	Selectivity[b] (%)	Yield[c] (%)	TOF[d] (1/h)	TON[e] (-)
Acetone	10.8	21.2	2.3	5.32	21.3
Dichloromethane	2.2	62	1.4	3.18	12.7
Acetonitrile	1.3	97	1.3	2.93	11.7
Pyridine	0.8	92	0.7	1.73	6.9
tert-Butyl alcohol	1.5	47	0.7	1.65	6.6
1-Butyl alcohol	1.5	10	0.2	0.35	1.4
Ethyl alcohol	1.3	8	0.1	0.25	1

(Benzene = 11 cm^3; % Fe(III) loading = 5 wt%; catalyst weight = 0.2 g; benzene/H_2O_2 mole ratio = 0.5; solvent = 40 cm^3; ascorbic acid = 0.5 g; temperature = 303 K; pressure = 1 atm; reaction time = 4 h)

[a] Conversion calculated as moles of benzene reacted per initial moles of benzene*100 %

[b] Selectivity calculated as moles of phenol per mole of benzene reacted*100 %

[c] Yield calculated as moles of phenol per initial mole of benzene*100 %

[d] Turnover frequency calculated as moles of phenol per mole of Fe per h

[e] Turnover number calculated as moles of phenol per mole of Fe

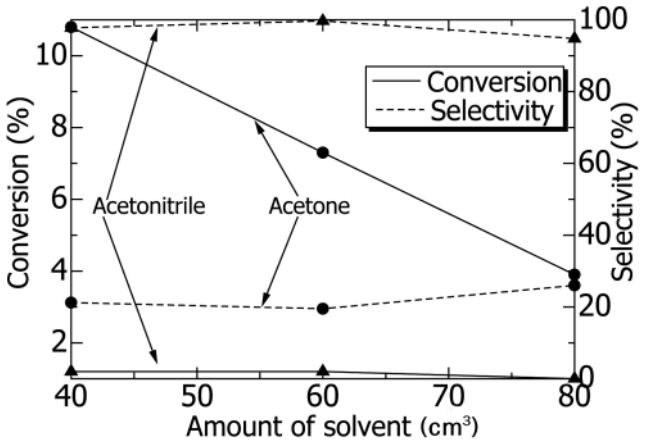

Figure 6. Effect of amount of solvent on benzene conversion and phenol selectivity.

from triphasic to biphasic at 60 cm^3. The benzene conversion dramatically decreased, while the selectivity increased slightly, when the system changed to biphasic and when more solvent was added in the biphasic system. In the case of acetonitrile, the system remained triphasic at 60 cm^3 and became biphasic at 80 cm^3. An almost insignificant effect of the amount of acetonitrile on the conversion and selectivity was observed, at least within the range of this study. Although it was expected that operation in biphasic systems would eliminate the presence of interfacial mass transfer resistance and, consequently, improve the catalytic performance of the reaction system, the dilution effect, as well as the poor mixing induced by the addition of extra solvent, retarded any such improvement. For both solvent cases, biphasic operation did not have a beneficial effect on the catalytic performance. This situation was particularly obvious in the case of acetone as solvent, which offered much lower performance. It should be noted that for the case of acetonitrile, which is not an inert solvent but participates directly in the reaction [10], no significant drop in the catalytic performance was observed upon increasing the amount of solvent. This study suggest that selection of a suitable amount of solvent is important, but operation in a biphasic system is not always advantageous.

Effect of the Amount of Ascorbic Acid

The amount of ascorbic acid was varied between 0.5 and 5 g using two types of solvent; i.e., acetone and acetonitrile.

The mechanism of Fenton's method is widely accepted as follows:

$$Fe(II) + H_2O_2 \rightarrow Fe(III) + OH^{o} + OH^{-} \quad (1)$$

The hydroxyl radical reacts directly with benzene to produce cyclohexadienyl (CHD) radical, which subsequently undergoes an H^+ abstraction as follows [22,23]:

$$OH^{o} + \text{benzene} \rightarrow CHD \quad (2)$$

$$CHD + Fe(III) \rightarrow \text{phenol} + Fe(II) + H^{+} \quad (3)$$

However, the CHD radical intermediate can react with H^+ and collapse to benzene as follows:

$$CHD + Fe(II) + H^{+} \rightarrow \text{benzene} + Fe(III) + \text{water} \quad (4)$$

Ascorbic acid is well known as a good reducing agent. It changes the state of the metal catalyst from Fe(III) to Fe(II).

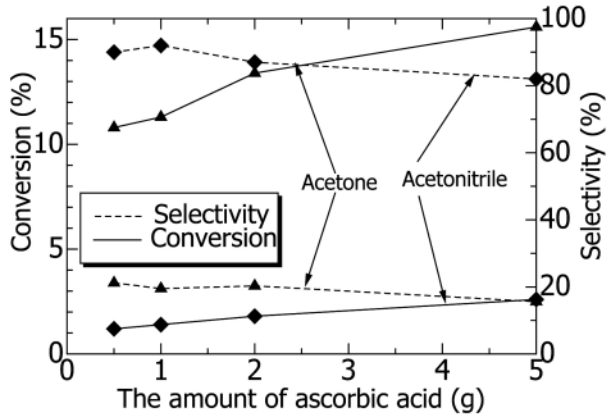

Figure 7. Effect of amount of ascorbic acid on benzene conversion and phenol selectivity.

2 Fe(III) + ascorbic acid + 0.5 O_2 → 2 Fe(II) + Dehydroascorbic acid + H_2O

2 Fe(II) + O_2+ 2H^+ → 2Fe(III) + H_2O_2

Fe(III) + H_2O_2 + H^+ → Fe(II) + OH^o + H_2O

Both Fe(III) and Fe(II) play important roles in the reaction system. Fe(III) helps to catalyze the conversion of the CHD radical intermediate to phenol, while Fe(II) promotes the decomposition of hydrogen peroxide to hydroxyl free radicals. The amount of generated hydroxyl radicals which affects phenol formation, could be controlled by the amounts of ascorbic acid and metal catalyst added.

As shown in Figure 7 the benzene conversion increased with increasing the amount of ascorbic acid, while the selectivity decreased slightly, in both the acetone and acetonitrile systems.

This situation can be explained by considering that increasing the amount of ascorbic acid activated the state change from Fe(III) to Fe(II), which enhanced the decomposition of H_2O_2 to hydroxyl radicals (as shown in Eq. 1) and, consequently, increased the benzene conversion (Eq. 2). However, too much ascorbic acid, which functioned as a reducing agent, suppressed the formation of Fe(III), which resulted in a decrease in the formation of phenol via the H^+ abstraction of CHD (Eq. 3). In addition, CHD can easily collapse to benzene when the Fe(II) content increased (Eq. 4) and also phenol can be further reacted with excess hydroxyl radicals to yield catechol, hydroquinone, and benzoquinone, resulting in the decrease of selectivity.

It is should be noted that ascorbic acid was highly soluble in the aqueous phase, but not in the organic phase. The addition of solvent was necessary to promote the reaction in this system by dissolving H_2O_2, ascorbic acid, and benzene into one phase.

Conclusion

The liquid phase hydroxylation of benzene to phenol with hydrogen peroxide catalyzed by Fe(III)/TiO_2 catalysts was investigated. The most suitable Fe(III) precursor and %Fe(III) loading were iron(III) acetylacetonate and 5 wt%, respectively. Among the solvents studied (acetone, dichloromethane, acetronitrile, pyridine, *tert*-butyl alcohol, 1-butyl alcohol, and ethyl alcohol), acetone showed the highest conversion and yield, but low selectivity. However, acetronitrile may be an attractive solvent because of its high selectivity. Biphasic operation was not attractive compared to triphasic operation because of the dilution effect. Benzene conversion increased with increasing the amount of ascorbic acid; however, too much ascorbic acid retarded the yield improvement because of lower phenol selectivity.

Acknowledgment

Financial support from the Thailand Research Fund and Commission on Higher Education are gratefully acknowledged.

References

1. R. J. Schmidt, *Appl. Catal. A*, **280**, 89 (2005).
2. G. I. Panov, A. K. Uriarte, M. A. Rodkin, and V. I. Sobolev, *Catal. Today*, **41**, 365 (1998).
3. Y. J. Seo, T. Tagawa, and S. Goto, *React Kinet. Catal. Lett.*, **54**, 265 (1995).
4. H. Kanzaki, T. Kitamura, R. Hamada, S. Nishiyama, and S. Tsuruya, *J. Mol. Catal. A*., **208**, 203 (2004).
5. Y. W. Chen and Y. H. Lu, *Ind. Eng. Chem. Res*., **38**, 1893 (1999).
6. J. Okamura, S. Nishiyama, S. Tsuruya, and M. Masai, *J. Mol. Catal. A*, **135**, 133 (1998).
7. Y. J. Seo, T. Tagawa, and S. Goto, *J. Mol. Catal. A*, **78**, 201 (1993).
8. T. Miyake, M. Hamada, H. Niwa, M. Nishizuka, and M. Oguri, *J. Mol. Catal. A*, **178**, 199 (2002).
9. J. Zhang, Y. Tang, G. Li, and C. Hu, *Appl. Catal. A*, **278**, 251 (2005).
10. M. Stockmann, F. Konietzni, and J. U. Notheis, *Appl. Catal. A*, **208**, 343 (2001)
11. F. S. Xiao, J. Sun, X. Meng, and R. Yu, *Appl. Catal. A*, **20**, 267 (2001).
12. Y. Liu, K. Murata, and M. Inaba, *Catal. Commun*., **6**, 679 (2005).
13. A. Dubey and S. Kannan, *Catal. Commun.*, **6**, 394 (2005).
14. J. S. Choi, T. H. Kim, K. Y., J. S. Sung, M. B.

Saidutta, S. O. Ryu, S. D. Song, B. Ramachandra, and Y. W. Rhee, *Appl. Catal. A*, **290**, 1 (2005).
15. K. D. Kim, L. B. Kim, J. B. Lee, and H. T. Kim, *J. Ind. Eng. Chem.*, **7**, 153 (2001).
16. M. S. Lee, G. D. Lee, S. S. Park, and S. S. Hong, *J. Ind. Eng. Chem.*, **9**, 89 (2003).
17. S. S. Hong, M. S. Lee, J. H. Kim, B. H. Ahn, K. T. Lim, and G. D. Lee, *J. Ind. Eng. Chem.*, **8**, 150 (2002).
18. H. H. Chung, M. J. Lee, J. Jung, and S. W. Choi, *J. Ind. Eng. Chem.*, **8**, 483 (2002).
19. H. H. Chungm and J. S. Rho, *J. Ind. Eng. Chem.*, **5**, 261 (1999).
20. H. Park and W. Choi, *Catal. Today*, **101**, 291 (2005).
21. S. S. Hong, C. S. Ju, C. G. Lim, B. H. Ahn, K. T. Lim, and G. D. Lee, *J. Ind. Eng. Chem.*, **7**, 99 (2001).
22. F. Gao and R. Hua, *Appl. Catal. A*, **270**, 223 (2004).
23. D. H. Bremmer, A. E. Burgess, and F. B. Li, *Appl. Catal. A*, **203**, 111 (2000).

Appendix 13

J. Ind. Eng. Chem., **Vol. 13**, No. 5, (2007) 870-877

Multi Transition Metal Catalysts Supported on TiO_2 for Hydroxylation of Benzene to Phenol with Hydrogen Peroxide

Garun Tanarungsun, Worapon Kiatkittipong*, Suttichai Assabumrungrat†, Hiroshi Yamada, Tomohiko Tagawa**, and Piyasan Praserthdam**

Center of Excellence in Catalysis and Catalytic Reaction Engineering, Department of Chemical Engineering, Faculty of Engineering, Chulalongkorn University, Bangkok 10330, THAILAND
**Department of Chemical Engineering, Faculty of Engineering and Industrial Technology, Silpakorn University, Nakhon Pathom 73000, THAILAND*
***Department of Chemical Engineering, Nagoya University, Chikusa, Nagoya, 464-8603, JAPAN*

Received April 24, 2007; Accepted June 13, 2007

Abstract: Liquid phase hydroxylation of benzene to phenol with hydrogen peroxide catalyzed by multi transition metals (Fe (III), V (V), and Cu (II)) supported on TiO_2 at room temperature was investigated. Particular focus was on the effects of second and third metal loading on the reaction performance. Bi- and tri-metal oxide catalysts showed obviously higher benzene conversion and phenol yield than single metal Fe supported on TiO_2. Among various solvents studied, i.e., acetone, acetonitrile, pyridine and water, acetonitrile was the most suitable solvent in terms of selectivity and yield. Operation with UV light in $FeVCu/TiO_2$ tri-metal catalyst could improve phenol yield without reduction of selectivity. The reactions could be explained as the Fenton-type mechanism for Fe (III), Cu (II), and V (V) metal catalysts. The effect of types of support on reaction performance was also investigated and their performances were ordered as follows: $TiO_2 > SiO_2 > \alpha$ - Al_2O_3.

Keywords: *oxidation of benzene, bi- and tri-metal, phenol production, hydrogen peroxide, Fe (III), V (V), Cu (II), TiO_2*

Introduction

Nowadays approximately 95 % of phenol production was produced by cumene process and the other 5 % by toluene oxidation process [1]. However, the cumene process is quite complicated as it consists of three main reaction steps, firstly, alkylation of benzene with propylene to cumene, secondly, oxidation of cumene to cumene hydroperoxide and finally, decomposition to phenol and propanone (acetone) co-product, which would be an oversupplied product in the future. The direct oxidation of benzene to phenol, a shortcut to one step reaction, is one of the attractive processes under investigation nowadays.

Many transition metal catalysts have been employed for catalyzing many oxidation reactions. However, most recent works revealed that Cu, Fe, and V containing catalysts are among the most desirable metal active species for the hydroxylation of benzene to phenol [2,3]. Stockmann and coworkers [4] used microporous mixed oxide catalysts with the transition metals (Cu, V, and Fe) whose catalytic activity was reported to follow the order of Fe > V > Cu. Acetonitrile solvent gave the best results with respect to phenol yield. Choi and coworkers [2] studied the transition metals (V (V), Fe (III), Cu (II)) supported on activated carbon. The activity of transition metals for the production of phenol was ordered as follow: V > Fe > Cu. It was found that iron and vanadium containing catalysts (with 5.0 wt% loading) gave phenol yield of over 15 %. Liu and coworkers [3] studied the transition metal substituted polyoxometalate compound for oxidation of benzene by O_2 with ascorbic acid as a reducing agent in an acetone/sulfolane/water mixed solvent. The catalytic performance of the metal species was ordered as follow: Cu > V > Fe. These transition metals

† To whom all correspondence should be addressed.
(e-mail: Suttichai.A@chula.ac.th)

Table 1. Details of Materials and Chemicals

Metal source	Iron (III) acetylacetonate 97 % (Aldrich) Cupric (II) nitrate 99 % (SIGMA) Ammonium metavanadate (V) 99.5 % (Carlo Erba reagenti)
Support	TiO_2 (JRC-TIO1) (Catalysis Society of Japan)
Solvent	Acetone 99.8 % (Carlo Erba) Acetonitrile 99.8 % (MERCK) Pyridine 99.7 % (MERCK)
Reducing agent	Ascorbic acid 99.7 % (Polskic Odczynniki Chemiczne S.A.)
Substrate	Benzene 99.7 % (MERCK)
Oxidant	Hydrogen peroxide 30 % wt. (MERCK)
Byproduct reference	Biphenyl 99.9 % (Fluka) Catechol 98 % (Fluka) Phenol 99 % (Panreac Sintesis) Quinol 99.8 % (APS) 1,4 Benzoquinone 98 % (ACROS)

were recently investigated by loading on clay support. The reactivity of metal species for phenol production was ordered as follow: V > Fe > Cu [5]. The differences in the order of metal activity were mainly arisen from the different supports. One of the interesting supports was TiO_2. When TiO_2 was photo-irradiated, its surfaces could generate OH・ radicals [6] which were important for phenol production from benzene. However, the hydroxylation of benzene to phenol with TiO_2 photocatalyst gave much lower conversion than that of the Fenton process. Therefore, TiO_2 could be used as a support accompanying with metal surface modification. In our previous works [7,8], the catalytic behavior of Fe (III), Cu (II), and V (V) catalysts impregnated on TiO_2 commercial support for the hydroxylation of benzene to phenol at room temperature was investigated. The activity of metal catalysts was ordered as follow: Fe (III) > Cu (II) > V (V); however, the phenol selectivity was in the reverse order [7]. The effect of second or third metal loading is yet to be examined in this study.

It should be noted that there are quite limited works focusing on the use of multi transition metals for direct hydroxylation of benzene to phenol. Dubey and coworkers [9] studied the multi transition metals over Cu-containing hydrotalcites with general formula of CuM(II)M(III)-HT. The ternary catalyst system offered higher activity than the binary systems; however, it was significantly influenced by the nature of bivalent metal ions as well as trivalent metal ions of HT-like lattice. Among the catalysts screened, CuCoAlHT and CuNiAlHT with (Cu + Co(or Ni))/Al = 3.0 and Cu/Co(or Ni) = 3.0 showed maximum activity with improved phenol selectivity. However, in their study low conversion of benzene was still obtained and it showed that the catalyst can catalyze phenol to catechol and hydroquinone [10]. Many researchers used titanium dioxide for photooxidation reaction and oxidation reaction [11-14].

In this study, the catalytic behaviors of Fe (III) impregnated on the TiO_2 support doped with Cu (II) and/or V (V) in bi- and tri-metal oxide catalyst systems on the hydroxylation of benzene to phenol were investigated. The influences of solvent species and UV light were studied. In addition, the effect of support type, i.e. TiO_2, -Al_2O_3 and SiO_2, was examined.

Experimental

Materials and Chemicals

Table 1 summarizes the details of materials and chemicals employed in this work. All chemicals were used without prior purification. Three supports; i.e., TiO_2 (JRC-TIO-1), α-Al_2O_3 (Aldrich), and SiO_2 (Aldrich), and three types of metal precursors; i.e., iron (III) acetylacetonate, Cupric (II) nitrate 99 % (SIGMA) and Ammonium metavanadate (V) 99.5 % (Carlo Erba reagenti) were used in the study.

Catalyst Preparation

Catalysts were prepared by impregnating a solution of metal precursor (Fe, Cu or V metal) on TiO_2, SiO_2, α-Al_2O_3 support powder at 353 K followed by evaporation and drying for overnight. The obtained catalysts were calcined in a furnace which was continuously fed with air flow (60 cm^3/min). The temperature was increased from room temperature to 773 K at a heating rate of 10 K/min and held for 5 h to remove the organic residues. After calcinations, the catalysts were stored in a dessicator. Percent loading of Fe (III) on TiO_2 was 5 wt% and loading of V (V) and Cu (II) was 2.5 wt% in the FeV/TiO_2 and FeCu/TiO_2. FeVCu/TiO_2 was 5 wt% loading of Fe (III) and 2.5 wt% loading of V (V) and Cu (II) each.

Characterization

XRD patterns of the metal supported catalysts were obtained by using X-ray diffractrometer, D 5000 (SIEMENS AG) using Cu Kα radiation equipped with Ni filter with a range of detection of (2θ) 20～80 and a resolution of 0.04.

BET surface area and porosity of the catalysts were measured by Micromeritics ASAP 2020. A sample of 0.3 g was degassed at 573 K for 3 h and the amount of N_2 adsorption was recorded.

XPS surface analysis was performed using a Kratos Amicus X-ray photoelectron spectroscopy. The XPS spectra were measured using the following conditions: Mg Ka X-ray source at current of 20 mA and 12 keV, resolution of 0.1 eV/step, and pass energy of 75 eV. The operating pressure was approximately 1×10^{-6} Pa. A

Table 2. Summary of BET Surface Area and Pore Volume of Supports and Catalysts

Catalyst	BET surface area (m^2/g)	Pore volume (cm^3/g)
TiO_2	76.6	0.29
α-Al_2O_3	2.1	0.001
SiO_2	257.3	1.50
Fe/TiO_2	68.5	0.25
FeV/TiO_2	57.5	0.19
FeCu/TiO_2	58.7	0.23
FeVCu/TiO_2	54.2	0.22
FeV/ α-Al_2O_3	2.0	0.0009
FeCu/ α-Al_2O_3	2.0	0.001
FeVCu/ α-Al_2O_3	2.1	0.001
FeV/SiO_2	239.4	1.24
FeCu/SiO_2	240.2	1.30
FeVCu/SiO_2	230.2	1.22

wide-scan survey spectrum was collected for each sample in order to determine the elements present on the surface. All the binding energies were calibrated internally with the carbon C 1s photoemission peak at 285.0 eV. Photoemission peak areas were determined after smoothing and background subtraction using a linear routine. Deconvolution of complex spectra were done by fitting with Gaussian (70 %) - Lorentzian (30 %) shapes using VISION 2 software equipped with the XPS system.

Experimental Setup and Product Analysis

The hydroxylation of benzene by H_2O_2 was carried out in a 125 cm^3 round flat bottomed flask at 303 K and 1 atm with a high speed stirrer at 600 rpm. In a typical experiment, 0.5 g of ascorbic acid (2.8 mmol) was added in a liquid mixture containing 40 cm^3 of solvent, 30 cm^3 of H_2O_2 (0.32 mol) and 11 cm^3 of benzene (0.16 mol). It should be noted that with this amount of solvent, the experiments were operated in a triphasic system consisting of solid catalyst, solvent phase and aqueous phase. For the photooxidation system, the ultraviolet light source of a black light blue fluorescent bulb (8 Watts) was included to the system which was kept in the black box.

The products were analyzed by a gas chromatogragh (SHIMADZU 9A) with a packed column of GP 10 % SP-2100. The operating conditions of GC were as follows: injection temperature of 523 K, detector temperature of 523 K, initial column temperature of 383 K, final column temperature of 443 K and temperature programmed rate of 10 K/min. The products were also analyzed by GC-MS especially for some product species which cannot be detected by the FID detector.

The terms of reaction performance were defined as follows.

Table 3. Results of % Metal Loading on TiO_2 Support Measured by XPS.

Catalyst	% metal loading*	Ratio of Fe/V or Fe/Cu
V/TiO_2 5 wt%	15.61	-
Cu/TiO_2 5 wt%	16.04	-
Fe/TiO_2 5 wt%	17.48	-
Fe, V/TiO_2 5 and 2.5 wt%	13.59, 5.73	2.37
Fe, Cu/TiO_2 5 and 2.5 wt%	13.39, 4.88	2.74
Fe, V, Cu/TiO_2 5, 2.5, and 2.5 wt%	12.20, 5.91, 5.47	2.06, 2.23

*% loading of metal calculated weight of metal / (TiO_2 added metal) × 100

$$\text{Conversion of benzene} = \frac{\text{mole of benzene reacted}}{\text{initial mole of benzene}}$$

$$\text{Yield of phenol} = \frac{\text{mole of phenol produced}}{\text{initial mole of benzene}}$$

$$\text{Selectivity of phenol} = \frac{\text{mole of phenol produced}}{\text{mole of benzene reacted}}$$

$$\text{Turn over number (TON)} = \frac{\text{mole of phenol produced}}{\text{mole of metal catalyst}}$$

$$\text{Turn over frequency (TOF)} = \frac{\text{mole of phenol produced}}{\text{mole of metal catalyst} \times \text{reaction time}}$$

Results and Discussion

Catalyst Characterization

XRD patterns of different catalysts supported on TiO_2 and the blank TiO_2 support were determined (not shown). However, no obvious peaks of Fe, Cu, and V metals were observed when compared with the pattern of the blank anatase TiO_2. This is probably due to low metal loading on the support. The values of BET surface area and pore volume of various supports and metal supported catalysts were summarized in Table 2. As metals were loaded on the supports, the surface area and pore volume decreased compared to those of the blank supports. The surface area and pore volume were ordered as follow: $SiO_2 > TiO_2 > \alpha$-Al_2O_3. The amount of metal loading on TiO_2 surface was studied by XPS and the results are shown in Table 3. The amount of metal loading (Fe (III), Cu (II), and V (V)) on the TiO_2 surface were higher than percent metal loading on the support, suggesting that the metal species were deposited more on the surface of the support. For the single metal catalysts, Fe showed the

Table 4. Catalytic Performances for Hydroxylation of Benzene to Phenol of Single Metal Fe (III), Cu (II), V (V)/TiO_2 Catalysts and bi-metal FeCu/TiO_2 and FeV/TiO_2 in Various Solvent-added Systems

Catalyst	Solvent	Conversion (%)[a]	Selectivity (%)	Yield (%)[b]	TOF (h^{-1})[c]	TON (-)[d]
5 wt%Fe/TiO_2	acetone	4.5	32	1.44	3.35	13.39
5 wt%Fe/TiO_2	acetonitrile	1.2	90	1.08	2.51	10.04
10 wt%Fe/TiO_2	acetone	13.2	20	2.65	3.08	12.32
5 wt%Cu/TiO_2	acetone	3.1	32	0.99	2.62	10.48
5 wt%Cu/TiO_2	acetonitrile	1	88	0.88	2.33	9.31
5 wt%V/TiO_2	acetone	2.1	39	0.82	1.74	6.97
5 wt%V/TiO_2	acetonitrile	0.9	84	0.76	1.62	6.46
FeCu/TiO_2*	acetone	10.5	62	6.51	10.53	42.10
FeCu/TiO_2*	acetonitrile	8.5	75	6.34	10.25	41.00
FeCu/TiO_2*	pyridine	3.6	83	2.99	4.84	19.34
FeCu/TiO_2*	Water	0.5	90	0.45	0.73	2.91
FeV/TiO_2**	acetone	8.8	70	6.16	9.26	37.04
FeV/TiO_2**	acetonitrile	7.8	85	6.63	9.97	39.86
FeV/TiO_2**	pyridine	2.4	95	2.28	3.43	13.71
FeV/TiO_2**	Water	0.3	100	0.30	0.45	1.80

Benzene: 11 cm^3 catalyst 0.2 g; benzene/H_2O_2 mole ratio: 0.5; acetone solvent 40 cm^3; ascorbic cid 0.5 g; temperature 303 K; pressure 1 atm; Reaction time 4 h;

[a]Conversion calculated as moles of benzene reacted per initial moles of benzene × 100

[b]Yield calculated as moles of phenol per initial moles of benzene × 100

[c]Turn over frequency calculated as moles of product per mole of metal per h

[d]Turn over number calculated as moles of phenol per mole of metal

* loading 5 wt%Fe and 2.5 wt%Cu

** loading 5 wt%Fe and 2.5 wt%V

highest metal dispersion on the surface. This result was corresponding well with the binary and ternary metal oxide catalysts whose Fe/Cu and Fe/V ratios were higher than 2.

Effects of Second Metal (Cu or V) and Solvent Type on the Reaction Performance

From our previous work [7], among three single metal catalysts, i.e., Fe (III), Cu (II), and V (V) supported on TiO_2, Fe showed the best performance for phenol production in terms of conversion and yield. Therefore, in this study, the effects of second metal (and third metal as will be mentioned later) on Fe-containing TiO_2 catalyst was investigated.

Some data of phenol production performances of single metal catalysts supported on TiO_2 from our previous work [7] were compared with those of bi-metal oxide catalysts from this study as shown in Table 4.

Considering the case with acetone as a solvent, the addition of a second metal, i.e., Cu, and V at 2.5 wt% on 5 wt% Fe/TiO_2 catalyst resulted in higher benzene conversion and phenol yield compared to those of Fe/TiO_2 with Fe loading of 5 wt%. Their obtained yields were also higher than those of Fe/TiO_2 with Fe loading of 10 wt%, indicating the improvement of catalytic performance by the presence of the second metal. As the kind and amount of active metals are different, discussions based on turnover frequency (TOF) should provide a better insight. At 5 wt% loading, the TOFs for Fe, Cu, and V are 3.35, 2.62, and 1.74 h^{-1}, respectively for the case of acetone solvent. It is clear that Fe is superior to Cu and V. At a higher metal loading, 10 wt% Fe/TiO_2 showed slightly lower TOF than did the 5 wt% Fe/TiO_2. It is likely due to the poorer metal dispersion at higher metal loading. With the binary metal system, the values of TOF significantly increased to 10.5 and 9.3 h^{-1} for Fe-Cu and Fe-V, respectively, compared to those of the single metal catalysts. Similar trend was observed on TON; i.e. the value increased from 13.39 (5 wt% Fe/TiO_2) to 42.1 (FeCu/TiO_2) and 37.04 (FeV/TiO_2). These higher values suggest the synergistic effect from the addition of the second components on the catalyst. The synergistic effect has been reported in some other systems. For example, Chou and coworkers [28] reported that small amount of Al loading to Cu-MCM-41 improved the conversion and selectivity of 2,3,6-trimethylphenol hydroxylation to 2,3,5-trimethylbenzoquinone; however, the selectivity decreased with high Al loading, leading to lower obtained yield.

Considering the bi-metal oxide catalyst system with different solvents, i.e., acetone, acetonitrile, pyridine and water, acetone and acetonitrile showed the substantial re-

Table 5. Catalytic Performances for Hydroxylation of Benzene to Phenol of Tri-metal FeVCu/TiO_2 Catalysts in Various Solvent-added Systems with and Without UV

Condition	Catalyst*	Solvent	Conversion (%)[a]	Selectivity (%)	Yield (%)[b]	TOF (h^{-1})[c]	TON (-)[d]
Without UV	FeVCu/TiO_2	acetone	16.5	45	7.2	8.43	33.72
	FeVCu/TiO_2	acetonitrile	10.2	70	7.14	8.36	33.44
	FeVCu/TiO_2	dichloromethane	5.2	90	4.68	5.48	21.92
	FeVCu/TiO_2	pyridine	3.9	95	3.71	4.34	17.37
	FeVCu/TiO_2	-	2.5	60	1.5	1.76	7.02
	FeVCu/TiO_2	water	0.9	100	0.9	1.05	4.21
	FeVCu/TiO_2	Ethanol	7.5	4	0.3	0.35	1.40
With UV	FeVCu/TiO_2	acetone	18.61	52	9.68	11.33	45.31
	FeVCu/TiO_2	acetonitrile	14.27	68	9.7	11.36	45.43
	FeVCu/TiO_2	pyridine	7.9	90	7.11	8.32	33.29

Benzene: 11 cm^3 catalyst 0.2 g; benzene/H_2O_2 mole ratio: 0.5; solvent 40 cm^3; ascorbic cid 0.5 g; Temperature 303 K; pressure 1 atm; Reaction time 4 h;

[a]Conversion (%) calculated as moles of benzene reacted per initial moles of benzene × 100

[b]Yield (%) calculated as moles of phenol per initial moles of benzene × 100

[c]Turn over frequency calculated as moles of phenol per mole of metal per h

[d]Turn over number calculated as moles of phenol per mole of metal

* loading 5 wt%Fe (III), 2.5 wt%V (V), and 2.5 wt%Cu (II)

action performance. In the case of acetone solvent, loading with the second metal significantly increased conversion and phenol selectivity, as discussed in the last paragraph. In the case of acetonitrile solvent, Fe/TiO_2 catalyst showed very high selectivity (~90%), and loading with the second metal increased conversion without a pronounced reduction of the selectivity. Even though pyridine and water solvents gave high selectivity, they were not attractive due to the poor benzene conversion and phenol yield. Their TOF and TON are much lower than those of the system with acetone and acetonitrile solvents.

FeVCu/TiO_2 Ternary-metal Catalyst for Hydroxylation of Benzene to Phenol with and Without UV in Various Solvents

The reaction performances of FeVCu/TiO_2 tri-metal catalyst with and without UV in various solvents were shown in Table 5. Comparing with Table 4 when using the same operating condition (without UV), FeCuV/TiO_2 tri-metal catalyst showed the improvement in terms of conversion and yield but it gave lower selectivity than the bi-metal catalysts, FeCu/TiO_2, and FeV/TiO_2, in both acetone and acetonitrile solvents. Although, the TOF value of the tri-metal catalyst was lower than those of the bi-metal catalysts, the value was still higher than those of the single-metal systems, indicating that the second and third components are still effective to promote the catalytic performance. It was further observed that acetone gave a yield as high as acetonitrile; however, the selectivity was lower. Therefore, acetonitrile was considered as the best solvent in this system.

Like the bi-metal catalysts, the selectivity achieved in the tri-metal catalyst system with pyridine and water solvents was still very high (almost 100 %). Compared to the case without solvent, pyridine gave higher benzene conversion but the value was still small. For the case of water as the solvent, the decrease of H_2O_2 concentration according to the increase of the aqueous phase volume may lead to a dilution effect. Therefore, phenol yield was lower than that of the case without solvent. It can be concluded that the performance of the solvent can be ordered as follow: acetonitrile > acetone > dichloromethane > pyridine > water > ethanol. It is probably because the polarity index of acetonitrile (5.8) was higher than that of acetone (5.1), and therefore, acetonitrile can dissolve more hydroxyl peroxide to react with benzene in the organic phase than does the acetone. The increased ratio of benzene per oxidant in the benzene phase results in a higher catalytic reaction in the system. The results showed a similar tendency with the study of Zhang and coworkers [29] which showed an order as: acetonitrile > acetone > alcohol for the system catalyzed by $NaVO_3$ catalyst.

The mechanism of Fenton's method is widely accepted as follows [16,31].

$$Fe(II) + H_2O_2 \rightarrow Fe(III) + OH^{o} + OH^{-} \quad (1)$$

The hydroxyl radical reacts directly with benzene to produce cyclohexadienyl (CHD) radical, which subsequently undergoes an H^+ abstraction as follows.

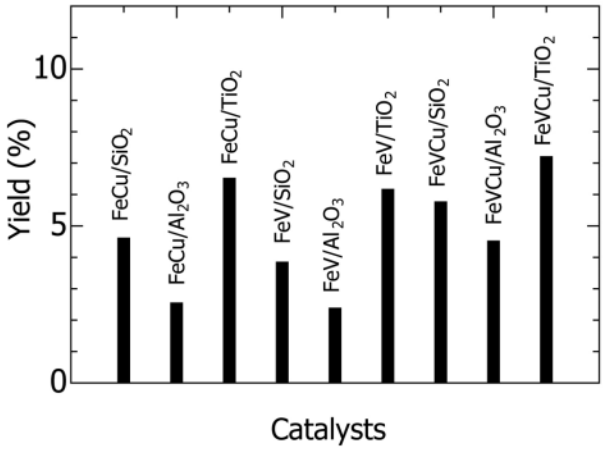

Figure 1. Comparison of phenol yield of different catalysts.

$$OH^{o} + \text{benzene} \rightarrow \text{CHD} \quad (2)$$

$$\text{CHD} + \text{Fe (III)} \rightarrow \text{phenol} + \text{Fe (II)} + H^{+} \quad (3)$$

However, the CHD radical intermediate can react with H^+ and collapse to benzene as follows.

$$\text{CHD} + \text{Fe (II)} + H^{+} \rightarrow \text{benzene} + \text{Fe (III)} + \text{water} \quad (4)$$

The ascorbic acid is well known as a good reducing agent. It changes the state of metal catalyst from Fe (III) to Fe (II).

$$2\ \text{Fe (III)} + \text{ascorbic acid} + 0.5\ O_2 \rightarrow 2\ \text{Fe (II)} + \text{Dehydroascorbic acid} + H_2O$$

$$2\ \text{Fe (II)} + O_2 + 2H^{+} \rightarrow 2\text{Fe (III)} + H_2O_2$$

$$\text{Fe (III)} + H_2O_2 + H^{+} \rightarrow \text{Fe (II)} + OH^{o} + H_2O$$

In the cases of Cu and V, the formation of phenol proceeds through the similar mechanism as that of Fenton chemistry by replacing the redox of Fe (III)/Fe (II) to that of Cu (II)/Cu (I) as well as V (V)/V (IV) [7,16,20]. The synergistic effect of Cu and V might be arisen from: a) increasing redox rate of Fe to increase the rate reaction (1), b) increasing the oxidation of Fe (II) to prevent the reverse reaction (4) and c) stabilizing phenol to prevent the further oxidation of phenol. More detailed studies should be carried in order to elucidate this effect.

The effect of UV light was also provided in Table 5. The use of UV light obviously improved conversion for all solvent systems. In this study, only a simple comparison was done on the photocatalytic oxidation of benzene. Selectivity slightly increased in the case of acetone while slightly decreased in the cases of acetonitrile and pyridine. The UV light enhanced the decomposition of H_2O_2 by increasing the hydroxyl radicals which reacted with benzene [21]; however, if the amount of the hydroxyl radicals was excessive, it can convert phenol to hydroquinone and benzoquinone. The optimum of UV intensity may be further studied for each case of different solvent and catalyst.

Effect of Support on the Reaction Performance

Three types of metal doping, i.e., FeCu, FuV, and FeVCu were loaded on three supports, i.e., SiO_2, α-Al_2O_3 and TiO_2. The results of the obtained yields were compared as shown in Figure 1. The orders of the performance of the support are the same for all three types of metal doping, i.e., $TiO_2 > SiO_2 > \alpha$-Al_2O_3. The results of BET measurement summarized in Table 2 showed that the values of specific surface area of the supported catalysts followed the order of $SiO_2 > TiO_2 > \alpha$-Al_2O_3, indicating that the surface area is not the only major influencing factor on the catalytic performance and, therefore, the interaction between the metal-support should be an important issue. It was reported in some studies that in the case of supporting acidic Fe species, SiO_2 is preferred to give strong surface acidity. However, in this case with neutral Fe species, rather polar support (TiO_2) gave better results. Also TiO_2 support is essential for the photocatalytic reactions [32]. It was also reported that difference in metal species loading provided a different support behavior. With 5 wt% Cu loading, the catalytic activity of benzene oxidation with respect to support was ordered as follows: γ-$Al_2O_3 > TiO_2 > SiO_2$ [21] and that of 0.5 wt% V was $ZrO_2 > \alpha$-$Al_2O_3 > SiO_2$ [23].

Comparison with other Results from Literatures

Many researchers have studied the hydroxylation of benzene to phenol in different reaction conditions, i.e., solvent and oxidant species, active catalyst and support, reaction temperature, reaction time, etc. Therefore, it is difficult to compare their performance of each parameter directly. The ratios of benzene per catalyst and oxidant type are ones of the most important parameters. As shown in Table 6, although our system was operated with comparatively moderate benzene per catalyst, low residence time and low temperature (room temperature), the obtained yields are relatively high compared with others.

Conclusion

The liquid phase hydroxylation of benzene to phenol with hydrogen peroxide catalyzed by multi transition metal (Fe-) containing TiO_2 catalyst was investigated. Doping with 2.5 wt% Cu or V as a second metal loading to 5 wt% Fe component for bi-metal oxide catalyst obviously improved phenol yield and selectivity. FeVCu/TiO_2 tri-metal catalyst showed higher benzene conver-

Table 6. Comparison of Experimental Results from Different Literatures

Catalyst	Benzene/catalyst (mol/g)	Oxidant	Reaction Temperature (K)	Solvent	Reaction time (h)	Yield (%)	Reference
TBA-$PW_{11}Cu$	3.54×10^{-3}	O_2	323	acetone, water, sulfolane	12	8.4	[9]
Cu/Al_2O_3	4.20×10^{-3}	O_2	303	acetic acid	24	2.5	[21]
$CsPMoV_2$	6.96×10^{-3}	O_2	353	acetic acid	24	7.2	[27]
V/Al_2O_3	7.14×10^{-1}	O_2	303	acetic acid	24	8.2	[22]
Fe/Activated carbon	NA	H_2O_2	338	acetonitrile	5	7	[2]
Cu/Activated carbon	NA	H_2O_2	338	acetonitrile	5	3.6	[2]
V/Activated carbon	NA	H_2O_2	338	acetonitrile	5	13.2	[2]
5.0Fe/NACH-600N	NA	H_2O_2	338	acetonitrile	3	20	[25]
Cu/TiO_2	9.43×10^{-4}	H_2O_2	303	acetone	4	1.3	[7]
Fe/TiO_2	1.08×10^{-3}	H_2O_2	303	acetone	4	2.3	[7]
V/TiO_2	1.18×10^{-3}	H_2O2	303	acetone	4	1.3	[7]
$PMO_{11}V$	1.25×10^{-3}	H_2O_2	338	acetonitrile	2	11.5	[24]
$FeCu/TiO_2$	1.55×10^{-3}	H_2O_2	303	acetone	4	6.5	this work
FeV/TiO_2	1.66×10^{-3}	H_2O_2	303	acetonitrile	4	6.6	this work
$FeVCu/TiO_2$	2.13×10^{-3}	H_2O_2	303	acetone	4	7.2	this work
$FeVCu/TiO_2$+ Photo	2.13×10^{-3}	H_2O_2	303	acetonitrile	4	9.7	this work
V/Clay	1.75×10^{-2}	H_2O_2	313	acetonitrile	4	10.6	[5]
TS-1	1.75×10^{-2}	H_2O_2	313	acetonitrile	4	5.2	[5]
VO_x/SiO_2	3.06×10^{-2}	H_2O_2	343	acetic acid	20	8.3	[26]
V-MCM-41	4.00×10^{-1}	H_2O_2	333	acetonitrile	3	9	[23]

sion and phenol yield; however, it slightly decreased in selectivity and also TOF. Acetonitrile was the most suitable solvent since the highest phenol yield with high selectivity were obtained. Operation with UV light in $FeVCu/TiO_2$ tri-metal catalyst improved also phenol yield without selectivity change. The performances of the support were ordered as follows: $TiO_2 > SiO_2 > \alpha$-Al_2O_3.

Acknowledgments

Financial supports from the Thailand Research Fund and Commission on Higher Education are gratefully acknowledged.

References

1. R. J. Schmidt, *Appl. Catal. A*., **280**, 89 (2005).
2. J. S. Choi, T. H. Kim, K. Y. Choo, J. S. Sung, M. B. Saidutta, S. D. Song, and Y. W. Rhee, *J. Porous Mater*., **12**, 301 (2005).
3. Y. Liu, K. Murata, and M. Inaba, *Catal. Com.*, **6**, 679 (2005).
4. M. Stockmann, F. Konietzni, and J. U. Notheis, *Appl. Catal. A.*, **208**, 343 (2001)
5. X. Gao and J. Xu, Appl. *Clay Sci.*, **33**, 1 (2006).
6. H. Park and W. Choi, *Catal. Today*, **101**, 291 (2005).
7. G. Tanarungsun, W. Kiatkittipon, S. Assabumrungrat, H. Yamada, T. Tagawa, and P. Prasertdam, *J. Chem. Eng. Japan*, **40**, 415 (2007).
8. G. Tanarungsun, W. Kiatkittipon, S. Assabumrungrat, H. Yamada, T. Tagawa, and P. Prasertdam, *J. Ind. Eng. Chem*., **13**, 444 (2007).
9. A. Dubey and S. Kannan, *Catal. Com.*, **6**, 394 (2005).
10. A. Dubey, V. Rives, and S. Kannan , *J. Mol. Catal. A*, **181**, 151 (2002).
11. H. H. Chungm and J. S. Rho, *J. Ind. Eng. Chem*., **5**, 261 (1999).
12. H. H. Chungm and J. S. Rho, *J. Ind. Eng. Chem.*, **5**, 81 (1999).
13. S. S. Hong, C. S. Ju, C. G. Lim, B. H. Ahn, K. T. Lim, and G. D. Lee, *J. Ind. Eng. Chem*., **7**, 99 (2001).
14. S. B. Kim, H. T. Jang, and S. C. Hang, *J. Ind. Eng. Chem.*, **8**, 156 (2002).
15. Y. J. Seo, Y. Mukai, T. Tagawa, and S. Goto, *J. Mol. Catal. A*, **120**, 149 (1997).
16. T. Miyahara, H. Kanzaki, R. Hamada, S. Kuroiwa, S. Nishiyama, and S. Tsuruya, *J. Mol. Catal. A*., **176**, 141 (2001).
17. K. D. Asim, B. Chaudhuri, S. Bhattacharjee, and B. K. Dutta, *J. Hazard. Mater.*, **64**, 91 (1999).
18. S. C. Kim, *J. Hazard. Mater*., **91**, 285 (2002).
19. K. Murata, R. Yanyong, and M. Inaba, *Catal. Lett*.,

102, 143 (2005).
20. H. Kanzaki, T. Kitamura, R. Hamada, S. Nishiyama, and S. Tsuruya, *J. Mol. Catal. A*., **208**, 203 (2004).
21. Y. K. Masumoto, R. Hamada, K. Yokota, S. Nishiyama, and S. Tsuruya, *J. Mol. Catal. A.*, **184**, 215 (2002).
22. Y. W. Chen and Y. H. Lu, *Ind. Eng. Chem. Res.*, **38**, 1893 (1999).
23. N. A. Alekar, V. Indira, S. B. Halligudi, D. Srinvas, S. Gopinathan, and C. Gopinathan, *J. Mol. Catal. A.*, **164**, 181 (2000).
24. J. S. Choi, T. H. Kim, K. Y. Choo, J. S. Sung, M. B. Saidutta, S. O. Ryu, S. D. Song, B. Ramachndra, and Y. W. Rhee, *Appl. Catal. A.*, **290**, 1 (2005).
25. K. Lemke, H. Ehrich, U. Lohse, H. Berndt, and K. Jahnisch, *Appl. Catal. A.*, **243**, 41 (2003).
26. S. T. Yamaguchi, S. Sumimoto, Y. Ichihashi, S. Nishiyama, and S. Tsuruya, *Ind. Eng. Chem. Res.*, **44**, 1 (2005).
27. K. I. Shimizu, H. Akahane, T. Kodama, and Y. Kitayama, *Appl. Catal. A*, **269**, 75 (2004).
28. B. Chou, J. L. Tsai, and S. Cheng, *Micropor. Mesopor. Mater.*, **48**, 309 (2001)
29. J. Zhang, Y. Tang, G. Li., and C. Hu, *Appl. Catal. A*, **278**, 251 (2005).
30. T. Mizuno, H. Yamada, T. Tagawa, and S. Goto, *J. Chem. Eng. Japan*, **38**, 849 (2005).
31. Y. J. Seo, T. Tagawa, and S. Goto, *J. Mol. Cat.*, **78**, 201 (1993).
32. Y. J. Seo, T. Tagawa, and S. Goto, *React. Kinet. Catal. Letters*, **54**, 265 (1995)

Appendix 14